2-P

NASA TECHNICAL NOTE

NASA TN D-7716

NASA TN D-7716

(NASA-TN-D-7716) WIND-TUNNEL FREE-FLIGHT INVESTIGATION OF A MODEL OF A SPIN-RESISTANT FIGHTER CONFIGURATION (NASA) 76 p HC $4.00 CSCL 01C

N74-26443

Unclas
H1/02 41970

WIND-TUNNEL FREE-FLIGHT INVESTIGATION OF A MODEL OF A SPIN-RESISTANT FIGHTER CONFIGURATION

by Sue B. Grafton, Joseph R. Chambers, and Paul L. Coe, Jr.

Langley Research Center
Hampton, Va. 23665

NATIONAL AERONAUTICS AND SPACE ADMINISTRATION • WASHINGTON, D. C. • JUNE 1974

19

1. Report No.	2. Government Accession No.	3. Recipient's Catalog No.
NASA TN D-7716		

4. Title and Subtitle	5. Report Date
WIND-TUNNEL FREE-FLIGHT INVESTIGATION OF A MODEL OF A SPIN-RESISTANT FIGHTER CONFIGURATION	June 1974
	6. Performing Organization Code
7. Author(s)	8. Performing Organization Report No.
Sue B. Grafton, Joseph R. Chambers, and Paul L. Coe, Jr.	L-9681
	10. Work Unit No.
9. Performing Organization Name and Address	501-26-04-02
NASA Langley Research Center Hampton, Va. 23665	11. Contract or Grant No.
	13. Type of Report and Period Covered
12. Sponsoring Agency Name and Address	Technical Note
National Aeronautics and Space Administration Washington, D.C. 20546	14. Sponsoring Agency Code

15. Supplementary Notes

Paul L. Coe, Jr., is an Assistant Research Professor in Engineering, The George Washington University, Joint Institute for Acoustics and Flight Sciences.

Technical Film Supplement L-1152 available on request.

16. Abstract

An investigation was conducted to provide some insight into the features affecting the high-angle-of-attack characteristics of a high-performance twin-engine fighter airplane which in operation has exhibited excellent stall characteristics with a general resistance to spinning. Various techniques employed in the study included wind-tunnel free-flight tests, flow-visualization tests, static force tests, and dynamic (forced-oscillation) tests. In addition to tests conducted on the basic configuration, tests were made with the wing planform and the fuselage nose modified.

The results of the study showed that the model exhibited good dynamic stability characteristics at angles of attack well beyond that for wing stall. The directional stability of the model was provided by the vertical tail at low and moderate angles of attack and by the fuselage forebody at high angles of attack. The wing planform was found to have little effect on the stability characteristics at high angles of attack. The tests also showed that although the fuselage forebody produced beneficial contributions to static directional stability at high angles of attack, it also produced unstable values of damping in yaw. Nose strakes located in a position which eliminated the beneficial nose contributions produced a severe directional divergence.

The investigation identified configuration features which promote spin resistance and also defined test techniques and methods of analysis which can be applied early in design of future configurations.

17. Key Words (Suggested by Author(s))	18. Distribution Statement
Stall/spin Dynamic stability High-performance fighter	Unclassified – Unlimited STAR Category 02

19. Security Classif. (of this report)	20. Security Classif. (of this page)	21. No. of Pages	22. Price*
Unclassified	Unclassified	~~76~~ 79	$4.00

*For sale by the National Technical Information Service, Springfield, Virginia 22151

WIND-TUNNEL FREE-FLIGHT INVESTIGATION OF A MODEL OF A SPIN-RESISTANT FIGHTER CONFIGURATION

By Sue B. Grafton, Joseph R. Chambers,
and Paul L. Coe, Jr.*
Langley Research Center

SUMMARY

An investigation was conducted to provide some insight into the features affecting the high-angle-of-attack characteristics of a high-performance twin-engine fighter airplane which in operation has exhibited excellent stall characteristics with a general resistance to spinning. Various techniques employed in the study included wind-tunnel free-flight tests, flow-visualization tests, static force tests, and dynamic (forced-oscillation) tests. In addition to tests conducted on the basic configuration, tests were made with the wing planform and the fuselage nose modified.

The results of the study showed that the model exhibited good dynamic stability characteristics at angles of attack well beyond that for wing stall. The directional stability of the model was provided by the vertical tail at low and moderate angles of attack and by the fuselage forebody at high angles of attack. The wing planform was found to have little effect on the stability characteristics at high angles of attack. The tests also showed that although the fuselage forebody produced beneficial contributions to static directional stability at high angles of attack, it also produced unstable values of damping in yaw. Nose strakes located in a position which eliminated the beneficial nose contributions produced a severe directional divergence.

The investigation identified configuration features which promote spin resistance and also defined test techniques and methods of analysis which can be applied early in design of future configurations.

---

*Assistant Research Professor in Engineering, The George Washington University, Joint Institute for Acoustics and Flight Sciences.

INTRODUCTION

Experience has shown that many high-performance fighter airplanes are susceptible to a lateral-directional divergence (sometimes referred to as nose-slice) at high angles of attack. (See, e.g., ref. 1.) This type of divergence usually leads to inadvertent spins, and spin recovery for present-day fighters is often difficult or impossible. Therefore, there is an urgent need to develop guidelines for use in the design of future tactical aircraft in order to eliminate instabilities and insure good inherent characteristics at high angles of attack. The National Aeronautics and Space Administration currently has a broad research program underway to provide these guidelines. One element of the program involves identification of airframe design features which promote good stall and spin characteristics.

The present investigation was conducted in order to provide some insight into the features affecting the stability characteristics at high angles of attack of a high-performance twin-engine fighter which in operation has exhibited outstanding stall and spin characteristics. These characteristics, which result in a general resistance to spins, include positive directional stability through the stall with no tendency to diverge and no significant adverse yaw due to aileron deflection at high angles of attack.

A wind-tunnel investigation was made with a 0.17-scale model of the airplane in order to define some of the more important geometric and aerodynamic characteristics responsible for the good stall and spin characteristics. The study included wind-tunnel free-flight tests, flow-visualization tests, static force tests, and dynamic (forced-oscillation) force tests.

In addition to the tests conducted for the basic configuration, tests were made with the wing planform changed to swept and delta designs. The basic and delta wings were also tested in a high position on the fuselage, and fuselage forebody strakes were added in order to determine the effects of these features on stability and control at high angles of attack.

Selected scenes from a motion picture of the free-flight tests have been prepared as a film supplement available on loan. A request card and a description of the film (L-1152) are included at the back of this report.

SYMBOLS

All longitudinal forces and moments are referred to the wind-axis system and all lateral-directional data are referred to the body-axis system shown in figure 1. All force-test data are referred to a moment reference center located longitudinally at 18 percent of the mean aerodynamic chord for the basic wing. The vertical location of the moment reference center was 0.02 percent of the mean aerodynamic chord above the wing-chord reference line at the plane of symmetry. All measurements were reduced to standard coefficient form on the basis of the geometric characteristics of each individual wing planform. In order to facilitate international usage of data presented, dimensional quantities are presented both in the International Systems of Units (SI) and in the U.S. Customary Units. Measurements and calculations were made in the U.S. Customary Units. Conversion factors for the two systems may be found in reference 2.

b wing span, m (ft)

$\bar{c}$ mean aerodynamic chord, m (ft)

C_A axial-force coefficient, $F_A/q_\infty S$

C_D drag coefficient, $F_D/q_\infty S$

C_L lift coefficient, $F_L/q_\infty S$

C_l rolling-moment coefficient, $M_X/q_\infty Sb$

C_m pitching-moment coefficient, $M_Y/q_\infty S\bar{c}$

C_n yawing-moment coefficient, $M_Z/q_\infty Sb$

C_N normal-force coefficient, $F_N/q_\infty S$

C_Y side-force coefficient, $F_Y/q_\infty S$

f frequency of oscillation, Hz

F_A axial force, N (lb)

F_D drag force, N (lb)

F_L lift force, N (lb)

F_N normal force, N (lb)

F_Y side force, N (lb)

I_X moment of inertia about X body axis, kg-m^2 (slug-ft^2)

I_Y moment of inertia about Y body axis, kg-m^2 (slug-ft^2)

I_Z moment of inertia about Z body axis, kg-m^2 (slug-ft^2)

k reduced-frequency parameter, $\frac{\omega b}{2V}$ or $\frac{\omega \bar{c}}{2V}$

M_X rolling moment, m-N (ft-lb)

M_Y pitching moment, m-N (ft-lb)

M_Z yawing moment, m-N (ft-lb)

p roll rate, rad/sec

q pitch rate, rad/sec

q_∞ dynamic pressure, N/m^2 (lb/ft^2)

r	yaw rate, rad/sec
S	wing area, m^2 (ft^2)
u,v,w	components of resultant velocity V along X, Y, and Z body axes, respectively, m/sec (ft/sec)
V	free-stream velocity, m/sec (ft/sec)
X,Y,Z	body reference axes (fig. 1)
α	angle of attack, deg
$\dot{\alpha}$	rate of change of angle of attack, rad/sec
β	angle of sideslip, deg
$\dot{\beta}$	rate of change of sideslip, rad/sec
δ_a	aileron deflection (per side), positive for left roll, deg
$\delta_{f,le}$	leading-edge flap deflection, deg
δ_h	horizontal-tail deflection, positive for nose-down pitch, deg
δ_r	rudder deflection, positive for nose-left yaw, deg
ΔC_l	incremental rolling-moment coefficient
ΔC_n	incremental yawing-moment coefficient
ΔC_Y	incremental side-force coefficient
ω	angular frequency, $2\pi f$, rad/sec

$$C_{l_\beta} = \frac{\partial C_l}{\partial \beta} \qquad C_{n_\beta} = \frac{\partial C_n}{\partial \beta} \qquad C_{Y_\beta} = \frac{\partial C_Y}{\partial \beta}$$

$$C_{n_{\beta,dyn}} = C_{n_\beta} - \frac{I_Z}{I_X} C_{l_\beta} \sin \alpha$$

$$C_{l_p} = \frac{\partial C_l}{\partial \frac{pb}{2V}} \qquad C_{n_p} = \frac{\partial C_n}{\partial \frac{pb}{2V}} \qquad C_{Y_p} = \frac{\partial C_Y}{\partial \frac{pb}{2V}}$$

$$C_{l_{\dot{\beta}}} = \frac{\partial C_l}{\partial \frac{\dot{\beta} b}{2V}} \qquad C_{n_{\dot{\beta}}} = \frac{\partial C_n}{\partial \frac{\dot{\beta} b}{2V}} \qquad C_{Y_{\dot{\beta}}} = \frac{\partial C_Y}{\partial \frac{\dot{\beta} b}{2V}}$$

$$C_{l_r} = \frac{\partial C_l}{\partial \frac{rb}{2V}} \qquad C_{n_r} = \frac{\partial C_n}{\partial \frac{rb}{2V}} \qquad C_{Y_r} = \frac{\partial C_Y}{\partial \frac{rb}{2V}}$$

$$C_{m_q} = \frac{\partial C_m}{\partial \frac{q\bar{c}}{2V}} \qquad C_{N_q} = \frac{\partial C_N}{\partial \frac{q\bar{c}}{2V}} \qquad C_{A_q} = \frac{\partial C_A}{\partial \frac{q\bar{c}}{2V}}$$

$$C_{m_{\dot{\alpha}}} = \frac{\partial C_m}{\partial \frac{\dot{\alpha}\bar{c}}{2V}} \qquad C_{N_{\dot{\alpha}}} = \frac{\partial C_N}{\partial \frac{\dot{\alpha}\bar{c}}{2V}} \qquad C_{A_{\dot{\alpha}}} = \frac{\partial C_A}{\partial \frac{\dot{\alpha}\bar{c}}{2V}}$$

MODEL, APPARATUS, AND TESTING TECHNIQUES

Basic Configuration

A three-view sketch showing the basic configuration of the model is presented in figure 2, photographs of the model are presented in figure 3, and mass and geometric characteristics are listed in table I. The model was

constructed primarily of molded fiberglass and was a 0.17-scale model of the full-scale airplane.

The model was powered by compressed air which was brought into the top of the model by flexible plastic tubing and ejected from metal tubes located inside the model near the rear of the fuselage. This ejector system simulated flow through the engines, since the model was tested with the engine inlets and interior of the model open.

The longitudinal control surface consisted of an all-movable horizontal tail, the lateral control surfaces were conventional ailerons, and the directional control surface was a conventional rudder. For manual control by the pilot, the control surfaces were actuated by electropneumatic servos which provided a full-on or full-off flicker-type deflection. Each actuator had a motor-driven trimmer which was electrically operated by the pilots so that controls could be rapidly trimmed in flight. The systems for pitch and roll control were also connected to individual rate damper systems. The rate dampers consisted of rate gyroscopes driven by compressed air which actuated the surfaces in proportion to pitch and roll rates. The control-surface deflections used during the flights were as follows:

Control	Pilot (flicker)	Damper (proportional)	Maximum available
Horizontal tail, deg	±5	±5	5 to -25
Ailerons (per side), deg . . .	±10	±5	±30
Rudder, deg	±10 to ±30	--	±30

Deflection of the horizontal tail on the full-scale airplane is limited to 17° trailing edge up, but increased travel was provided for the model in order to investigate angles of attack beyond those obtainable in 1 g flight at full scale.

Modified Configuration

One airframe component expected to have significant effects on the stability and control of the model at high angles of attack was the wing. Past studies (see refs. 3 and 4, e.g.) have shown that wing planform

characteristics, such as sweepback and taper ratio, together with the vertical location of the wing on the fuselage can have large effects on lateral-directional stability at high angles of attack. In order to evaluate the effects of wing modifications, the additional wings and wing-fuselage combinations shown in figures 4, 5, and 6 were tested. In addition to the basic wing, a swept wing (similar in planform to that employed by the configuration of ref. 1) and a delta wing were tested. As shown in figure 5, the basic wing and the delta wing were also tested in a high position with modified engine inlets. (The engine inlets were modified in order to smooth the intersection of the high wing and the fuselage.) All wings were of equal area and of relatively equal weights, so that the flight tests were conducted with a constant value of wing loading. Aspect ratio and wing span varied with each wing design. (See table I.) The location of the $0.25\bar{c}$ point was constant for all configurations tested. The additional wings incorporated conventional ailerons for roll control. Plan views of the configuration with the various wings are shown in figure 6.

Tests were also conducted to determine the effects of the symmetrical nose strakes shown in figure 7. The strakes were designed to eliminate asymmetric yawing moments and unstable values of damping in yaw at high angles of attack, as discussed in reference 5. As a further element of studies of the effects of the fuselage nose, the aerodynamic characteristics of the isolated nose of the basic configuration were determined in tests of the nose alone (fig. 8).

Free-Flight Test Technique

The test setup for the free-flight tests is shown in figure 9. The model was flown without restraint in the 9- by 18-m (30- by 60-ft) open-throat test section of the Langley full-scale tunnel and was remotely controlled about all three axes by two human pilots. One pilot, who controlled the model about its roll and yaw axes, was stationed in an enclosure at the rear of the test section. The second pilot, who controlled the model in pitch, was stationed at one side of the tunnel. Pneumatic and electric power and control signals were supplied to the model through a flexible trailing cable which was made up of wires and light plastic tubes. The trailing cable also incorporated a

0.318-cm-diameter (1/8-in.) steel cable that passed through a pulley above the test section. This section of flight cable was used to catch the model when an uncontrollable motion or mechanical failure occurred. The entire flight cable was kept slack during the flights by a safety-cable operator using a high-speed pneumatic winch. A further discussion of the free-flight technique, including the reasons for dividing the piloting tasks, is given in reference 6.

TESTS

Free-Flight Tests

Free-flight tests were conducted to determine the dynamic stability and control characteristics of the following model configurations at high angles of attack:

1. Low-wing configurations
   (a) Basic
   (b) Swept
   (c) Delta
2. High-wing configurations
   (a) Basic
   (b) Delta

The flight tests included steady flights at high angles of attack up to and including stall, studies of pilot lateral-control techniques at high angles of attack, and evaluation of the effects of artificial rate damping. In addition, a few flight tests were made to determine the effects of wing leading-edge flap deflection and wing-tip fuel tanks on the characteristics of the basic configuration. The results of the flight tests were mainly qualitative and consisted of pilot opinion of the behavior of the model. Motion-picture records were made of all flights and selected scenes are included in the film supplement to this report.

Force and Flow-Visualization Tests

Static and dynamic (forced-oscillation) tests were conducted in the Langley full-scale tunnel at a Reynolds number, based on the mean aerodynamic chord of the basic wing, of about 0.65×10^6. This value of Reynolds number

was about the same as that for the flight tests, which, of course, varied with lift coefficient. Static tests were made for a range of angle of attack from -10° to 40° over a range of angle of sideslip of $\pm 40^{\circ}$ for the configurations flown and included component-buildup tests and control-effectiveness tests. The forced-oscillation tests were made in pitch, roll, and yaw to determine the dynamic stability derivatives for the low-wing configurations. The tests were made with an angular amplitude of $\pm 5^{\circ}$ and an oscillation frequency of 1 Hz, which resulted in values of the reduced-frequency parameter k of 0.181 for the rolling and yawing tests and 0.056 for the pitching tests. Conventional wind-tunnel corrections for flow angularity have been applied to all force data. A limited number of tuft, smoke, and oil flow-visualization tests were also conducted to determine flow characteristics around the model.

RESULTS AND DISCUSSION OF FORCE TESTS

Static Longitudinal Characteristics

Basic configuration.- The static longitudinal characteristics of the basic configuration are presented in figures 10 to 12. The data of figure 10 show the effects of horizontal-tail deflection on the longitudinal characteristics. The model was statically stable and the horizontal tail was effective over the range of angle of attack tested. With the tail removed, the lift curve indicated major wing stall near $\alpha = 17^{\circ}$; this condition was verified by tuft flow-visualization tests. With the tail on, the lift curve did not exhibit a sharp break. The data also show that for the particular center of gravity of the tests ($0.18\bar{c}$), deflection of the tail to the maximum available on the full-scale airplane $\left(\delta_h = -17^{\circ}\right)$ would trim the model at about $\alpha = 21^{\circ}$ for 1 g flight. As previously pointed out, the horizontal-tail travel was extended to $\delta_h = -25^{\circ}$ for the present model in order to investigate stability and control characteristics at angles of attack higher than those obtained in 1 g flight.

The data of figure 11 show that deflection of the wing leading-edge flap produced a small increase in lift at high angles of attack and no effect on longitudinal stability. Addition of wing-tip tanks to the basic configuration had no significant effects on the longitudinal aerodynamic characteristics of the model, as shown in figure 12.

Modified configuration.- The longitudinal characteristics of the model with the swept and delta wings are given in figure 13 for various values of δ_h and for the horizontal tail off. This figure shows that the swept- and delta-wing configurations were stable throughout the angle-of-attack range. Figure 14 shows the characteristics for the three wing configurations with $\delta_h = 0^\circ$ and with the tail off. These data indicate that with the tail on, the level of longitudinal stability was about the same for all three configurations and that the swept- and delta-wing configurations produced more lift than the basic configuration at angles of attack beyond 20°.

Static Lateral-Directional Characteristics

Basic configuration.- The static lateral-directional characteristics of the basic configuration are presented in figure 15 in terms of the static stability derivatives C_{Y_β}, C_{l_β}, and C_{n_β} for $\delta_h = 0^\circ$ and -17°. The data show that the static directional-stability derivative C_{n_β} was large and positive (stable) at low angles of attack. The magnitude of C_{n_β} decreased markedly when the wing stalled at an angle of attack near 17°; but C_{n_β} became increasingly stable at post-stall angles of attack, in contrast to trends shown by most current fighter configurations. (See ref. 1, e.g.) This unusual increase in directional stability at post-stall angles of attack is expected to be a major beneficial factor resulting in the excellent stall characteristics shown by the configuration.

The data of figure 15 show that the effective dihedral derivative also remained stable (negative) over the angle-of-attack range. This characteristic is beneficial to dynamic lateral-directional stability at high angles of attack, as will be discussed in a subsequent section. Deflection of the horizontal tail had little effect on the static lateral-directional stability derivatives.

A number of additional component-buildup tests were conducted to determine the airframe component responsible for the pronounced increase in C_{n_β} exhibited by the configuration beyond wing stall. The data shown in figure 16 indicate the contribution of the vertical tail to C_{n_β}. Two significant results are immediately apparent from these data: First, the tail contribution decreased markedly at angles of attack beyond that for wing stall; second, when the tail

was off, the directional stability increased markedly at angles of attack above 25°, with the result that the model was directionally stable at angles of attack above 31° without a vertical tail. The decrease in tail contribution to directional stability at angles of attack beyond that for wing stall ($\alpha > 17^{\circ}$) was due to the fact that the tail became immersed in the low energy wake of the stalled wing. The fact that the loss in tail effectiveness was the result of loss of dynamic pressure at the tail was verified by tests to determine rudder effectiveness and will be discussed in a later section dealing with those tests. Such loss in tail effectiveness at high angles of attack is not unusual. The more remarkable, and probably more significant, characteristic is the large increase in tail-off directional stability at high angles of attack.

Additional tests were made to determine the wing-fuselage component responsible for the stability at high angles of attack. The component found to be responsible was the fuselage forebody, shown in figure 8. Results of tests conducted with the isolated nose mounted on a balance at a distance ahead of the moment center representative of that for the nose of the basic configuration are presented in figure 17. The data show that the isolated nose was directionally unstable at low angles of attack, as would be expected. At high angles of attack, however, the isolated nose became directionally stable, and comparison of data for the nose alone and data obtained for the basic configuration with the vertical tail off indicates that virtually all the directional stability of the configuration at angles of attack above 32° was produced by the nose.

The geometric feature probably responsible for the aerodynamic characteristics of the fuselage forebody of the present configuration is the cross-sectional shape shown in figure 7. As shown in the sketch, the cross section is an elliptical shape with the major axis horizontal. It has been found in past investigations (refs. 7 to 10, e.g.) that a "flattened" nose similar to that of the present configuration tends to produce such stability; the relatively long nose of the present configuration tends to amplify this effect because of the long moment arm through which side forces produced by the nose can act.

Tuft, smoke, and oil flow-visualization tests were conducted to determine the flow pattern on the nose associated with the aforementioned aerodynamic characteristics. The results showed that two strong vortex sheets were shed

from the pointed nose at high angles of attack, and the proximity of the individual sheets to the upper surface of the nose probably resulted in a pressure field conducive to the generation of beneficial side forces on the nose. Shown in figure 18 are oil-flow photographs of the upper nose surface at $\alpha = 40^{\circ}$ for $\beta = 0^{\circ}$ and $\beta = \pm 10^{\circ}$. At $\beta = 0^{\circ}$, the reattachment lines associated with the two vortex sheets are clearly seen to be fairly symmetrical on the surface. When the nose was sideslipped to the left, as shown for $\beta = 10^{\circ}$, the downwind vortex sheet did not impinge on the upper surface, but the vortex sheet on the windward side was close to the surface. This flow pattern probably produced low pressures on the windward side of the nose which resulted in a net side force on the nose to the right. Because of the long distance between the nose and the center of gravity, a substantial nose-right, or statically stabilizing, yawing moment was created.

The results of additional force tests also served to verify the importance of the nose on the stability characteristics of the present configuration. For example, shown in figure 19 are the results of tests to determine the effects of the fuselage forebody strakes (fig. 7). The results indicate that the strakes eliminated the stabilizing influence of the nose at high angles of attack. In addition, the data indicate that substantial beneficial interference effects existed between the flow field shed by the nose and the wing, as evidenced by large changes in C_{l_β} with the strakes on. Evidently, the strakes fixed the separation point on the forebody so that the beneficial flow field described previously was eliminated. Experience has shown that nose strakes are normally used to provide a substantial increase in directional stability at high angles of attack for other nose shapes. The results of the present investigation and of reference 5 indicate, however, that improperly placed nose strakes can severely degrade C_{n_β} at high angles of attack.

Presented in figures 20 and 21 are the results of tests to determine the effects of leading-edge flap deflection and wing-tip tanks on static lateral-directional stability. The data show that deflection of the leading-edge flap produced small beneficial effects for both C_{n_β} and C_{l_β}, as would be expected because of the small increase in lift discussed previously. Addition of tip tanks increased C_{l_β} somewhat, particularly near the stall.

Modified configurations.- The static lateral-directional stability characteristics of the swept- and delta-wing configurations are presented in figure 22 and the characteristics of these configurations are compared with those of the basic configuration in figure 23. As shown in figure 23, the swept- and delta-wing configurations had levels of directional stability equal to or higher than those of the basic configuration, and the trends of C_{n_β} at high angles of attack were dominated by the characteristics of the nose, as previously discussed for the basic configuration. It should also be noted that the apparent increase in C_{n_β} for the swept- and delta-wing configurations at low angles of attack was caused by the data-reduction procedure, in which the aerodynamic characteristics were based on the geometric characteristics of the individual wings. When compared for equal wing spans, the values of C_{n_β} for the individual wings are about equal at $\alpha = 0^\circ$. The relative unimportance of the large changes in wing planform for the present configuration at high angles of attack underlines the complexity of flow phenomena and the increased importance of what might be supposed to be secondary design features, such as fuselage forebody shape.

The complexity of the situation was emphasized by the results of the force tests for the high-wing configurations (see fig. 5) as presented in figure 24. Relocation of the basic wing to a high position (fig. 24(a)) resulted in a degradation of both C_{n_β} and C_{l_β}, whereas relocation of the delta wing to the high position (fig. 24(b)) resulted in a significant increase in C_{n_β} at high angles of attack for $\delta_h = 0^\circ$. Tests to determine the effects of horizontal-tail deflection for the configuration with the high delta wing indicated a severe deterioration of C_{n_β} due to δ_h. As shown in figure 25, deflection of the tail from $\delta_h = 0^\circ$ to $\delta_h = -25^\circ$ resulted in extremely unstable values of C_{n_β} above $\alpha = 23^\circ$ and a reduction in effective dihedral. This result was probably caused by a change in the vertical location of an adverse flow from the wing brought about by a change in the load on, and consequently the pressure field induced by, the horizontal tail.

Lateral-Directional Control Characteristics

Basic configuration.- The results of force tests conducted to determine the control effectiveness of the ailerons and rudder for the basic configuration are presented in figures 26 and 27. The data are presented in terms of the incremental values of C_Y, C_n, and C_l produced by a right-roll or right-yaw control input. The data of figure 26 show that the incremental rolling moment produced by aileron deflection for the basic configuration decreased markedly as wing stall was approached; the ailerons produced relatively small values of ΔC_l at post-stall angles of attack. The incremental yawing moments produced by aileron deflection were favorable (nose-right for right roll input) except for large control inputs $\left(\delta_a = -30^\circ\right)$ near stall. In addition, the favorable values of ΔC_n were produced by interference with the vertical tail, as shown by the data for $\delta_a = -30^\circ$ with the tail on and off. These favorable yawing moments are unusual for a high-performance fighter and are another factor producing the known spin resistance of the present configuration.

The incremental forces and moments produced by rudder deflection are presented in figure 27. The rudder was effective for angles of attack up to wing stall; at higher angles of attack the rudder effectiveness decreased rapidly. The reduced rudder effectiveness beyond wing stall was associated with immersion of the vertical tail in the low-energy wake of the stalled wing. Since this reduction in rudder effectiveness is almost exactly the same as the reduction in the vertical-tail contribution to C_{n_β} shown in figure 16, it is apparent that the loss in tail contribution to directional stability was caused primarily by reduced dynamic pressure. It should be noted, however, that the rudder effectiveness of the present configuration remains quite high to angles of attack substantially beyond wing stall.

Modified configuration.- The aileron effectiveness for the swept- and delta-wing configurations is compared with that for the basic configuration in figure 28. Both the swept and delta configurations exhibited equal or larger increments of ΔC_l at angles of attack above $\alpha = 12^\circ$ than did the basic configuration; however, both wing modifications produced large adverse yawing moments at and beyond wing stall. These adverse values of ΔC_n would be expected to degrade the post-stall control of the configuration considerably.

The rudder effectiveness of the various configurations is shown in figure 29. Although the results for the three configurations were about equal at $\alpha = 0^{\circ}$ (when compared for a constant value of b), the swept- and delta-wing configurations exhibited much higher values of rudder effectiveness at high angles of attack than did the basic configuration. This result was probably related to stall patterns on the individual wings and relative location of the stalled-wing wakes. It should be noted that the reduction in rudder effectiveness at high angles of attack for these two configurations was much less than the reduction in vertical-tail contribution to C_{n_β} (see fig. 22). This indicates, therefore, that the loss of stability was caused by both a loss in dynamic pressure and an adverse sidewash at the tail.

Dynamic Stability Derivatives

Basic configuration.- The results of the forced-oscillation tests in pitch for the basic configuration are presented in figure 30. The data show that the model had stable values of damping in pitch $\left(\text{negative values of } C_{m_q} + C_{m_{\dot{\alpha}}}\right)$ over the range of angle of attack and that the contribution of the horizontal tail to $C_{m_q} + C_{m_{\dot{\alpha}}}$ remained about constant over the range of angle of attack. The results of the forced-oscillation tests in roll are presented in figure 31. The damping-in-roll parameter $C_{l_p} + C_{l_{\dot{\beta}}} \sin \alpha$ was stable (negative) for angles of attack up to 27°, and unstable values were measured for values of α between 27° and 43°. The vertical tail had little effect on the damping-in-roll parameter, as might be expected. The results of the forced-oscillation tests in yaw are presented in figures 32 and 33. As shown in figure 32, the damping-in-yaw parameter $C_{n_r} - C_{n_{\dot{\beta}}} \cos \alpha$ was stable (negative) at angles of attack below stall but became unstable near $\alpha = 28^{\circ}$ and attained very large unstable values at higher angles of attack. The vertical tail had little effect on the unstable values or trends of the data at high angles of attack.

Additional forced-oscillation tests were conducted to determine the cause of the unstable values of $C_{n_r} - C_{n_{\dot{\beta}}} \cos \alpha$ at high angles of attack. As shown in figure 33, positive values of the parameter $C_{Y_r} - C_{Y_{\dot{\beta}}} \cos \alpha$ were obtained with the positive values of $C_{n_r} - C_{n_{\dot{\beta}}} \cos \alpha$. This result indicates that the nose was the principal cause of the unstable values of damping. Evidently, the

features of the nose which promoted the beneficial effects on static directional stability at high angles of attack also produced detrimental effects on dynamic damping in yaw. The physical cause of the unstable damping in yaw is illustrated by the sketches shown in figure 34. In figure 34(a) the configuration is shown in a steady sideslipped condition with the same value of β at both the nose and the center of gravity. As pointed out previously, for the present configuration, the nose produced a side force which acted through a relatively long moment arm to create a stabilizing yawing moment that tended to reduce the value of β. The sketch in figure 34(b) illustrates the situation for yawing flight, with zero sideslip at the center of gravity. Because the flight path is curved, the nose of the configuration is subjected to a local sideslip angle which produces a side force in a manner similar to that for the static situation. In this case, however, the resulting yawing moment is in a direction which tends to increase the value of yawing velocity and therefore results in unstable values of C_{n_r}.

Modified configuration.- The results of the forced-oscillation tests in pitch for the swept- and delta-wing configurations are compared with the results for the basic configuration in figure 35. The data show that all configurations had stable (negative) values of $C_{m_q} + C_{m_{\dot{\alpha}}}$ over the range of angle of attack, and that the delta configuration had significantly lower values of damping in pitch than the swept or basic configuration.

The results of the forced-oscillation tests in roll presented in figure 36 show that values of the damping-in-roll parameter for the swept and delta configurations were larger than those of the basic configuration at moderate angles of attack, but all configurations exhibited unstable values at angles of attack between 31° and 42°.

The results of the damping-in-yaw tests are presented in figure 37. The data show that the swept and delta configurations, like the basic configuration, exhibited unstable values of $C_{n_r} - C_{n_{\dot{\beta}}} \cos \alpha$ at high angles of attack, but the delta configuration remained stable to a much higher angle of attack than the basic configuration.

RESULTS AND DISCUSSION OF FLIGHT TESTS

A motion-picture film supplement with selected scenes from the free-flight tests has been prepared and is available on loan. A request form and a description of the film will be found at the back of this paper. For all the free-flight tests discussed herein, the center of gravity was at $0.18\bar{c}$.

Longitudinal Characteristics

Since the free-flight tests were intended primarily as an investigation of the lateral-directional characteristics of the model, the pitch damper was active for all tests and the pitch pilot's task was only to hold the model as closely as possible in place in the tunnel test section and to make changes in model trim as necessary. It should be noted, however, that no unusual or unsatisfactory characteristics were noted during the tests and the pilot expressed satisfaction with the stability and control characteristics up to the highest angles of attack flown.

Lateral-Directional Characteristics

Basic configuration.- During the flight tests it was found that the basic model without artificial damping in roll or yaw flew smoothly and with little effort by the pilots up to an angle of attack of about 20°. Above $\alpha = 20^{\circ}$ there was a slight nose wandering, or directional "looseness," noted by the lateral-directional pilot. The nose wandering (although small) increased the pilot effort required to fly the model smoothly. But the pilot was satisfied with the level of stability and considered that the major cause of the increased pilot effort was the rapid decrease in lateral-control effectiveness with increasing angle of attack. (See fig. 26.) At an angle of attack of about 30° the model diverged in yaw against full corrective controls. The yawing motion at the divergence appeared to be a fairly slow rotation about the Z body axis.

Flight tests were also made with the leading-edge flap deflected 20°. Although the lateral response of the model appeared to be better damped near $\alpha = 20^{\circ}$, the results were essentially the same as for the basic configuration and the slow divergence still occurred at about $\alpha = 30^{\circ}$. The model was flown

with the addition of wing-tip fuel tanks with no noticeable effect on the dynamic stability of the model. Similarly, the use of artificial damping in roll had no significant effect on the dynamic stability at high angles of attack.

When the strakes of figure 7 were added to the model, satisfactory flights were made up to about $\alpha = 18^{\circ}$. At slightly higher angles of attack, the model exhibited more serious nose wandering than the basic configuration, and at $\alpha = 23^{\circ}$ a very rapid nose slice, or directional divergence, occurred. This result serves to emphasize the importance of the fuselage forebody on the stability characteristics of the present configuration at the stall, as illustrated by the data of figure 19.

The possibility of directional divergence at high angles of attack is normally examined by means of the dynamic directional-stability parameter $C_{n_{\beta,dyn}}$ (ref. 11), where

$$C_{n_{\beta,dyn}} \doteq C_{n_\beta} - \frac{I_Z}{I_X} C_{l_\beta} \sin \alpha$$

Negative values of $C_{n_{\beta,dyn}}$ usually indicate the existence of a directional divergence. Values of $C_{n_{\beta,dyn}}$ calculated from data of figures 15 and 19 for the basic configuration with and without nose strakes are presented in figure 38. The parameter $C_{n_{\beta,dyn}}$ remained positive over the entire angle-of-attack range and therefore did not predict the directional divergence that was exhibited in the flight test at $\alpha = 23^{\circ}$ for the configuration with nose strakes and at $\alpha = 30^{\circ}$ for the basic configuration. For the configuration with the nose strakes, a minimum value of $C_{n_{\beta,dyn}}$ occurred around $\alpha = 27^{\circ}$ because of the unstable (negative) values of C_{n_β} at high angles of attack (fig. 19). For the basic configuration without nose strakes shown in figure 38, $C_{n_{\beta,dyn}}$ increased positively (stable) at the higher angles of attack. It appears, therefore, that the slow directional divergence exhibited by the model near $\alpha = 30^{\circ}$ was not predicted by $C_{n_{\beta,dyn}}$ but is probably associated with the unstable values of $C_{n_r} - C_{n_{\dot{\beta}}} \cos \alpha$ (fig. 32) and the low rudder effectiveness (fig. 29), neither of which is accounted for in the $C_{n_{\beta,dyn}}$ criterion.

The flights made to determine the effects of various pilot lateral control techniques at high angles of attack consisted of flying the model with rudder and ailerons individually and in an interconnected, or coordinated, mode. The results of these tests showed that flying the model with the rudder alone at high angles of attack was about as good as using both rudder and ailerons. When the wing-tip tanks were added and the rudder was used for lateral control, noticeable rolling motions due to control inputs were obtained, probably because of the increase in C_{l_β} produced by the tanks, as shown in figure 21. At angles of attack above 10°, the pilot could not use ailerons alone for lateral control because of apparently reduced control effectiveness. Some indication of the shortcomings of the aileron control at high angles of attack can be obtained from the aileron-effectiveness parameter (ref. 11) given by

$$C_{n_\beta} - C_{l_\beta} \frac{\Delta C_n}{\Delta C_l}$$

Negative values of this parameter indicate roll reversal; that is, a control input for right roll results in roll to the left. The calculated values of the parameter for the basic configuration are presented in figure 39, and the results indicate that roll reversal did not occur. This parameter does have a minimum value at an angle of attack a few degrees above wing stall, which occurred around $\alpha = 17^\circ$. The variations in magnitude of the aileron-effectiveness parameter are caused by variations in C_{n_β} and aileron yawing-moment characteristics.

Modified configuration.- The swept-wing configuration exhibited dynamic stability characteristics which were similar to those of the basic configuration. The model could be flown easily for angles of attack up to about 26°. At slightly higher angles of attack the lateral pilot noted a slight oscillation in roll ("wing rock"), and at $\alpha = 30^\circ$ the model diverged in yaw against full corrective control. The rate of divergence was about the same as for the basic configuration.

During the flight tests it was found that the delta-wing configuration exhibited the same general flight characteristics as the basic configuration.

Slight nose wandering occurred at about $\alpha = 20^{\circ}$, and at an angle of attack of about 35° the model again exhibited the slow divergence in yaw.

The variations of $C_{n_{\beta,dyn}}$ for the swept- and delta-wing configurations are compared with that for the basic configuration in figure 40. The values of $C_{n_{\beta,dyn}}$ were large and positive for all configurations, indicating no directional divergence, and it therefore appears that the slow divergences observed during the flights were caused by the unstable values of damping in yaw shown in figure 37.

When the basic wing was moved to a high position (as in fig. 5), the characteristics of the model were severely degraded. Nose wandering began near $\alpha = 18^{\circ}$ and the model exhibited a fairly slow directional divergence near $\alpha = 21^{\circ}$. In a similar manner, the high delta-wing configuration also showed degraded characteristics and a rapid directional divergence near $\alpha = 27^{\circ}$. The variation of $C_{n_{\beta,dyn}}$ for the basic- and delta-wing configurations in the high position is presented in figure 41. For the high basic wing the possibility of a mild directional divergence is indicated by a value of $C_{n_{\beta,dyn}}$ of about zero near $\alpha = 22^{\circ}$, which is in good agreement with results of the free-flight tests. The data for the high delta-wing configuration with the elevator deflected 25° show very small positive values of $C_{n_{\beta,dyn}}$ near $\alpha = 32^{\circ}$; however, the severe directional divergence near $\alpha = 27^{\circ}$ which occurred in the flight test was not indicated by $C_{n_{\beta,dyn}}$.

The results of the lateral-control tests for all the aforementioned modified configurations were similar to those for the basic configuration in that the rudder was the most effective means of roll control at high angles of attack. It was noted, however, that use of the ailerons appeared to be completely unsatisfactory because of noticeable adverse yaw. The degraded aileron effectiveness for these configurations is illustrated by the variation of the aileron-effectiveness parameter shown in figure 42. At high angles of attack the swept- and delta-wing configurations show negative values of the parameter, which indicate reversal of roll response due to the adverse aileron yaw shown in figure 28.

INTERPRETATION OF RESULTS

The results of the free-flight tests for the basic configuration are in very good agreement with the characteristics exhibited by the full-scale airplane. In particular, within the operational angle-of-attack range, the absence of any divergence, the good rudder effectiveness, and the absence of adverse yaw due to ailerons appear to have been adequately represented by the model. Of course, the low values of Mach and Reynolds numbers associated with the present tests could cause some characteristics, such as wing stall, to occur at slightly different angles of attack. In addition, the confined space available within the wind tunnel, the rapidity of the motions of the model, and the lack of piloting cues cause the evaluation of lateral-control techniques to be qualitative at best. It appears, however, that the results of the present tests are indicative of some of the factors which cause the basic configuration to have outstanding stall and spin characteristics.

It should be pointed out, however, that some of the factors, such as nose shape, which was found to have a large influence on the stability of the present configuration at high angles of attack, may be insignificant for other configurations. The blending of airframe components for good characteristics at high angles of attack is very configuration dependent and there are few general conclusions to be made. Instead, wind-tunnel test techniques and methods of analysis similar to those presented herein must be used early in design stages in order to insure good stall characteristics.

SUMMARY OF RESULTS

The results of a wind-tunnel and free-flight investigation to determine the factors responsible for the spin-resistant nature of a current fighter airplane may be summarized as follows:

1. The model exhibited exceptionally good dynamic stability characteristics for angles of attack substantially beyond wing stall.

2. The configuration was directionally stable over the angle-of-attack range of the tests. The directional stability was provided by the vertical tail

at low and moderate angles of attack and by the fuselage forebody (nose) at high angles of attack.

3. The wing planform had little effect on the stability characteristics at high angles of attack.

4. The fuselage forebody produced beneficial contributions to static directional stability, but it also produced unstable values of damping in yaw.

5. Use of nose strakes located in a position which eliminated the beneficial nose contributions resulted in a severe directional divergence at high angles of attack.

Langley Research Center,
National Aeronautics and Space Administration,
Hampton, Va., May 23, 1974.

REFERENCES

1. Chambers, Joseph R.; and Anglin, Ernie L.: Analysis of Lateral-Directional Stability Characteristics of a Twin-Jet Fighter Airplane at High Angles of Attack. NASA TN D-5361, 1969.

2. Mechtly, E. A.: The International System of Units - Physical Constants and Conversion Factors (Second Revision). NASA SP-7012, 1973.

3. Polhamus, Edward C.; and Spreeman, Kenneth P.: Subsonic Wind-Tunnel Investigation of the Effect of Fuselage Afterbody on Directional Stability of Wing-Fuselage Combinations at High Angles of Attack. NACA TN 3896, 1956.

4. Goodman, Alex: Effects of Wing Position and Horizontal-Tail Position on the Static Stability Characteristics of Models With Unswept and 45° Sweptback Surfaces With Some Reference to Mutual Interference. NACA TN 2504, 1951.

5. Chambers, Joseph R.; Anglin, Ernie L.; and Bowman, James S., Jr.: Effects of a Pointed Nose on Spin Characteristics of a Fighter Airplane Model Including Correlation With Theoretical Calculations. NASA TN D-5921, 1970.

6. Parlett, Lysle P.; and Kirby, Robert H.: Test Techniques Used by NASA for Investigating Dynamic Stability Characteristics of V/STOL Models. J. Aircraft, vol. 1, no. 5, Sept.-Oct. 1964, pp. 260-266.

7. Johnson, Joseph L.: Damping in Yaw and Static Directional Stability of a Canard Airplane Model and of Several Models Having Fuselages of Relatively Flat Cross Section. NACA RM L50H30a, 1950.

8. Paulson, John W.; and Johnson, Joseph L., Jr.: Free-Flight-Tunnel Investigation of the Low-Speed Stability and Control Characteristics of a Model Having a Fuselage of Relatively Flat Cross Section. NACA RM L52L22, 1953.

9. Bates, William R.: Static Stability of Fuselages Having a Relatively Flat Cross Section. NACA TN 3429, 1955. (Supersedes NACA RM L9I06a.)

10. Spencer, Bernard, Jr.; and Phillips, W. Pelham: Effects of Cross-Section Shape on the Low-Speed Aerodynamic Characteristics of a Low-Wave-Drag Hypersonic Body. NASA TN D-1963, 1963.

11. Moul, Martin T.; and Paulson, John W.: Dynamic Lateral Behavior of High-Performance Aircraft. NACA RM L58E16, 1958.

TABLE I.- MASS AND GEOMETRIC CHARACTERISTICS OF THE

LOW-WING MODEL CONFIGURATIONS

	Basic wing	Swept wing	Delta wing
Model weight	251.3 N (56.5 lb)	243.6 N (54.76 lb)	244.9 N (55.06 lb)
Model moments of inertia:			
I_X	0.56 kg-m^2 (0.41 slug-ft^2)	0.31 kg-m^2 (0.23 slug-ft^2)	0.41 kg-m^2 (0.30 slug-ft^2)
I_Y	8.53 kg-m^2 (6.29 slug-ft^2)	8.76 kg-m^2 (6.46 slug-ft^2)	8.64 kg-m^2 (6.37 slug-ft^2)
I_Z	8.95 kg-m^2 (6.60 slug-ft^2)	9.06 kg-m^2 (6.68 slug-ft^2)	9.04 kg-m^2 (6.67 slug-ft^2)
Wing:			
Span	1.34 m (4.39 ft)	1.17 m (3.85 ft)	1.01 m (3.31 ft)
Area	0.49 m^2 (5.24 ft^2)	0.49 m^2 (5.24 ft^2)	0.49 m^2 (5.24 ft^2)
Root chord	0.59 m (1.95 ft)	0.71 m (2.34 ft)	0.92 m (3.01 ft)
Tip chord	0.15 m (0.48 ft)	0.12 m (0.39 ft)	0.05 m (0.15 ft)
Mean aerodynamic chord	0.41 m (1.34 ft)	0.48 m (1.59 ft)	0.61 m (2.01 ft)
Aspect ratio	3.68	2.82	2.09
Taper ratio	0.25	0.17	0.05
Dihedral	0	3.69°	0
Aileron area (one side)	0.013 m^2 (0.14 ft^2)	0.014 m^2 (0.15 ft^2)	0.013 m^2 (0.14 ft^2)

TABLE I.- MASS AND GEOMETRIC CHARACTERISTICS OF THE

LOW-WING MODEL CONFIGURATIONS – Concluded

Horizontal tail:	
Area	0.165 m^2 (1.78 ft^2)
Span	0.75 m (2.46 ft)
Aspect ratio (exposed)	2.88
Taper ratio	0.33
Dihedral	-4.0
Vertical tail:	
Area (exposed)	0.12 m^2 (1.25 ft^2)
Aspect ratio (exposed)	1.22
Taper ratio (exposed	0.25
Rudder area (aft of hinge)	0.017 m^2 (0.18 ft^2)
Overall fuselage length	2.38 m (7.81 ft)

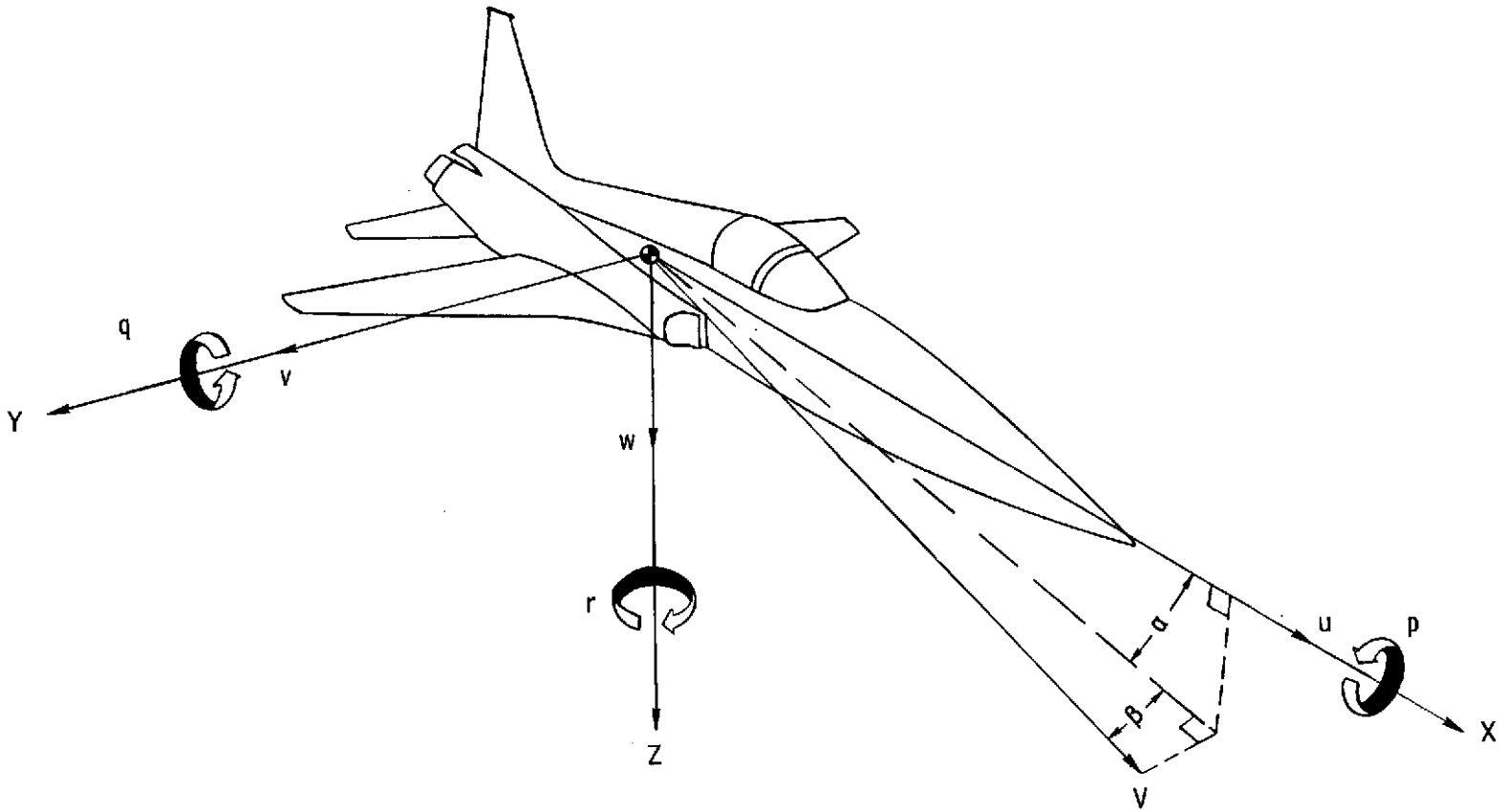

Figure 1.- The body system of axes.

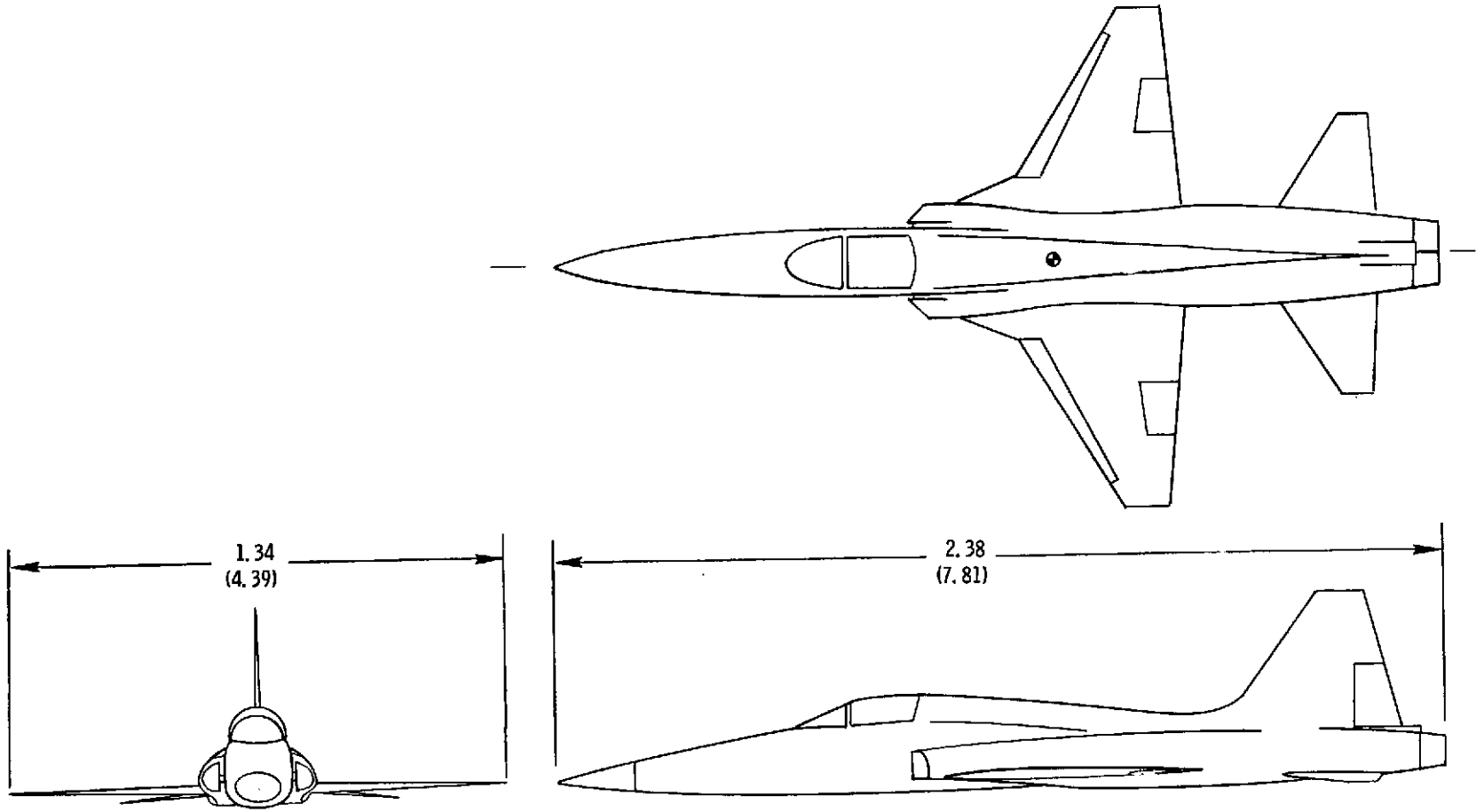

Figure 2.- Three-view sketch of basic model. Dimensions are given in m (ft).

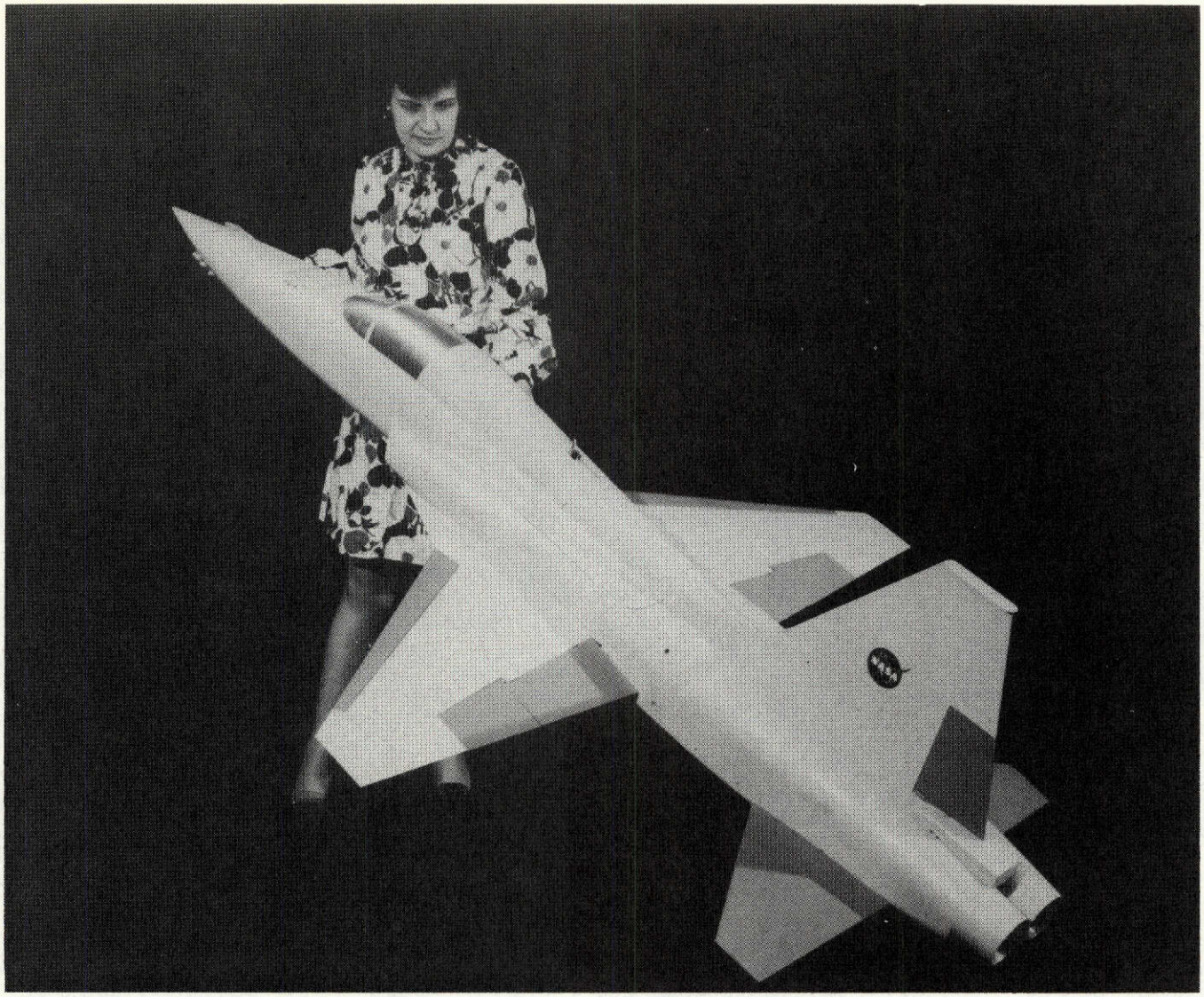

L-72-4472

(a) Three-quarter rear view.

Figure 3.- Photographs of model.

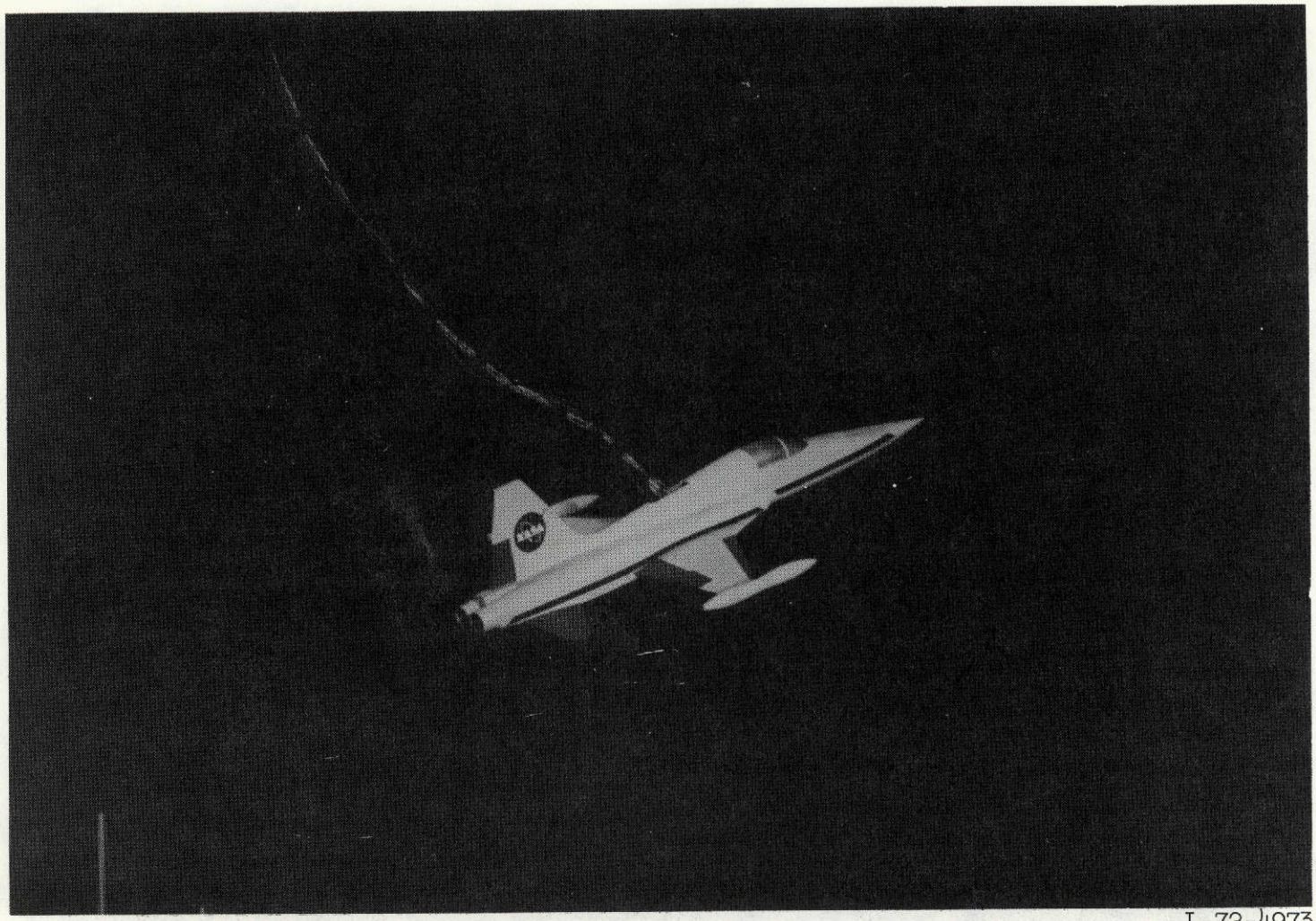

L-72-4973

(b) Model in free flight.

Figure 3.- Concluded.

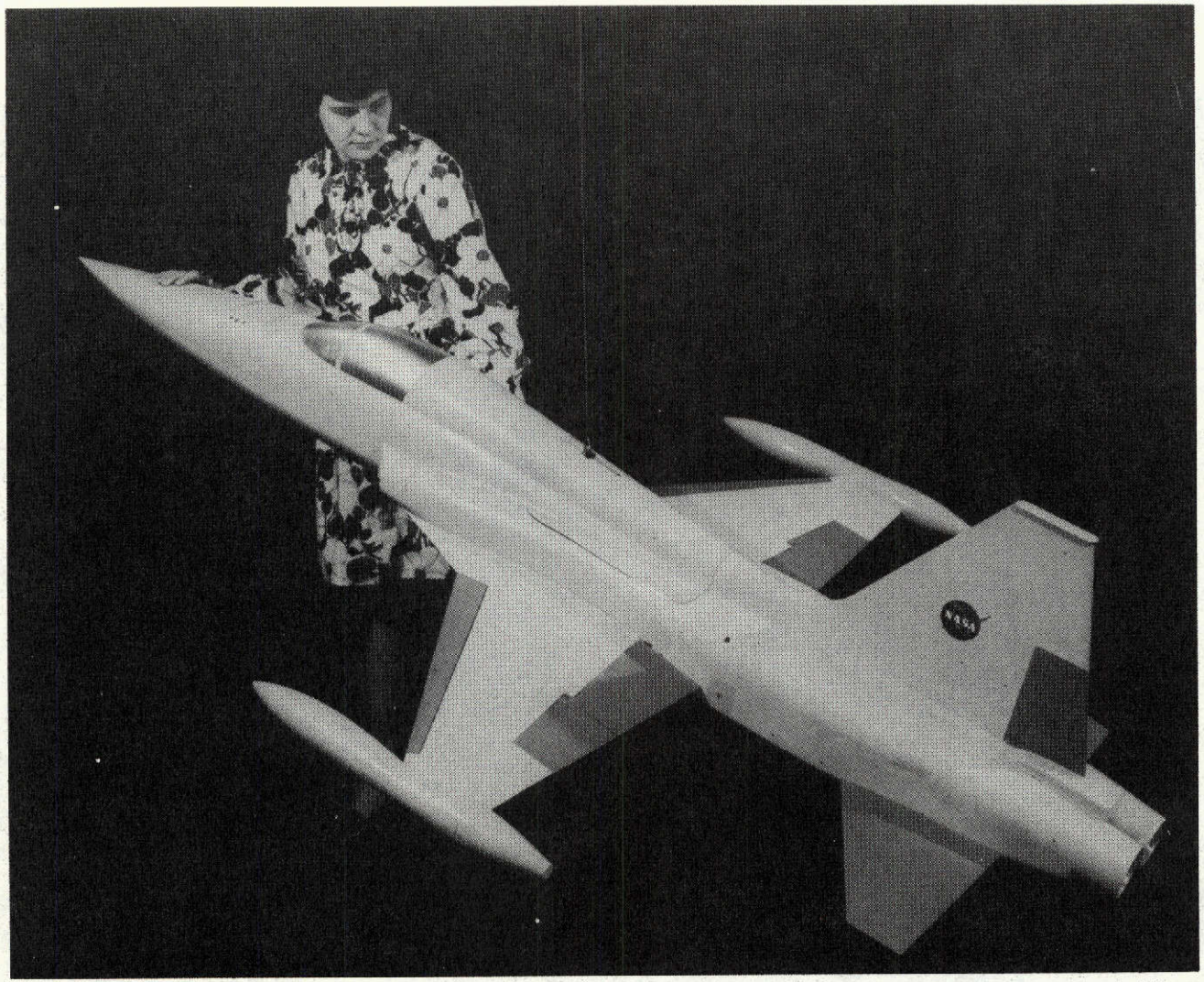

L-72-4473

(a) Basic wing with tip tanks.

Figure 4.- Photographs of model with various wings tested.

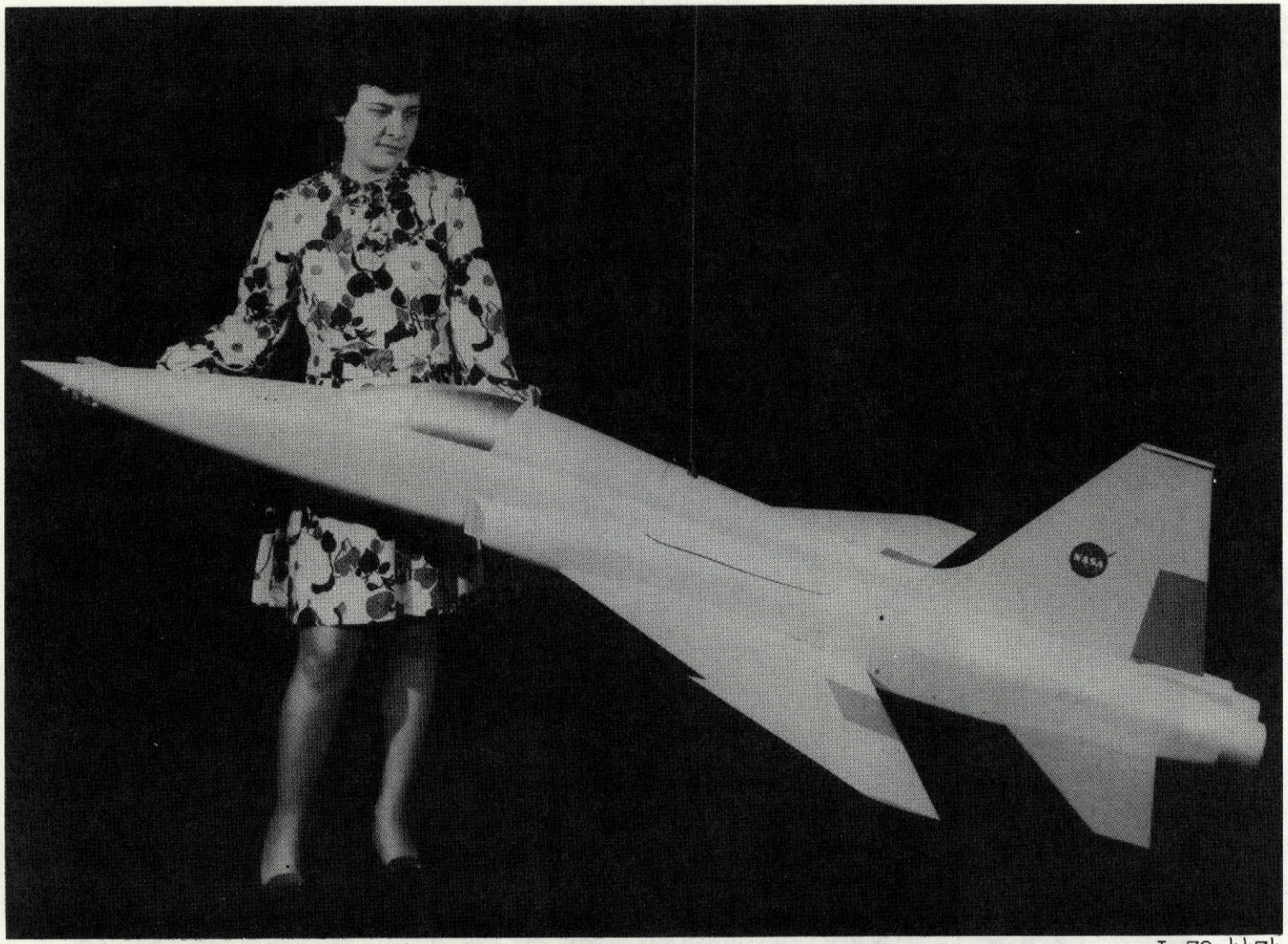

L-72-4474

(b) Swept wing.

Figure 4.- Continued.

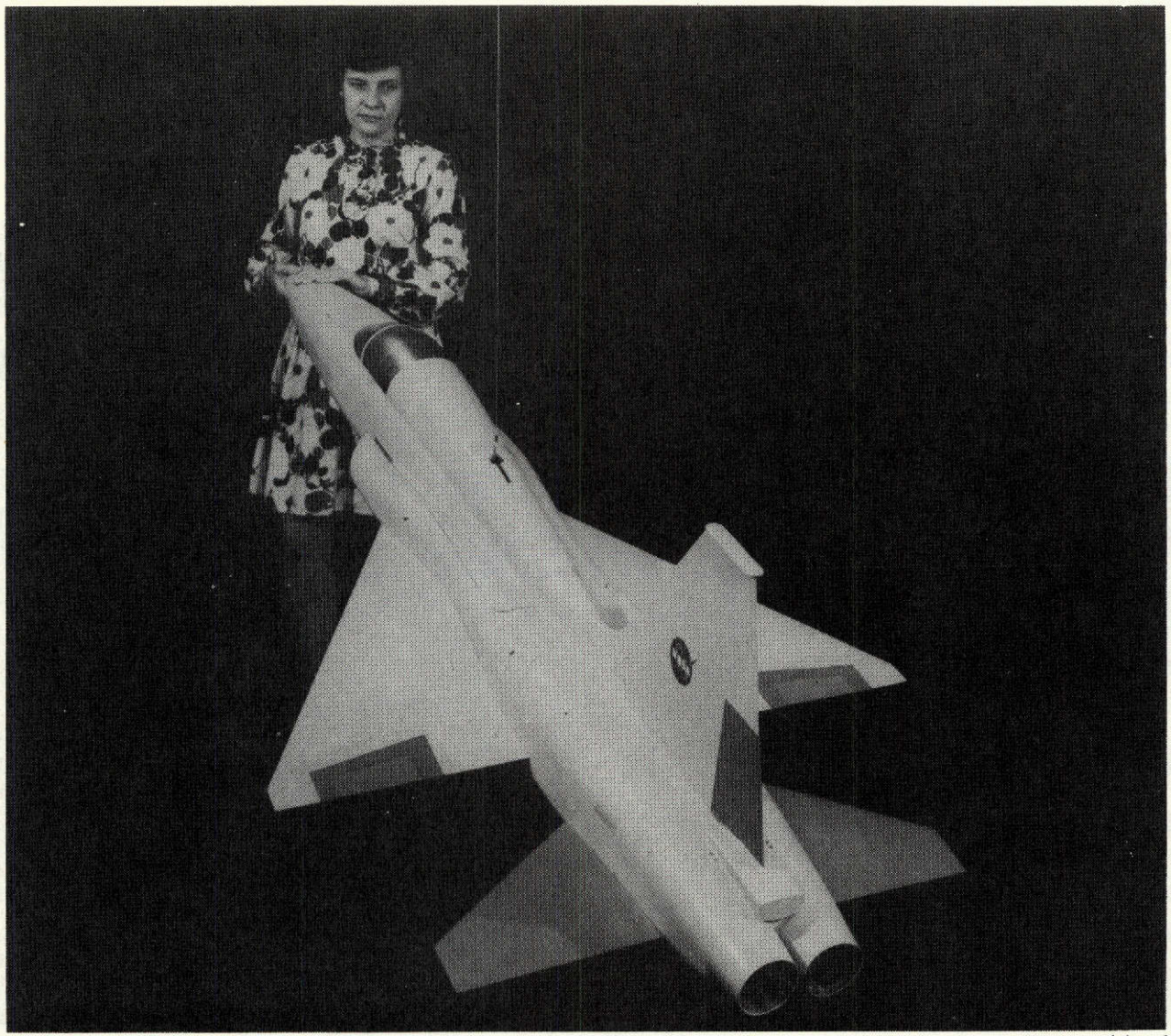

L-72-4476

(c) Delta wing.

Figure 4.- Concluded.

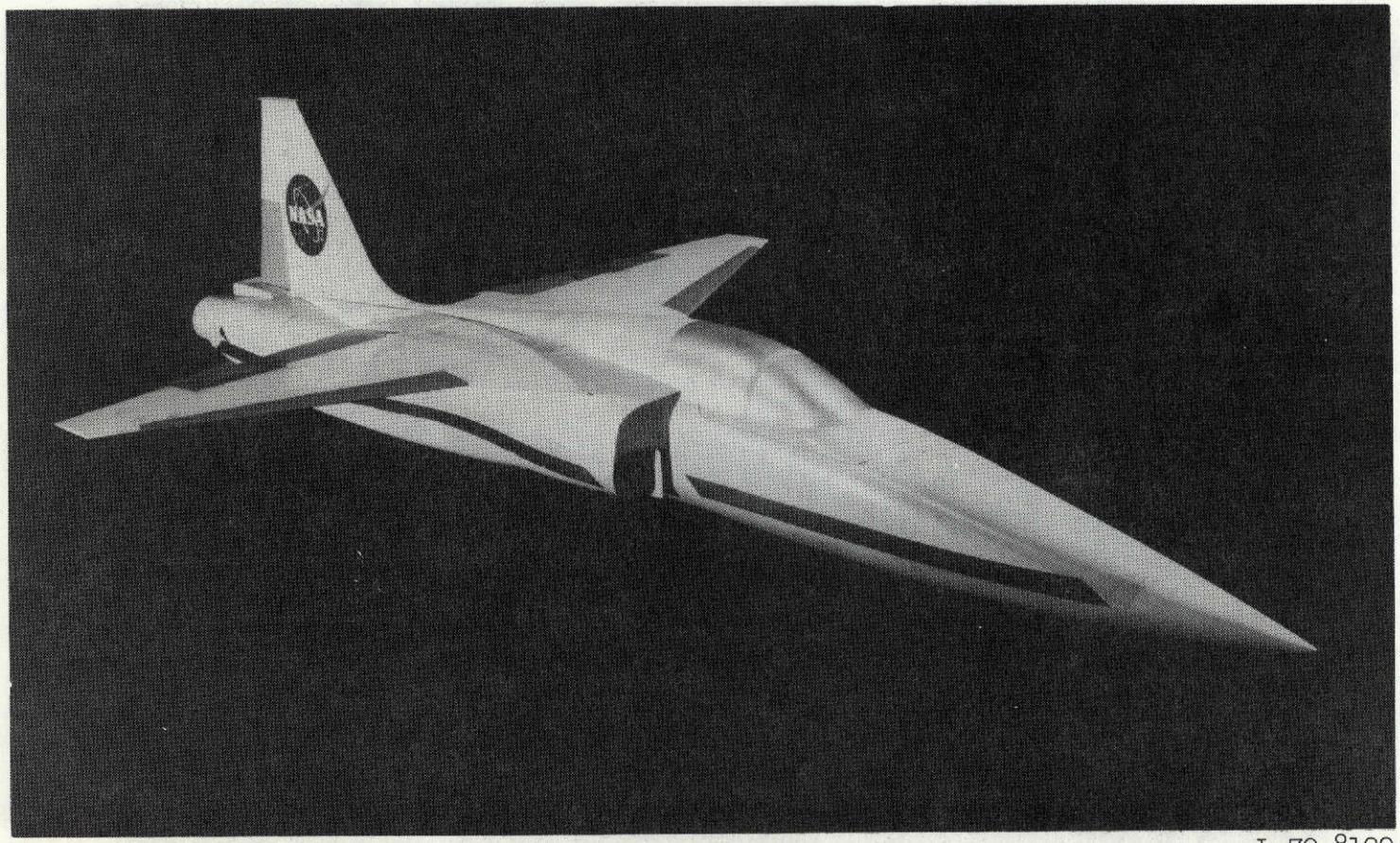

L-72-8122

(a) Basic wing in high position.

Figure 5.- Photographs of high-wing models.

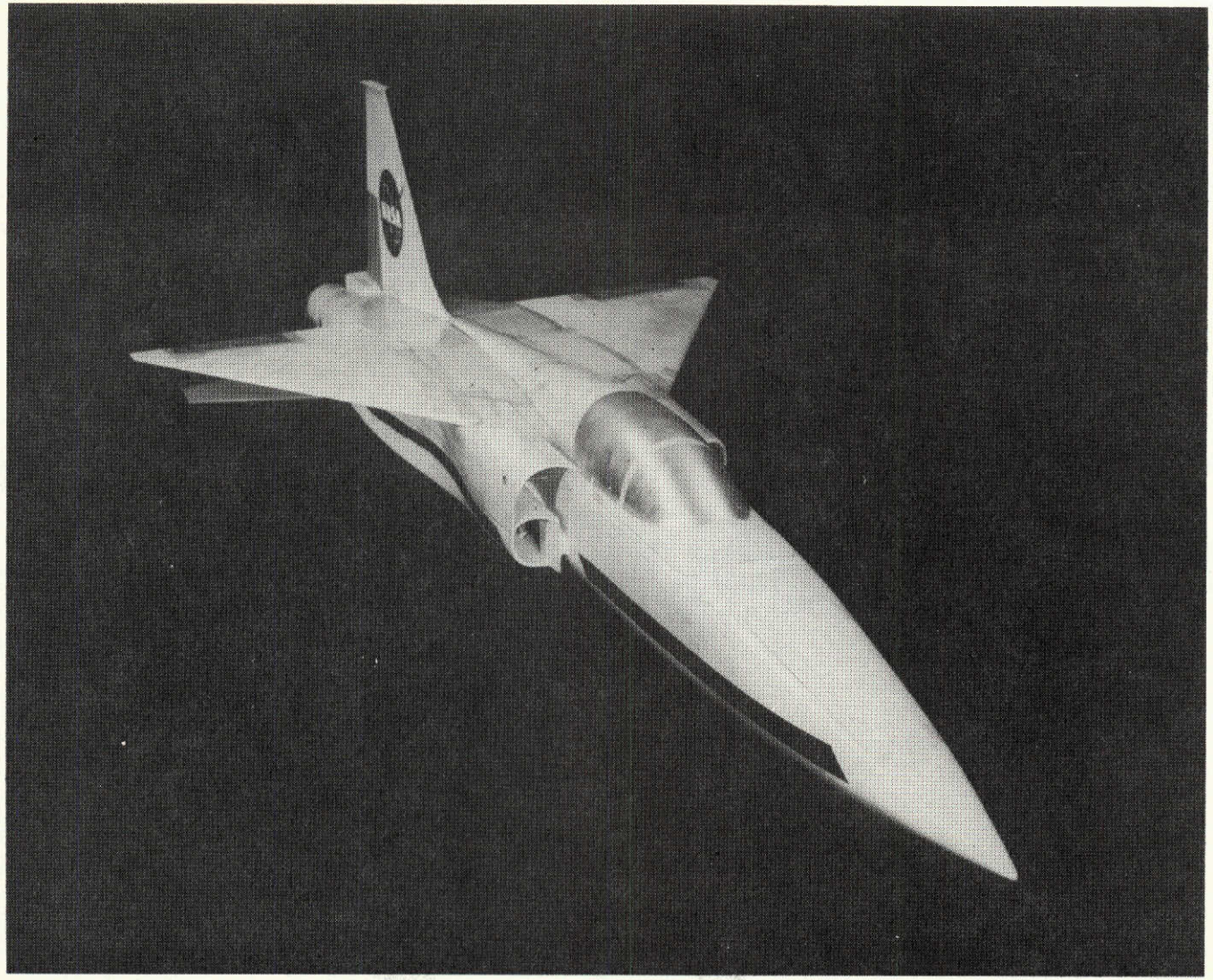

(b) Delta wing in high position. L-72-8168

Figure 5.- Concluded.

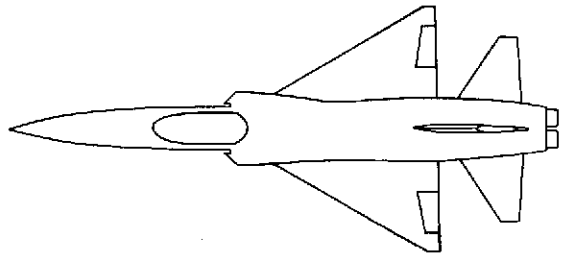

Delta

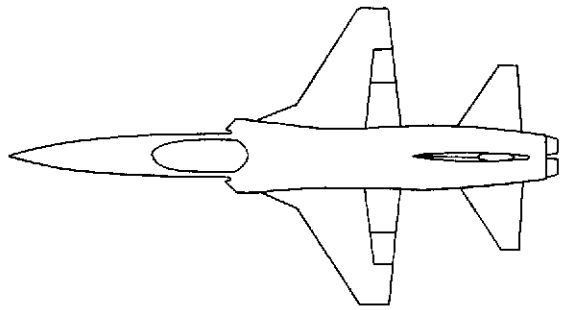

Basic

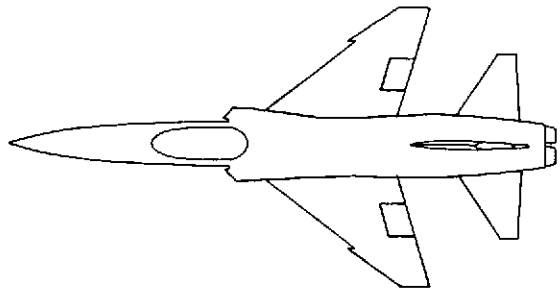

Swept

Figure 6.- Sketch of three wing configurations.

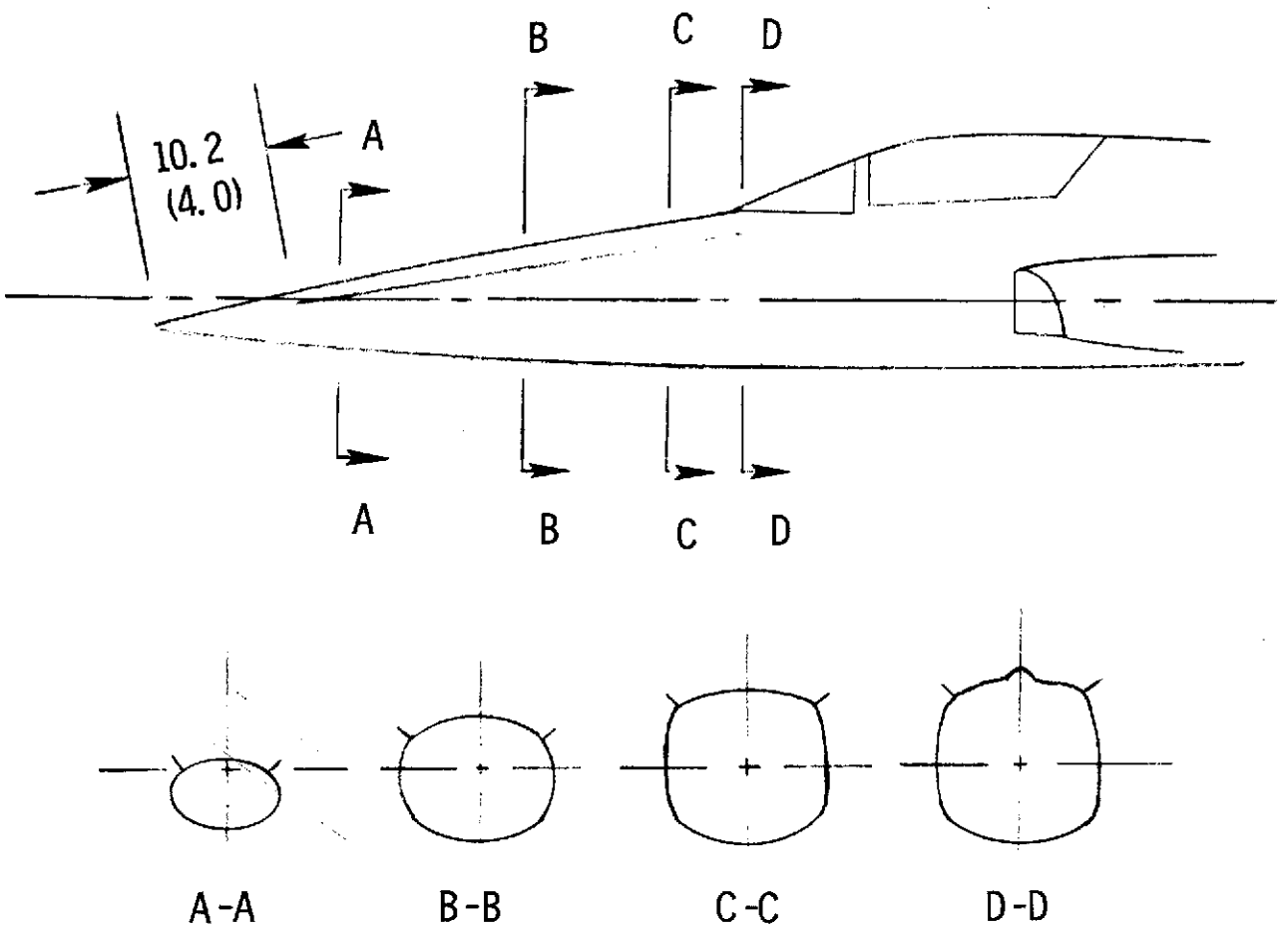

Figure 7.- Sketch of strake position. Dimension given is in cm (in.).

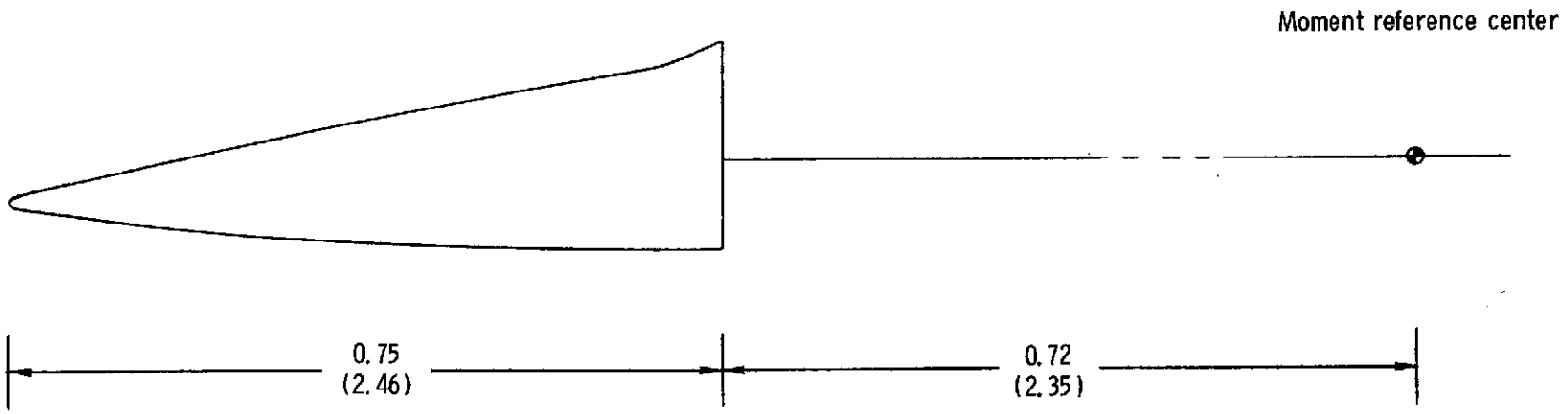

Figure 8.- Side view of nose alone. Dimensions are given in m (ft).

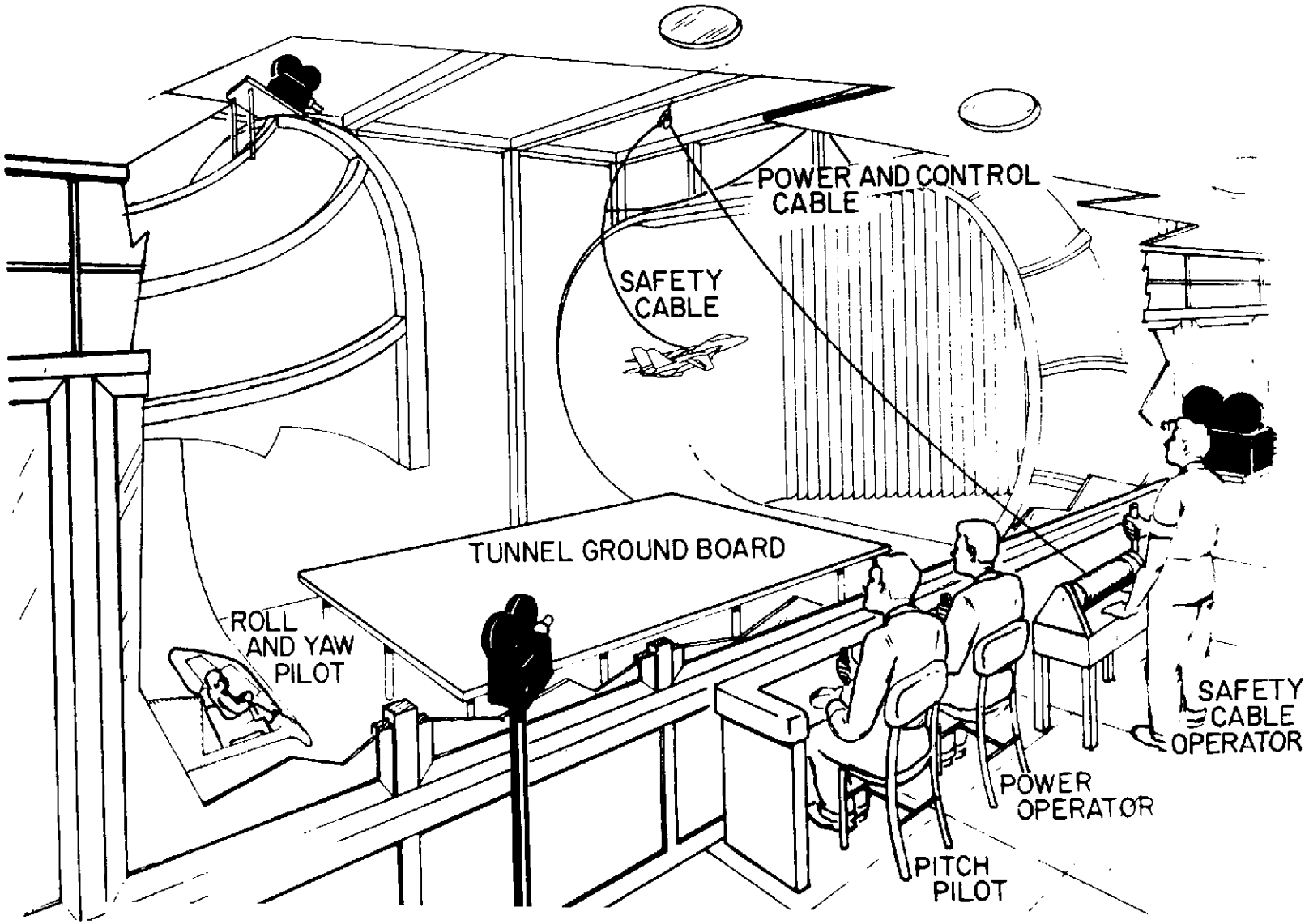

Figure 9.- Setup for free-flight tests.

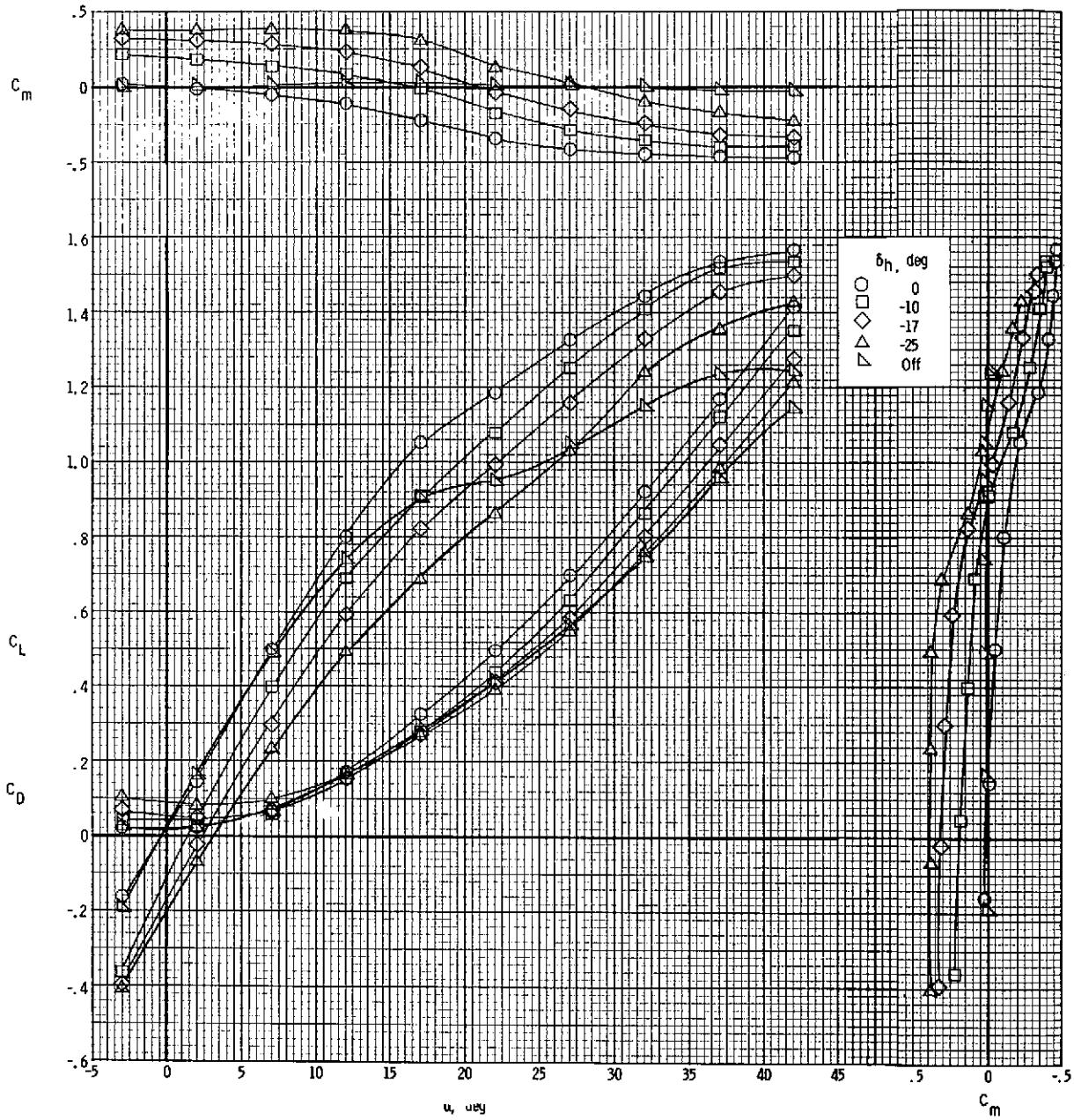

Figure 10.- Effect of horizontal-tail deflection on static longitudinal characteristics of the basic configuration.

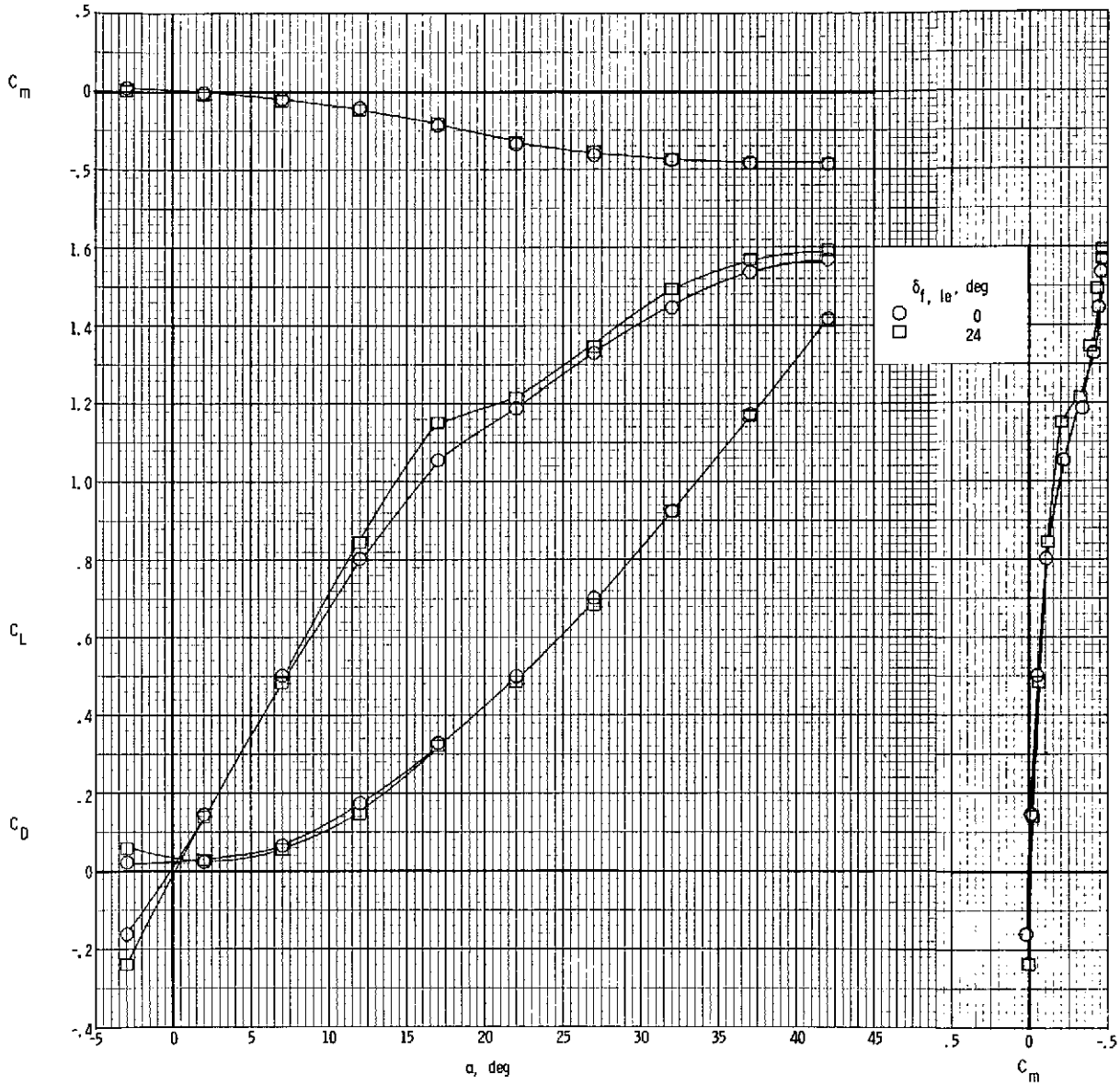

Figure 11.- Effect of leading-edge flap deflection on static longitudinal characteristics of the basic configuration.

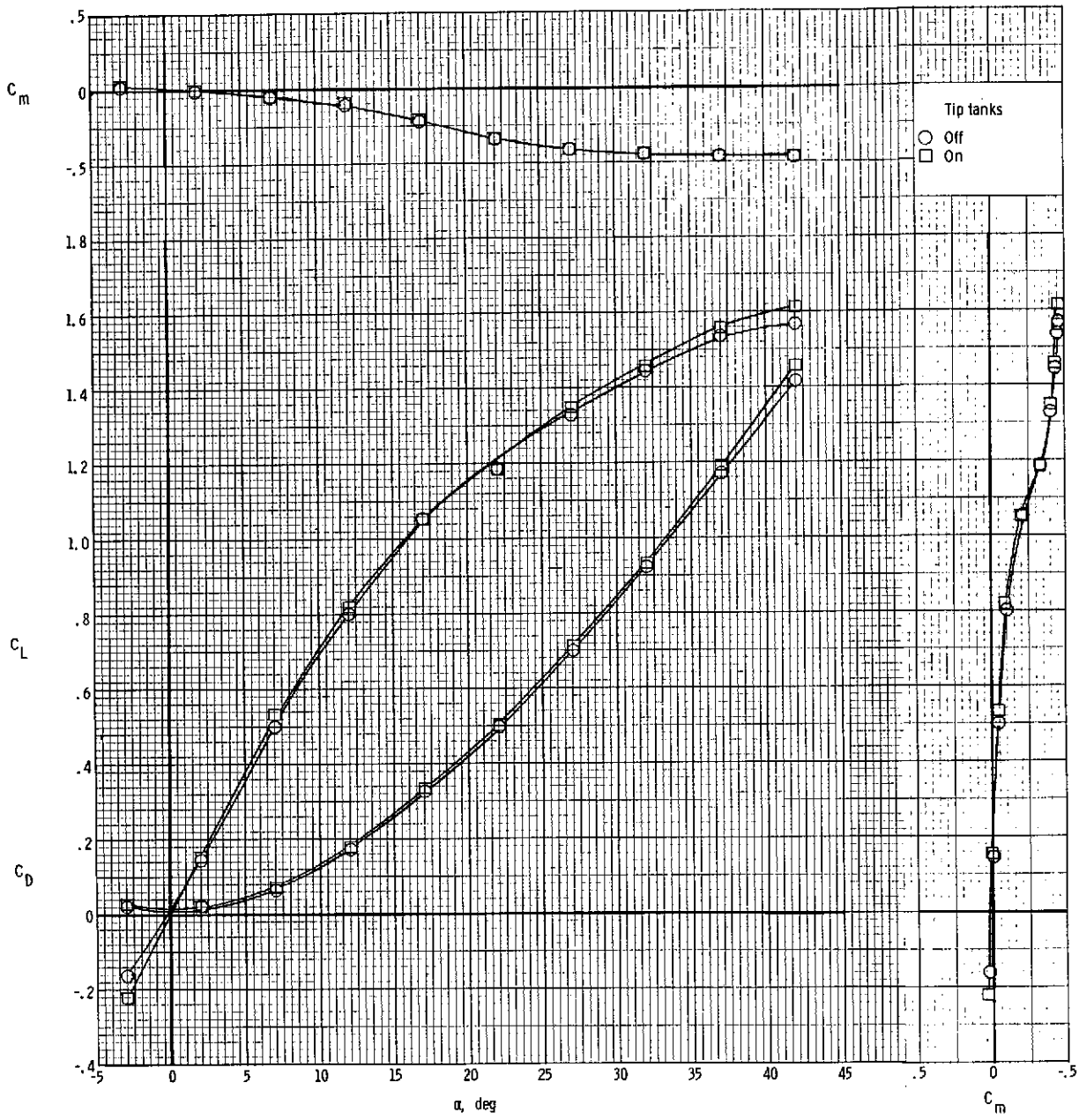

Figure 12.- Effect of wing-tip tanks on static longitudinal characteristics of the basic configuration.

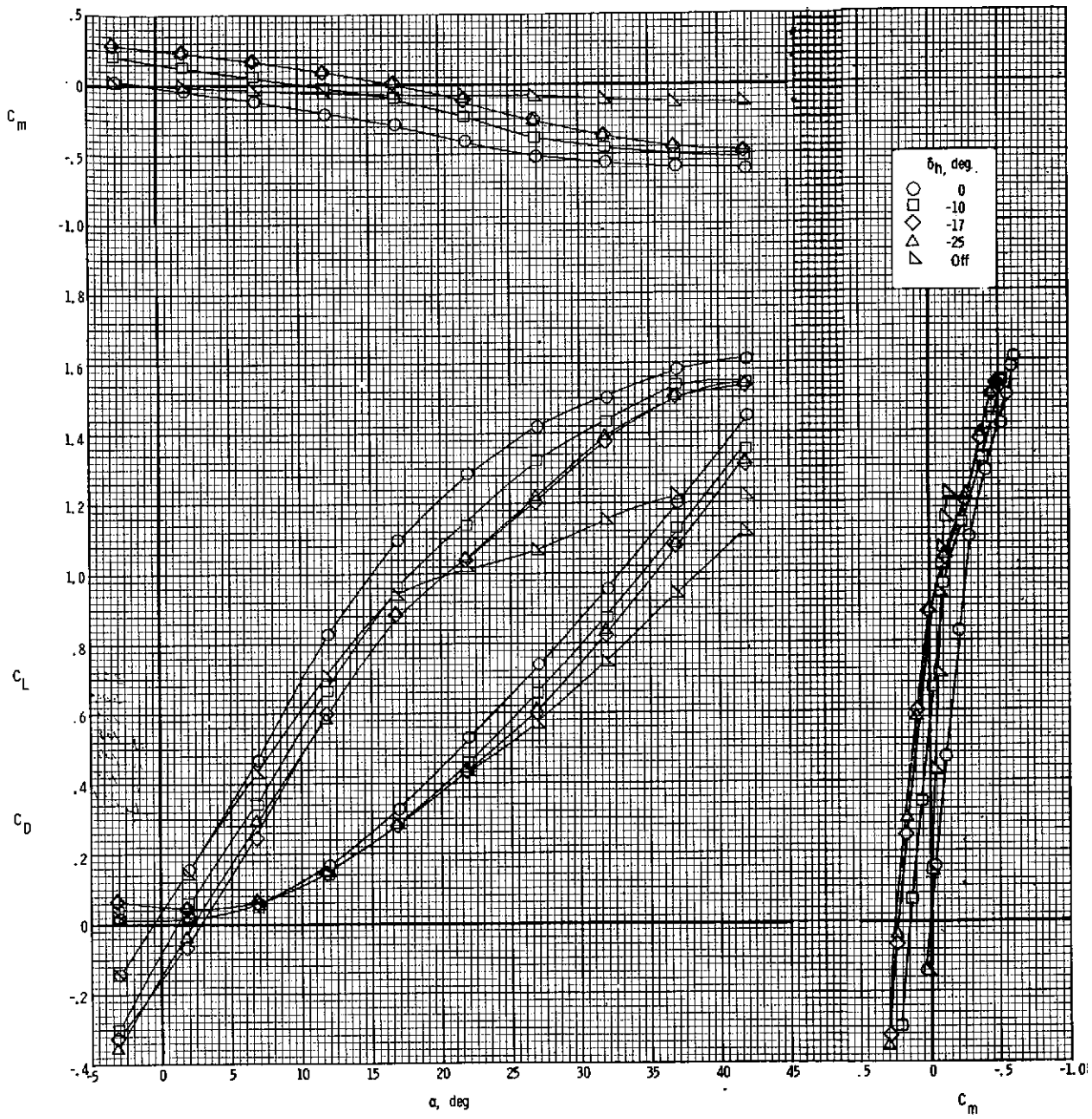

(a) Swept wing.

Figure 13.- Variation of static longitudinal characteristics with angle of attack for modified configurations.

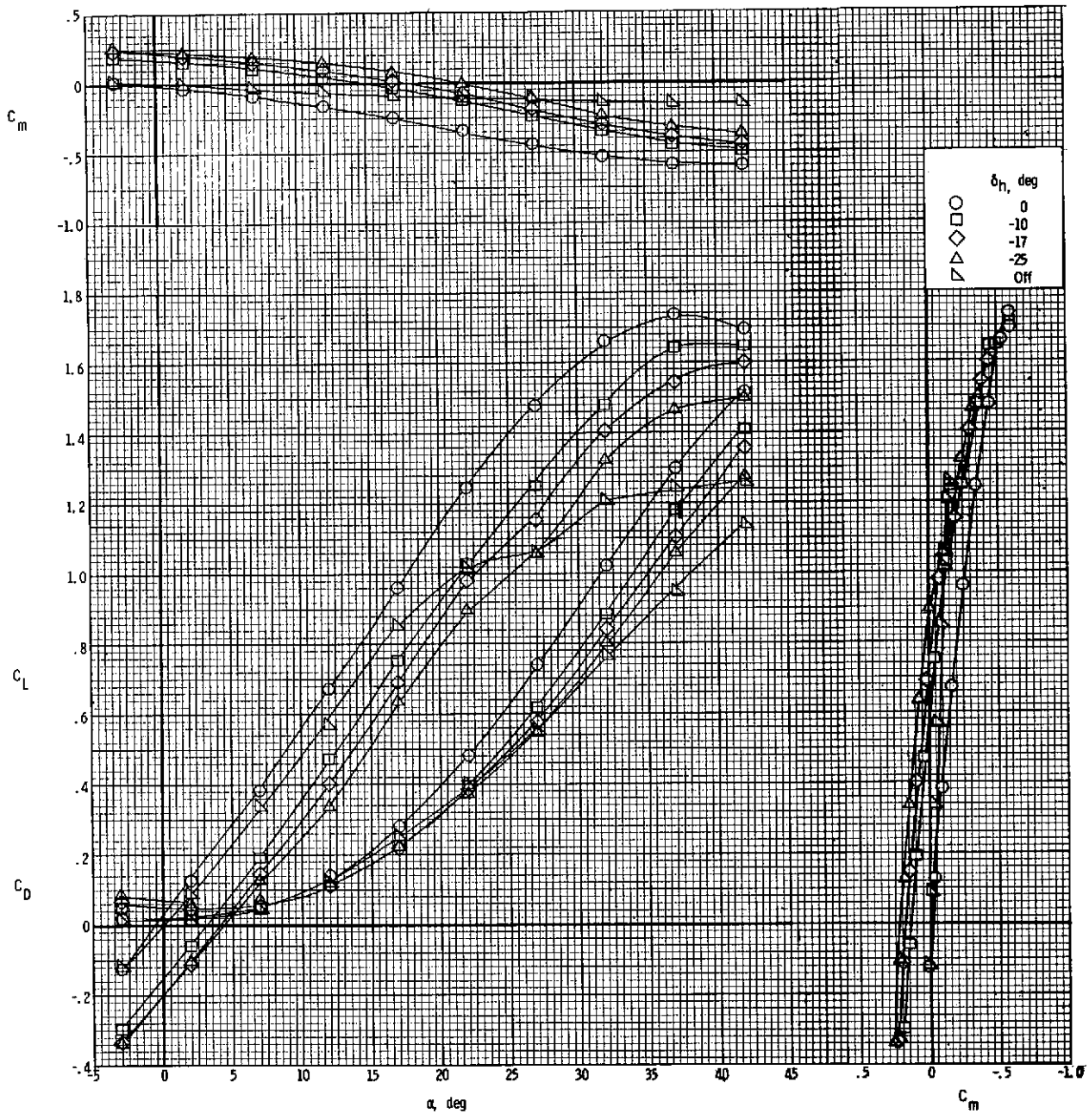

(b) Delta wing.

Figure 13.- Concluded.

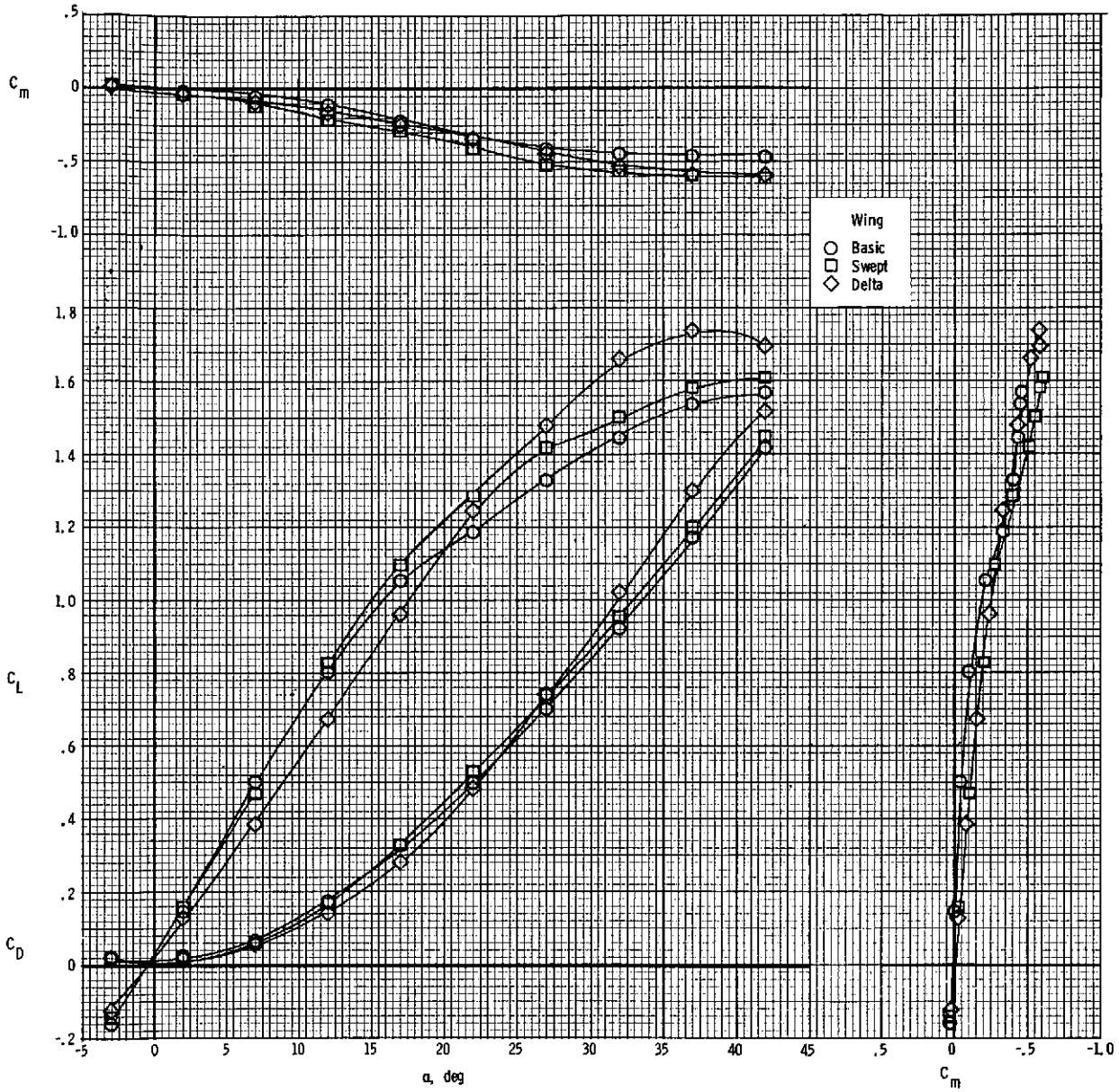

(a) Horizontal tail on. $\delta_h = 0^{\circ}$.

Figure 14.- Variation of static longitudinal characteristics with angle of attack for three wing configurations.

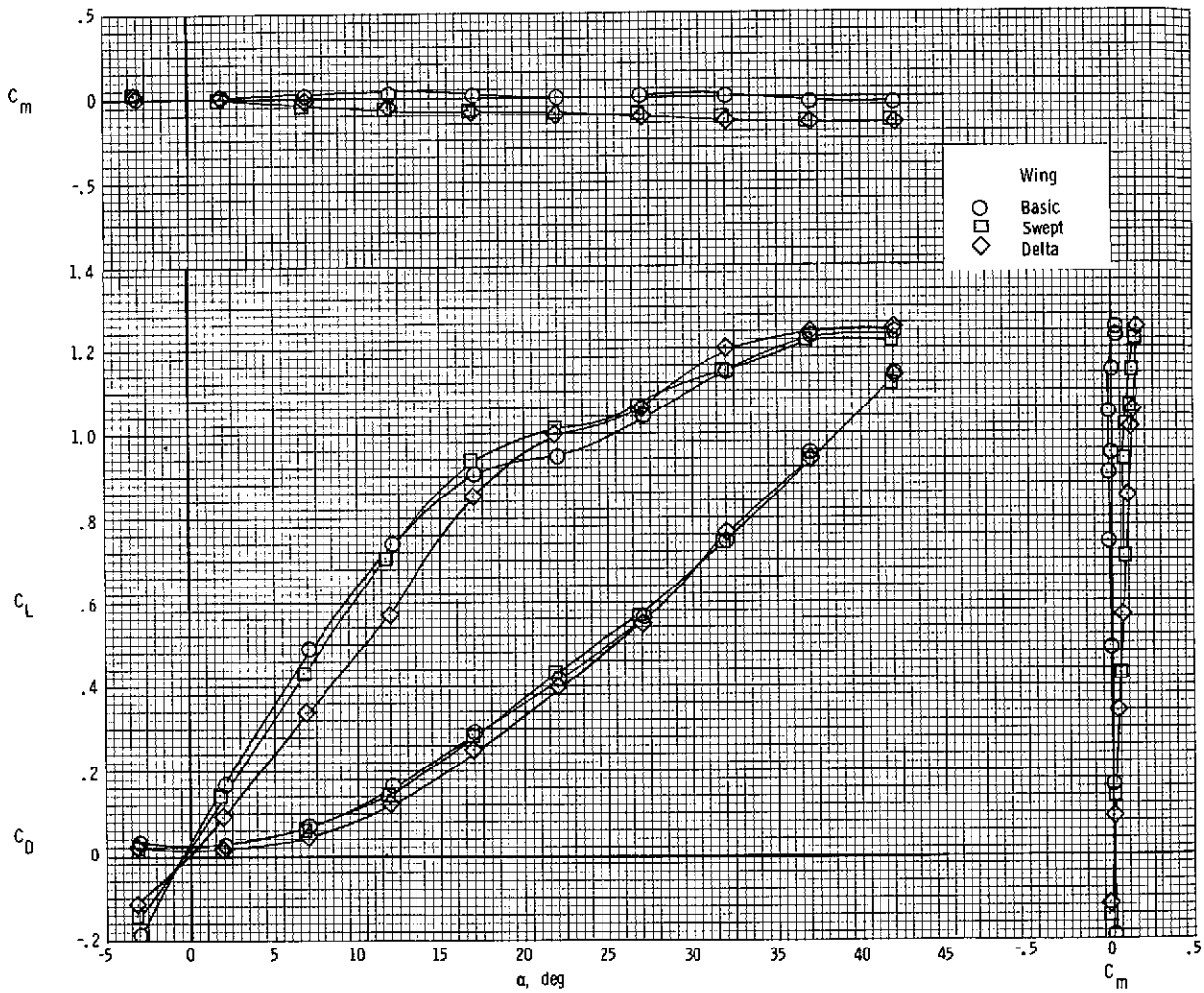

(b) Horizontal tail off.

Figure 14.- Concluded.

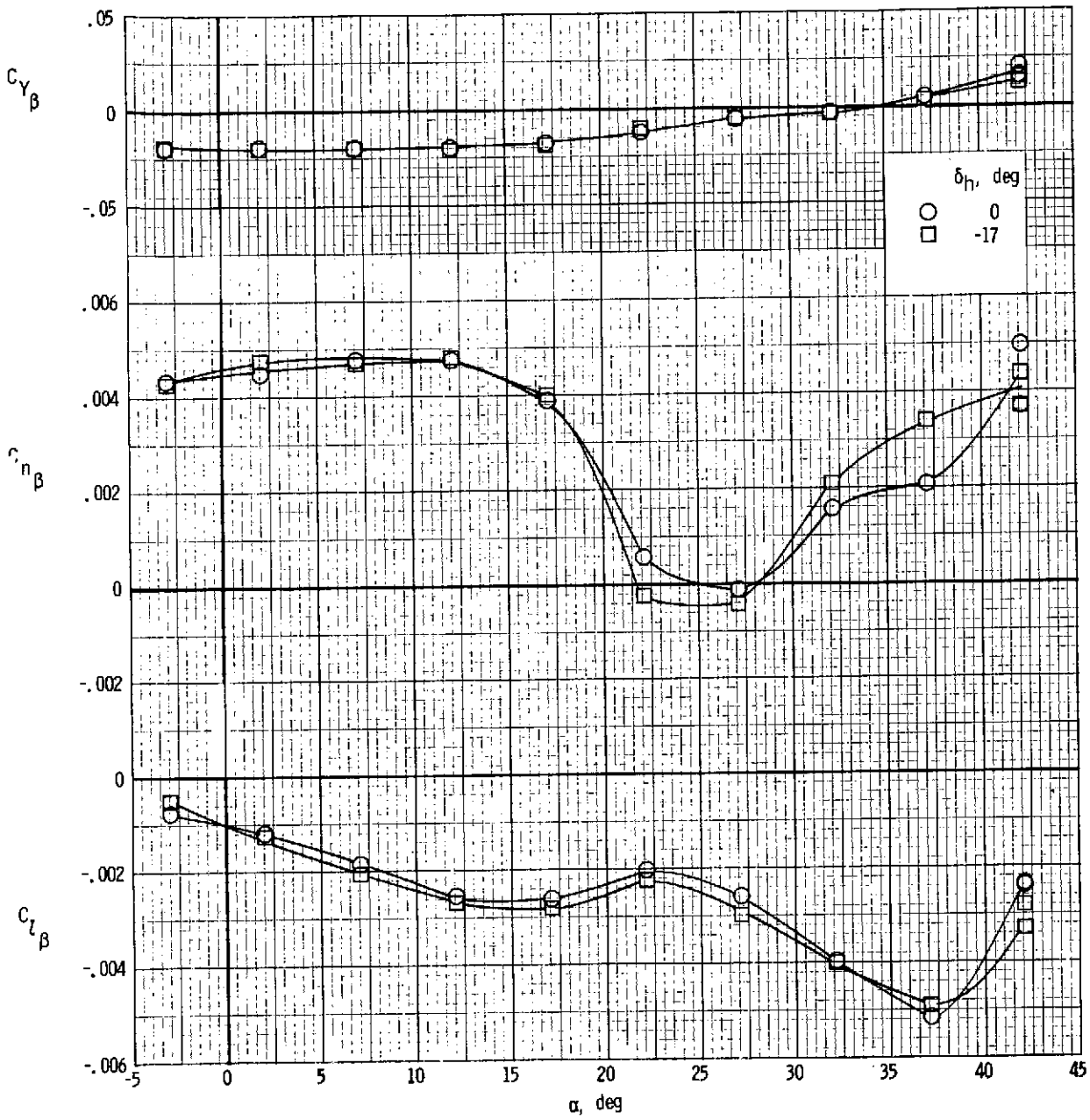

Figure 15.- Effect of horizontal-tail deflection on static lateral-directional stability. Basic configuration; $\delta_{f,le} = 0^{\circ}$.

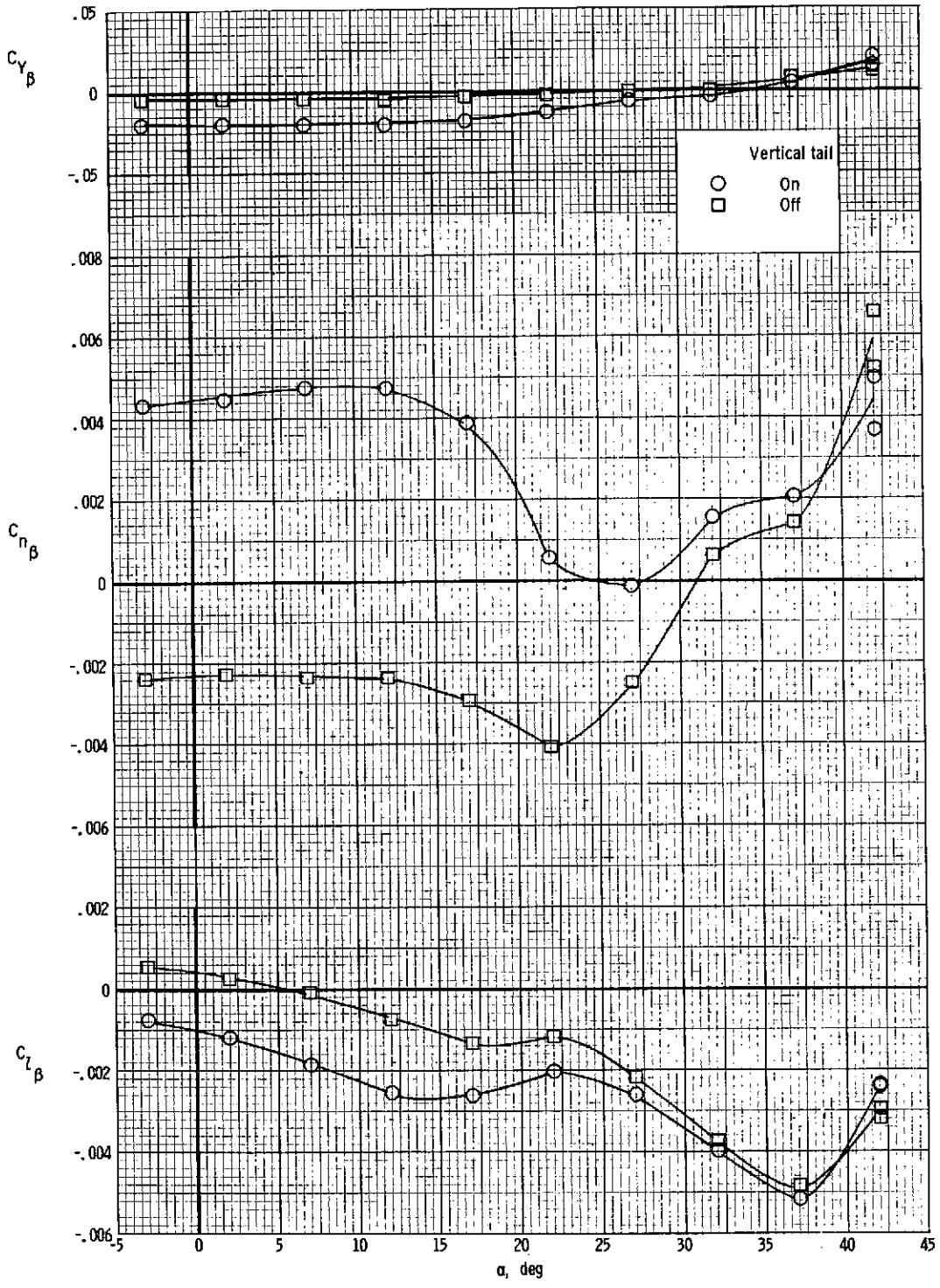

Figure 16.- Effect of the vertical tail on static lateral-directional stability for basic configuration.

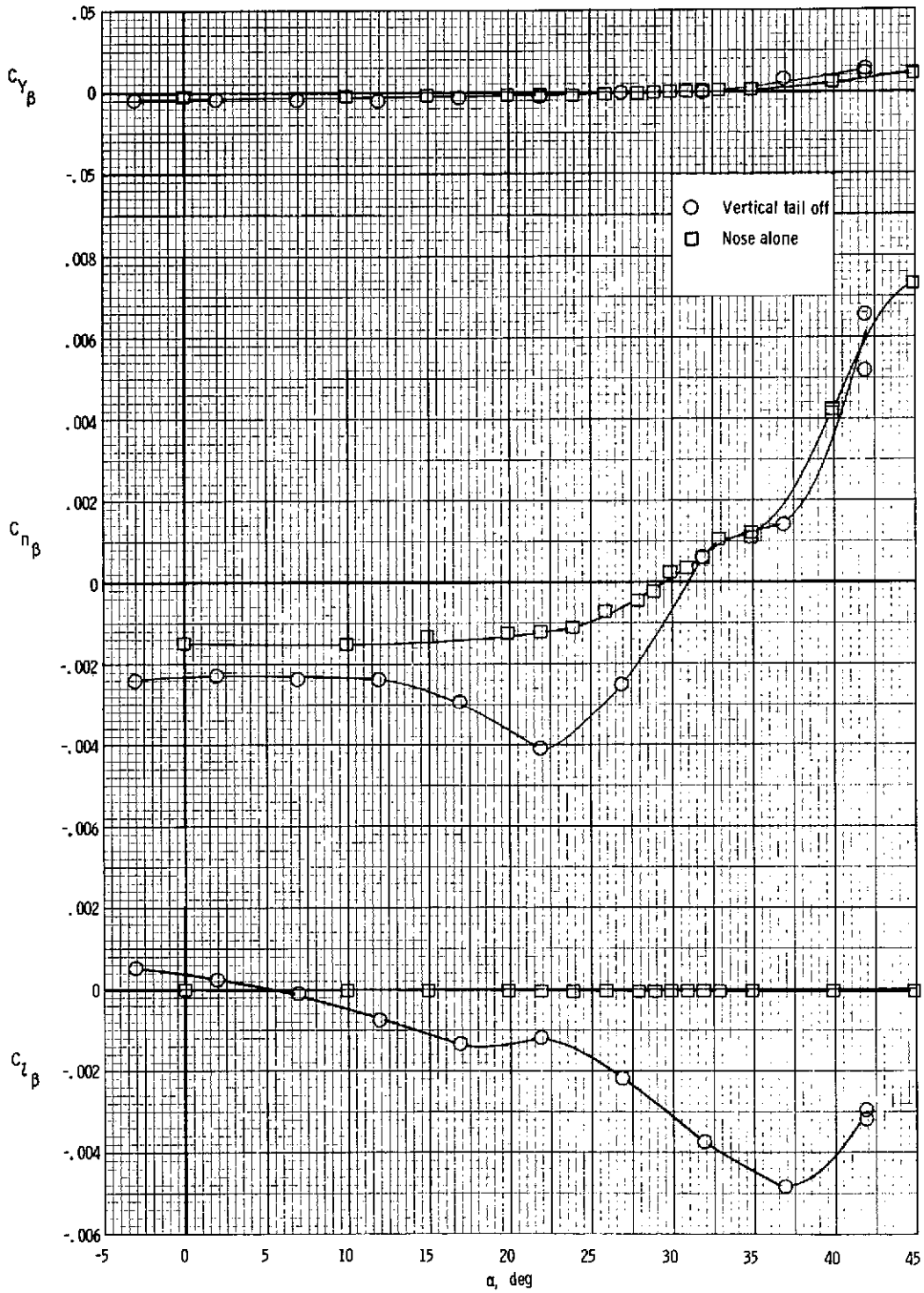

Figure 17.- Variation of static lateral-directional characteristics with angle of attack for isolated nose and for basic configuration with vertical tail off.

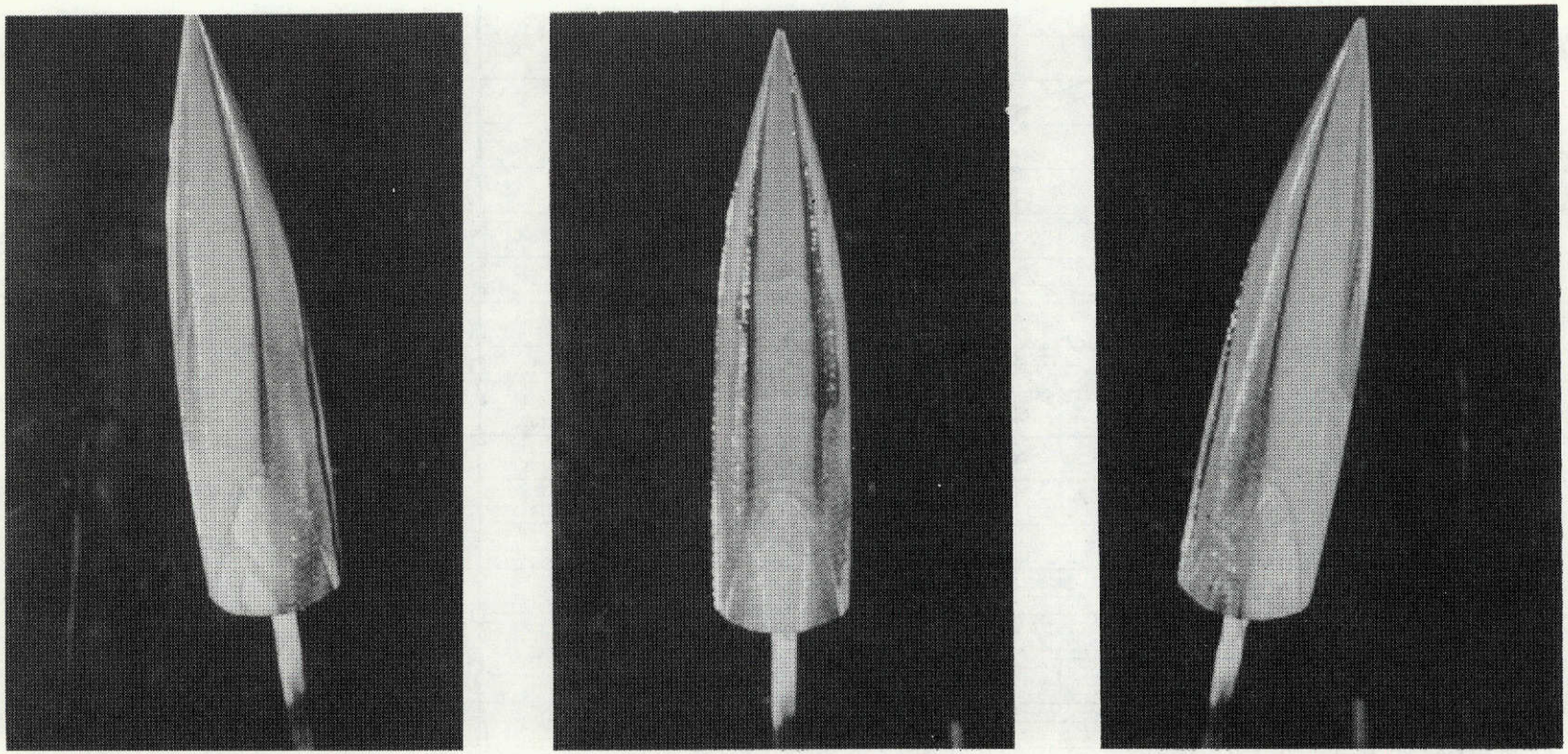

$\beta = 10^{\circ}$ $\beta = 0^{\circ}$ $\beta = -10^{\circ}$

Figure 18.- Variation of oil-flow patterns on the nose with angle of sideslip. $\alpha = 40^{\circ}$.

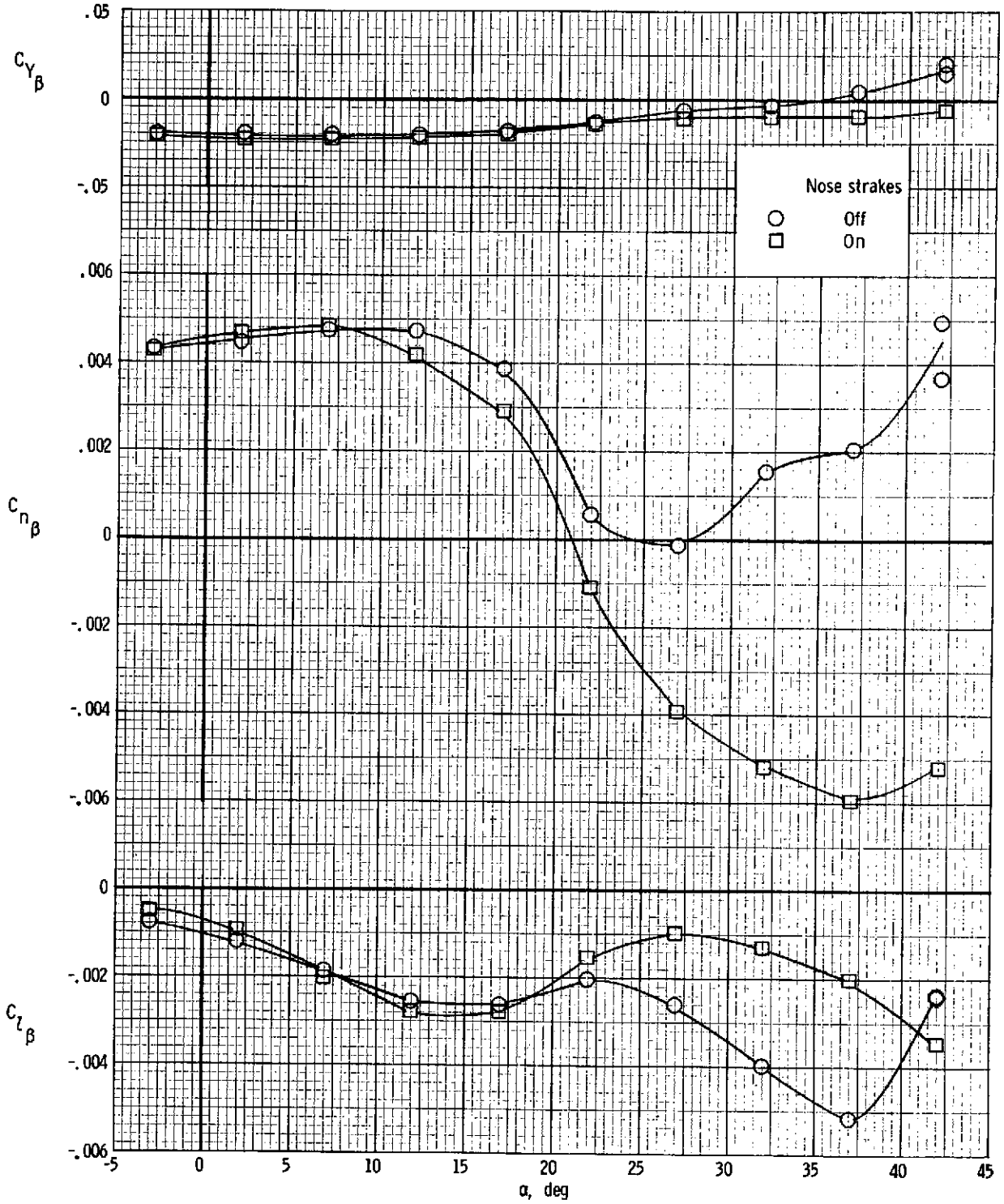

Figure 19.- Effect of nose strakes on static lateral-directional stability. Basic configuration; $\delta_h = 0^\circ$; $\delta_{f,le} = 0^\circ$.

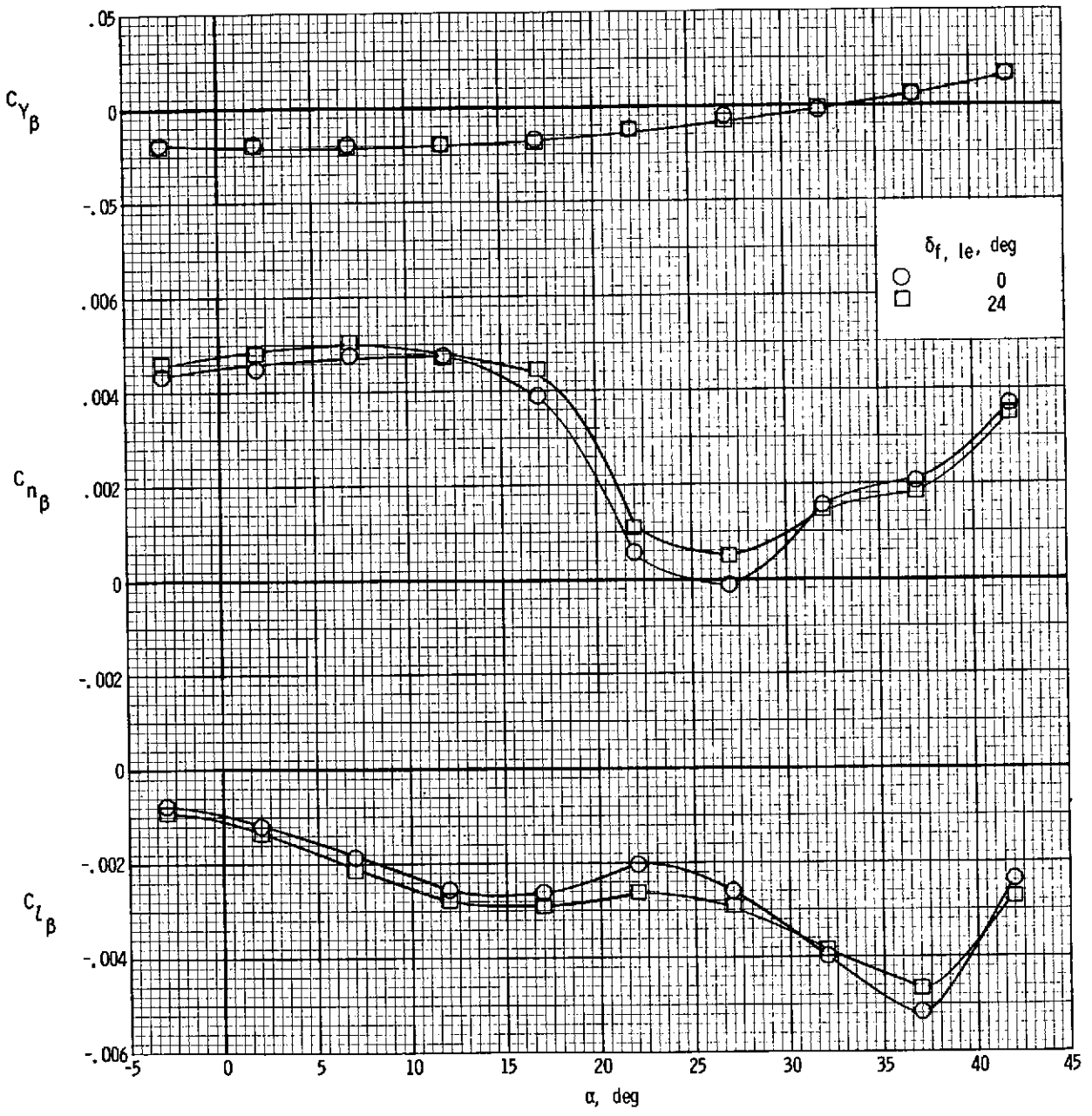

Figure 20.- Effect of leading-edge flap deflection on static lateral-directional stability for basic configuration.

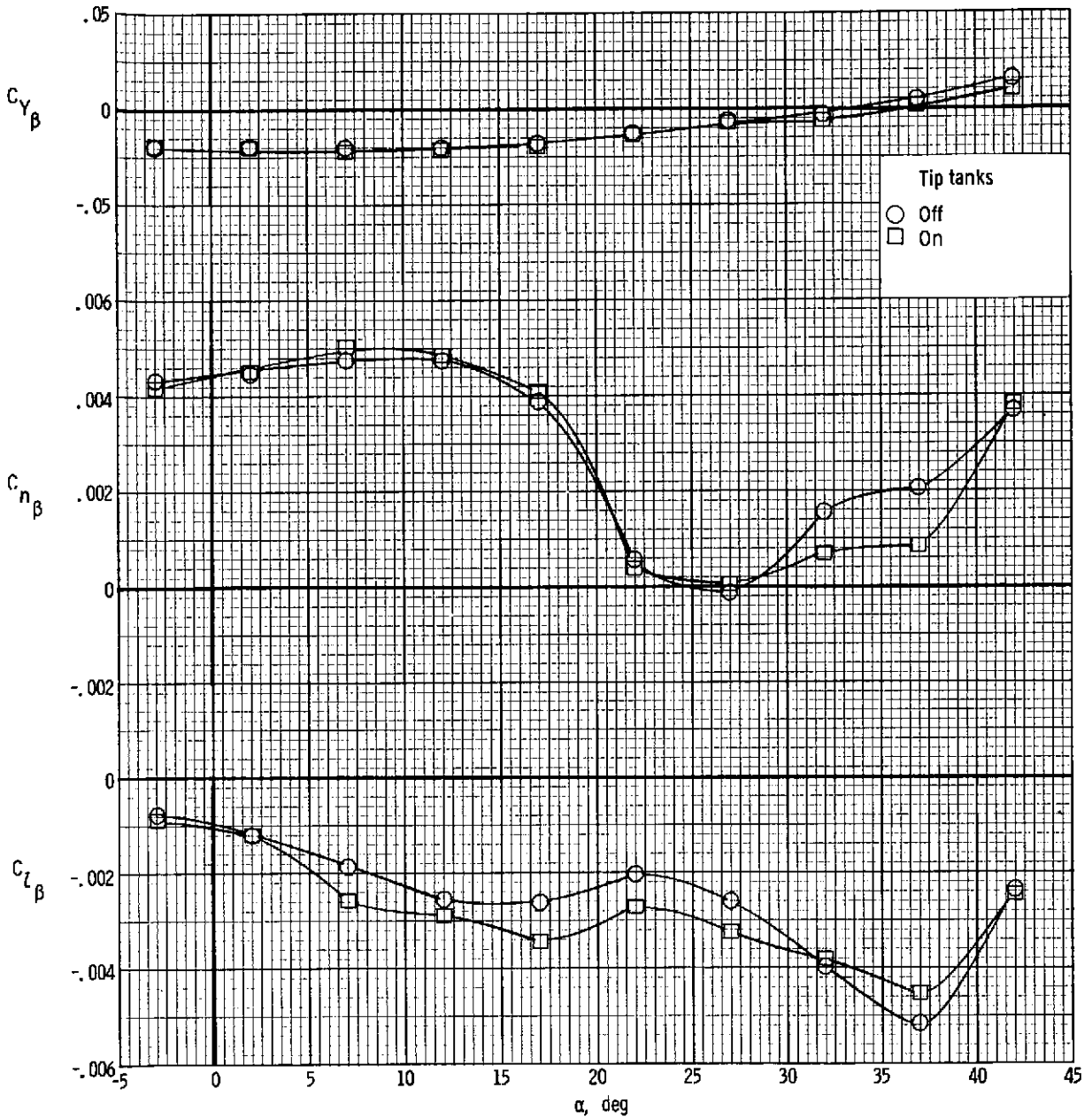

Figure 21.- Effect of wing-tip tanks on static lateral-directional stability for basic configuration.

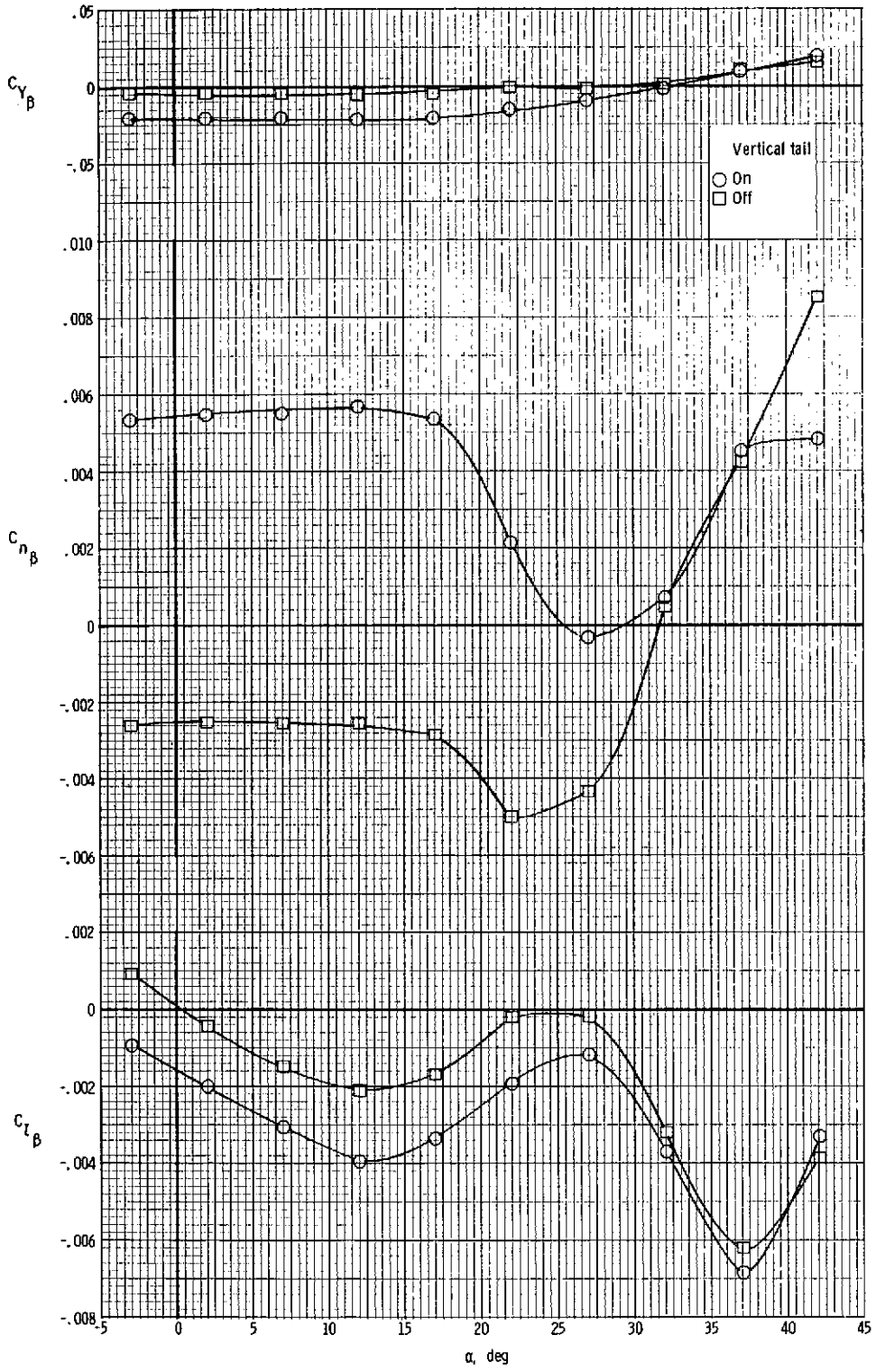

(a) Swept wing.

Figure 22.- Effect of vertical tail on static lateral-directional stability for modified configurations.

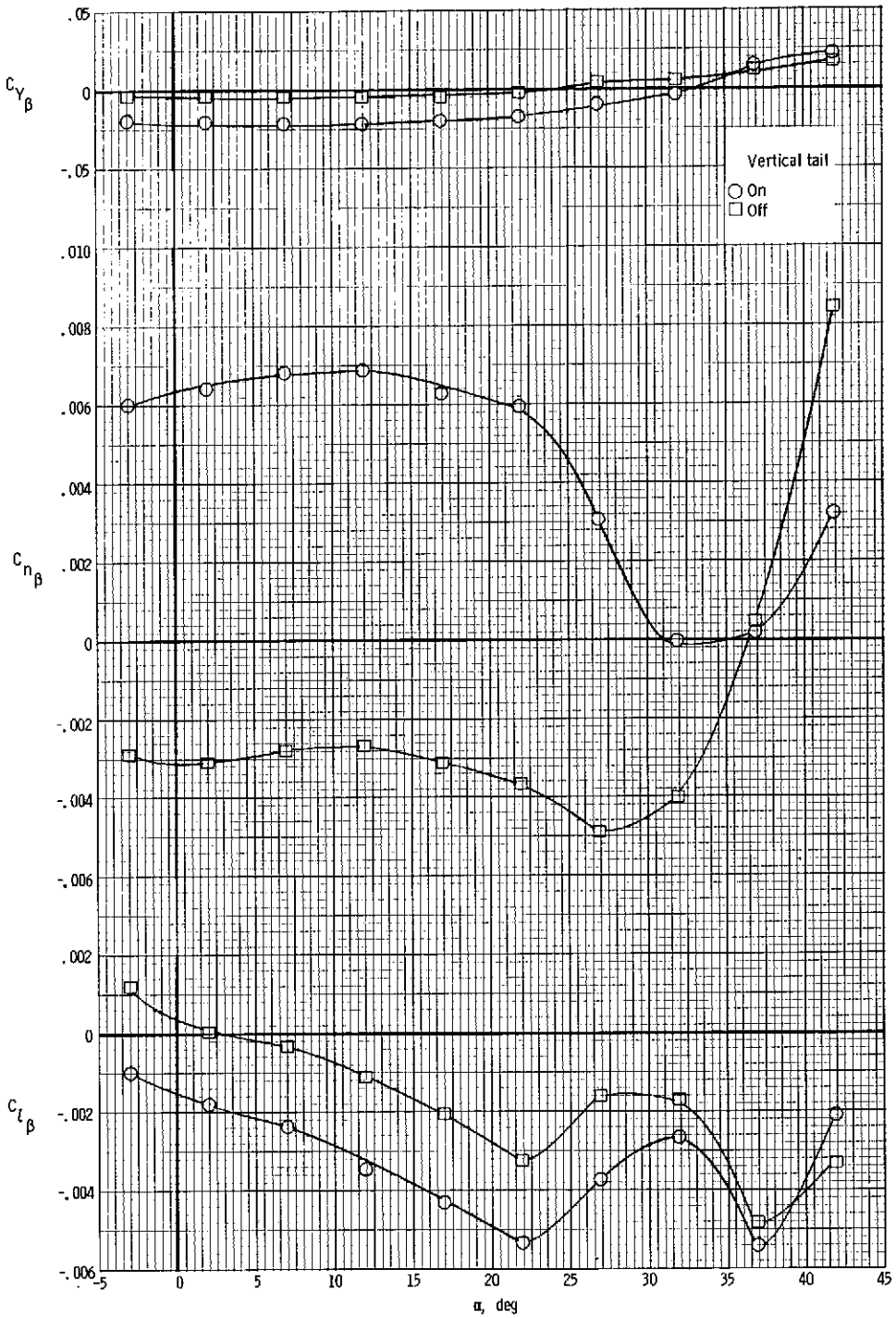

(b) Delta wing.

Figure 22.- Concluded.

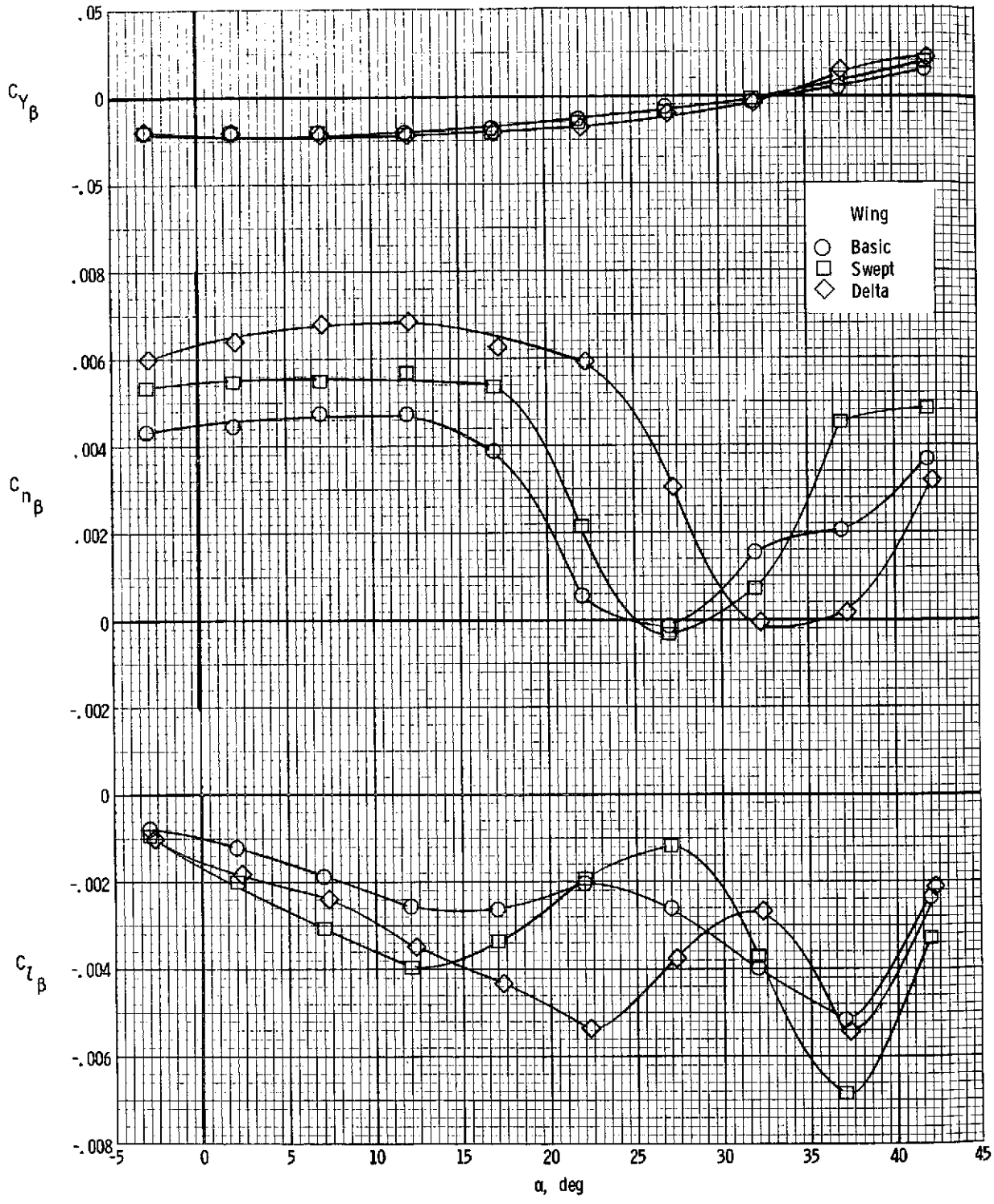

Figure 23.- Variation of static lateral-directional stability with angle of attack for three wing configurations.

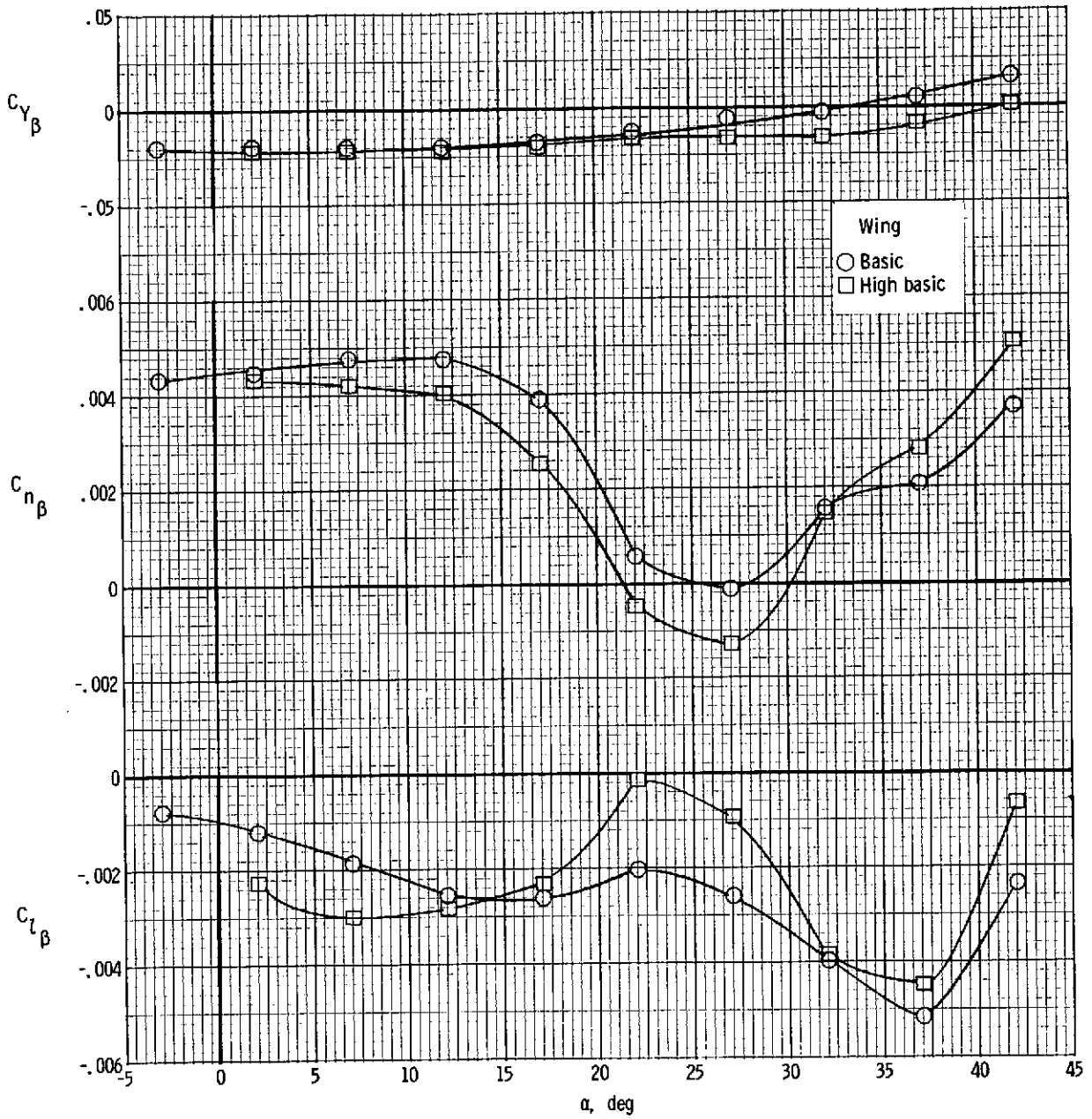

(a) Basic wing.

Figure 24.- Effect of wing position on static lateral-directional stability.

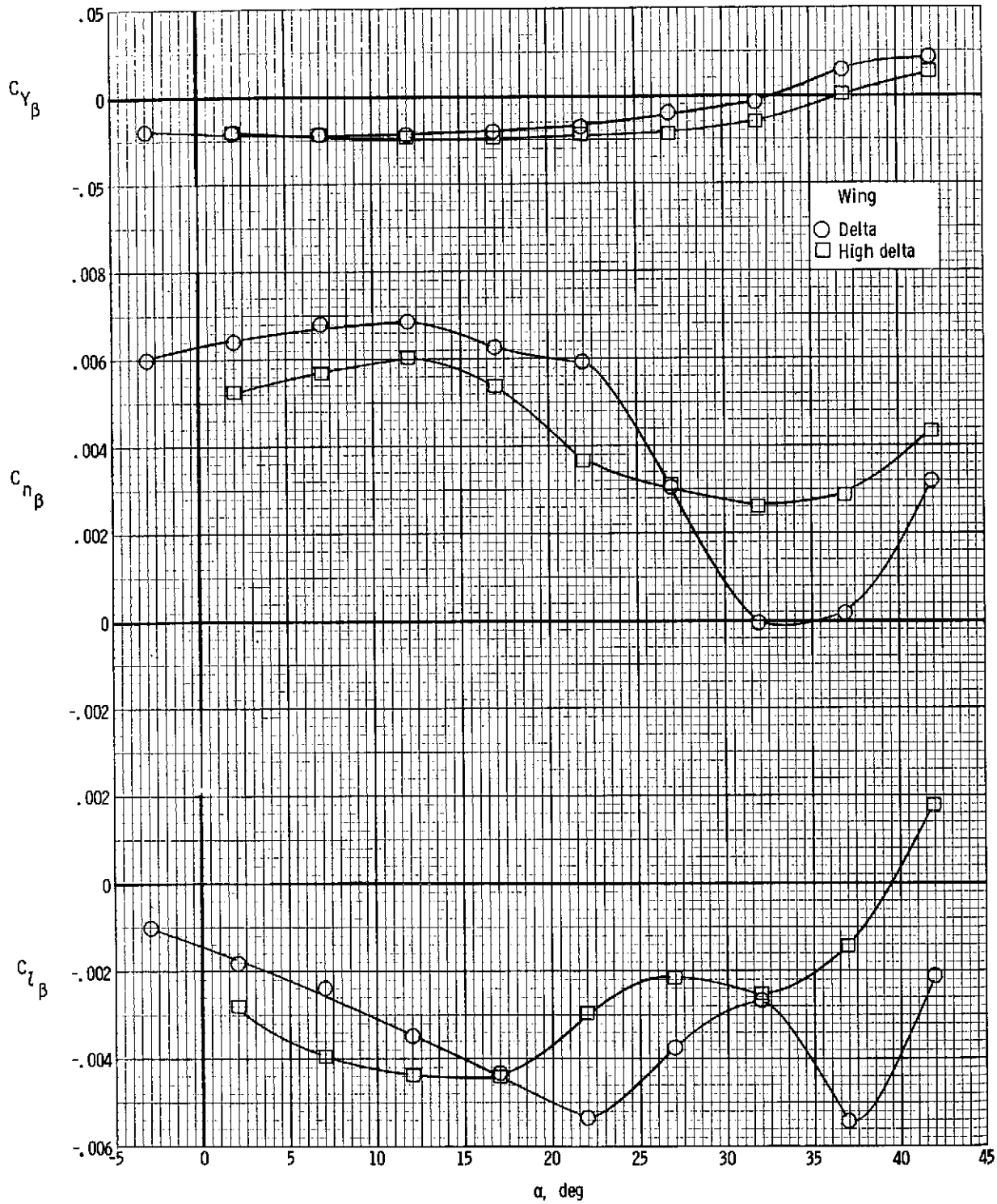

(b) Delta wing.

Figure 24.- Concluded.

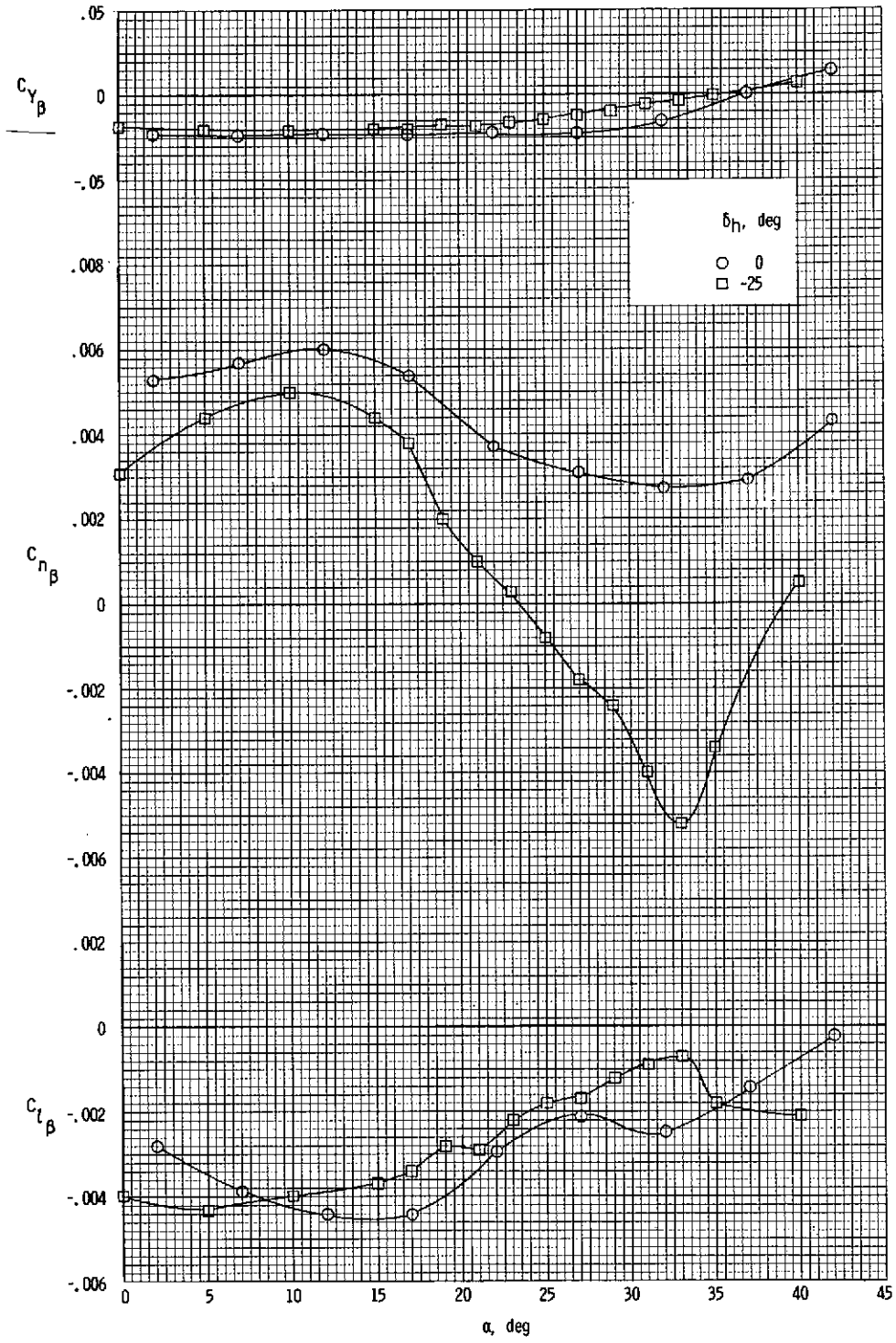

Figure 25.- Effect of horizontal-tail deflection on static lateral-directional stability. High delta wing; $\delta_{f,le} = 0^{\circ}$.

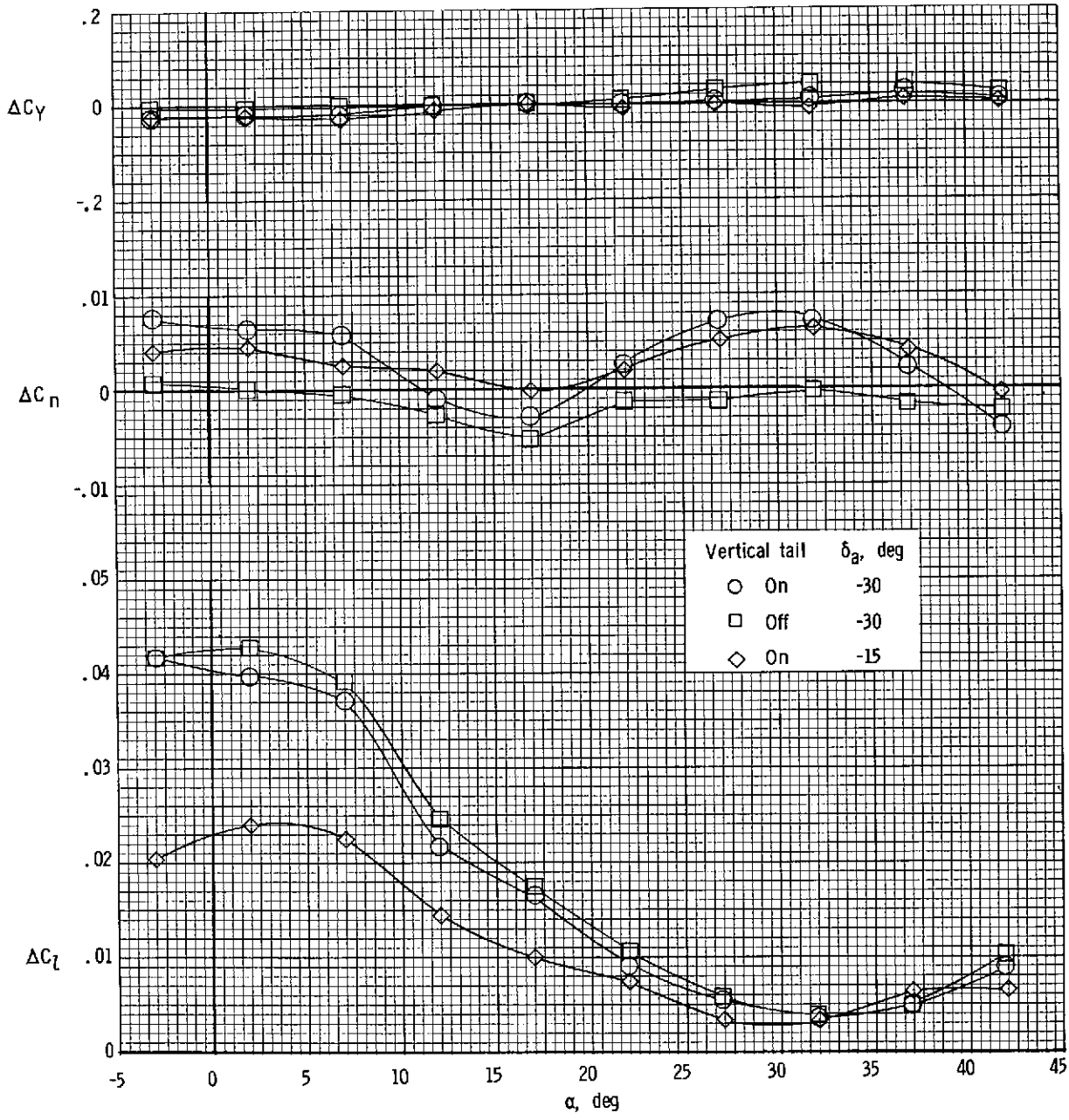

Figure 26.- Effect of aileron deflection for the basic configuration.

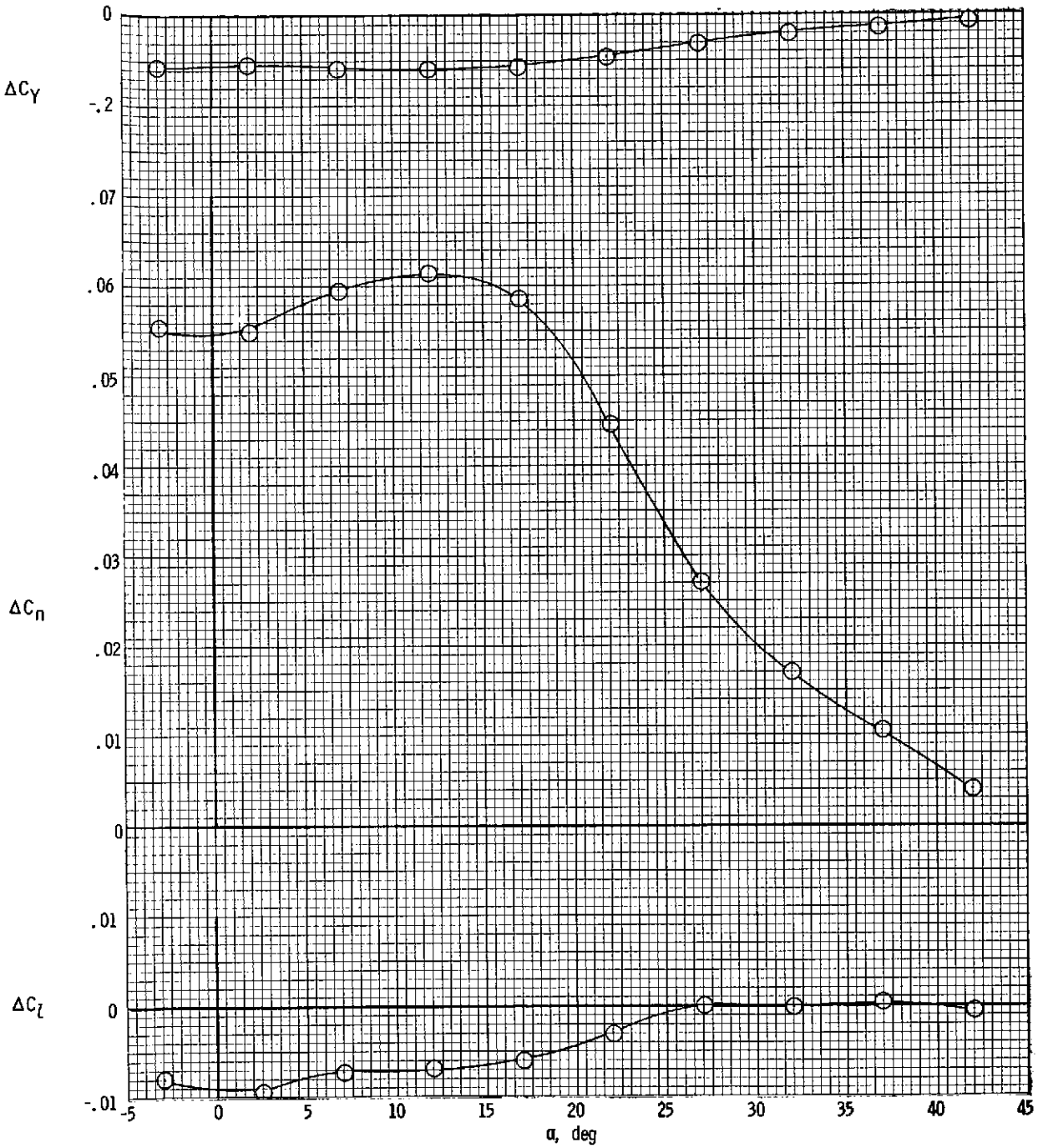

Figure 27.- Effect of rudder deflection for the basic configuration. $\delta_r = -30^\circ$.

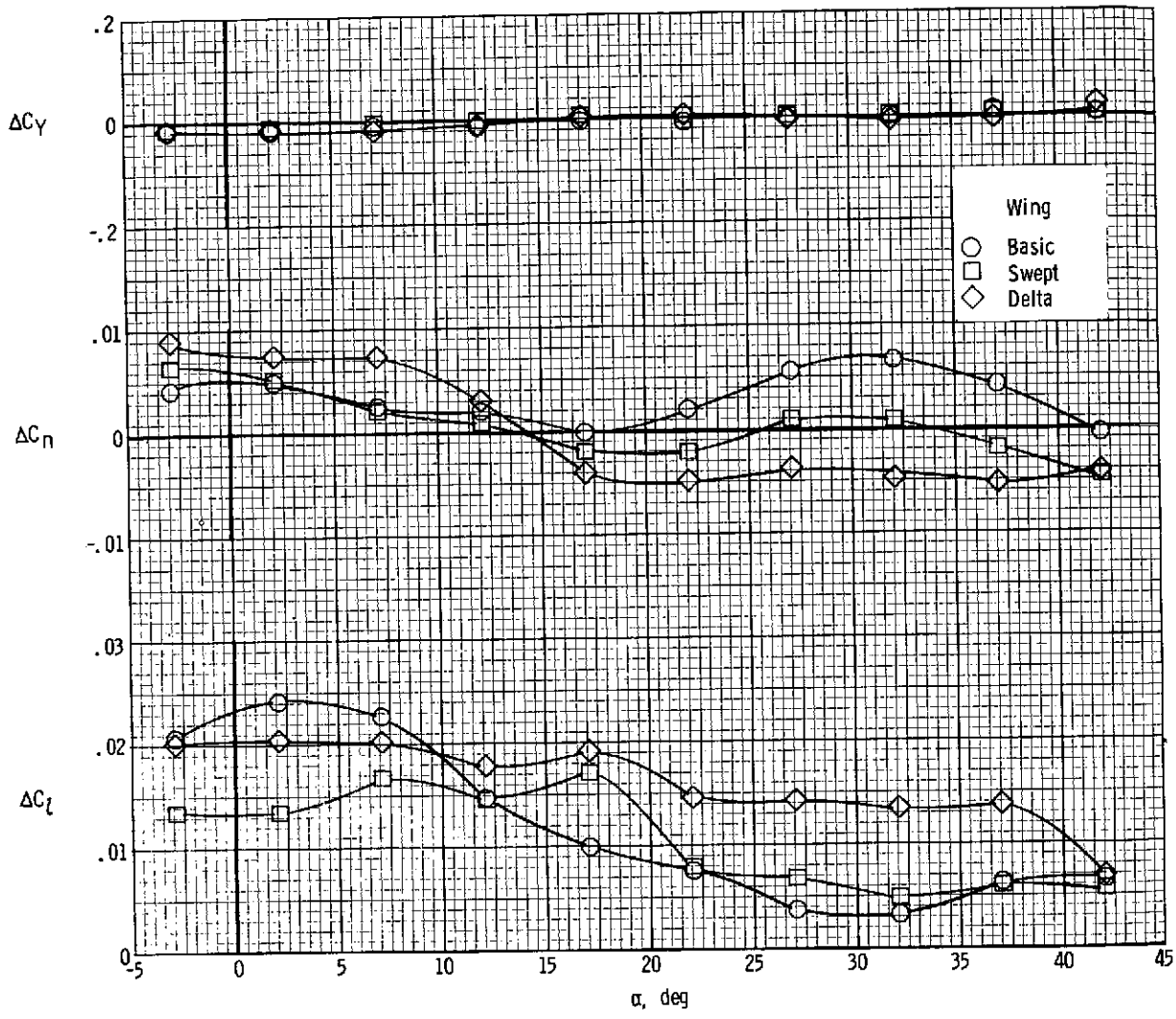

Figure 28.- Effect of aileron deflection for three wing configurations. $\delta_a = -15^\circ$.

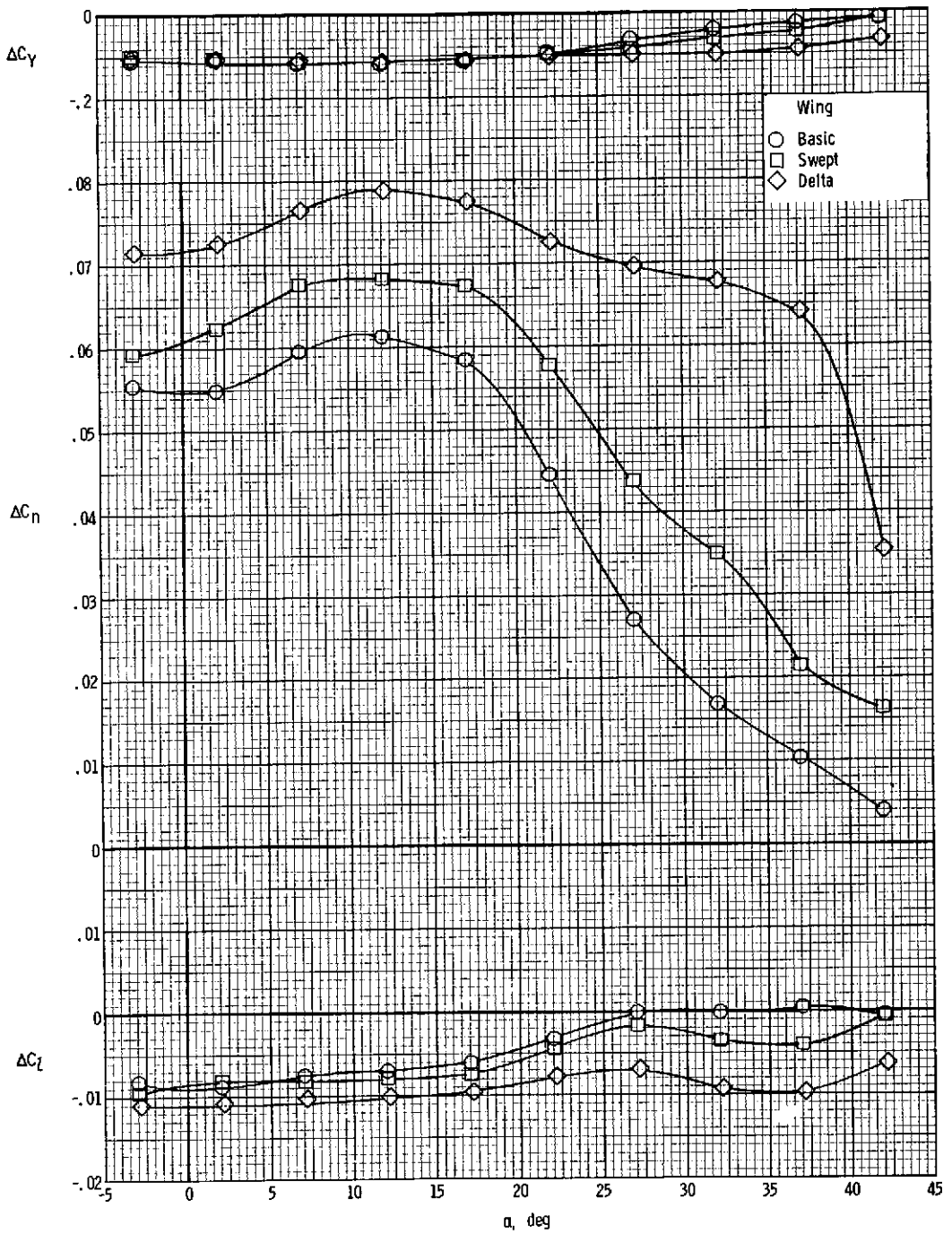

Figure 29.- Effect of rudder deflection for three wing configurations. $\delta_r = -30^\circ$.

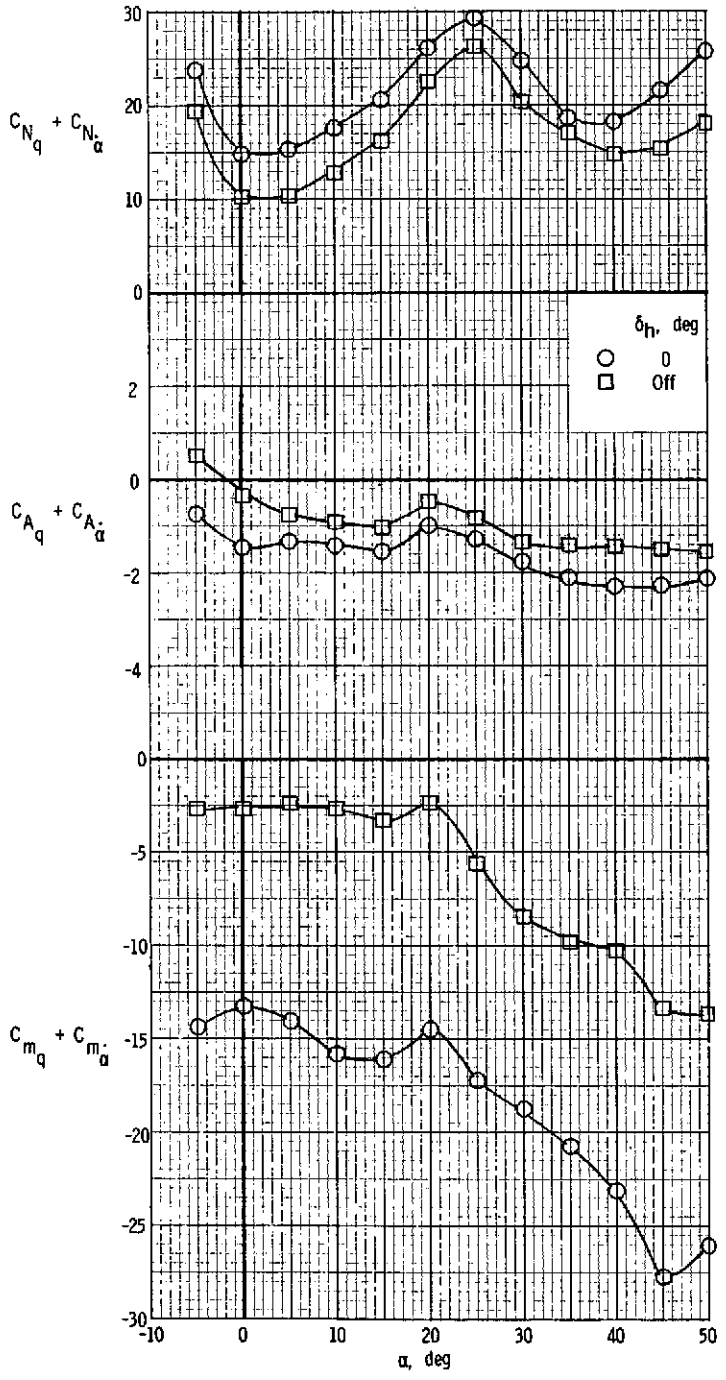

Figure 30.- Effect of horizontal tail on dynamic longitudinal-stability derivatives obtained during pitching-oscillation tests. Basic configuration; $\delta_{f,le} = 0^{\circ}$.

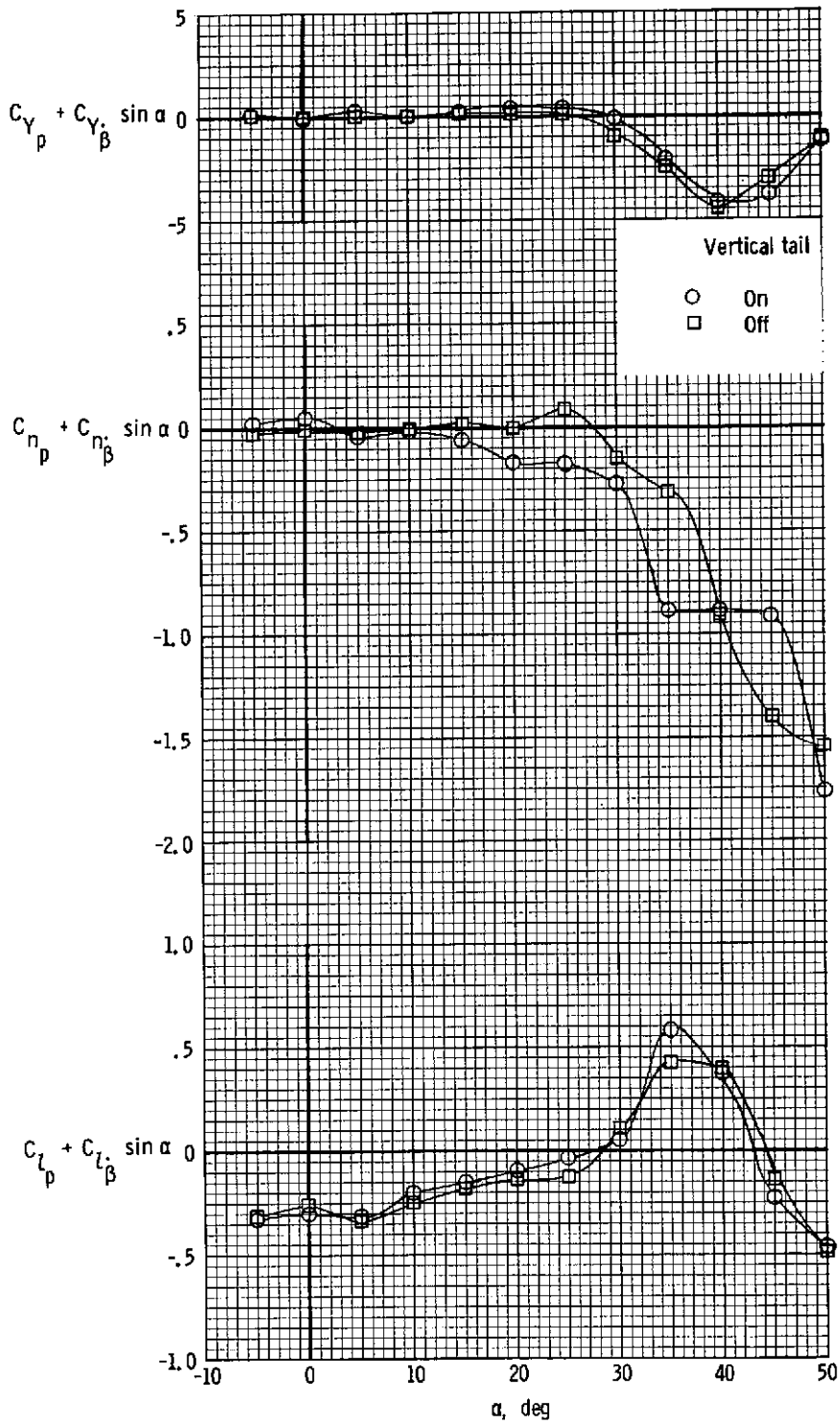

Figure 31.- Effect of vertical tail on dynamic lateral-directional stability derivatives obtained during rolling-oscillation tests.

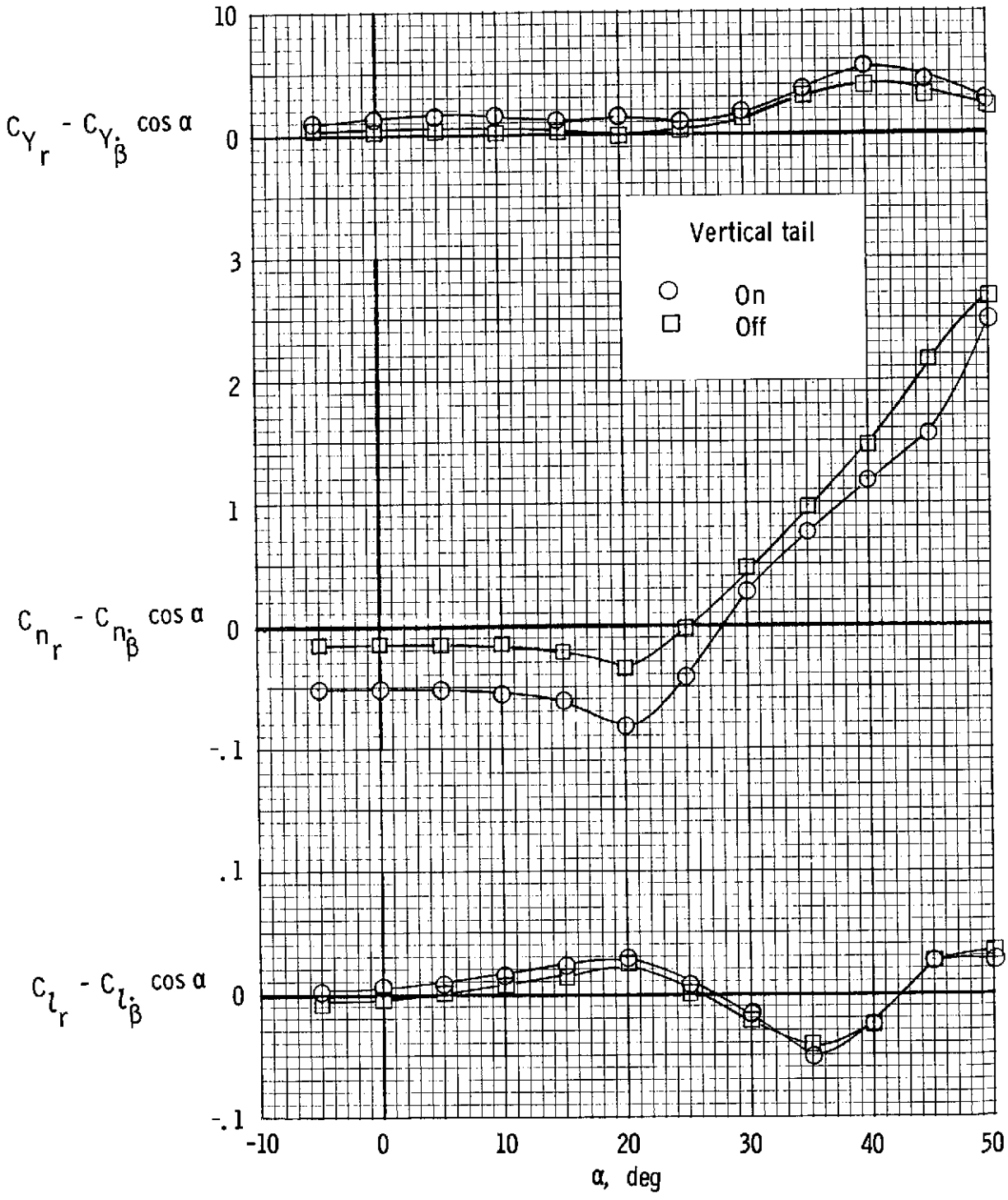

Figure 32.- Effect of vertical tail on dynamic lateral-directional stability derivatives obtained during yawing-oscillation tests.

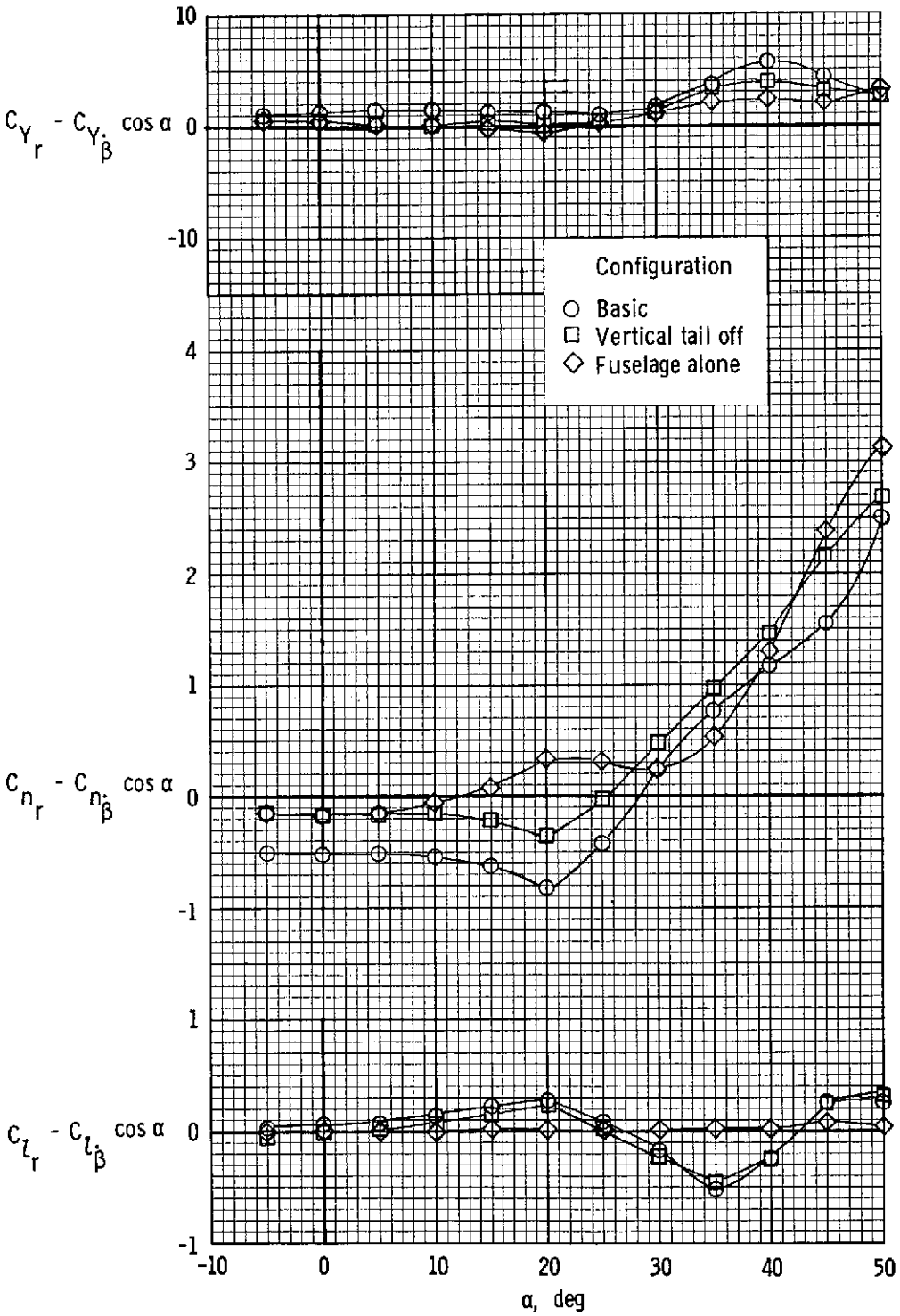

Figure 33.- Dynamic lateral-directional stability derivatives obtained during yawing-oscillation tests.

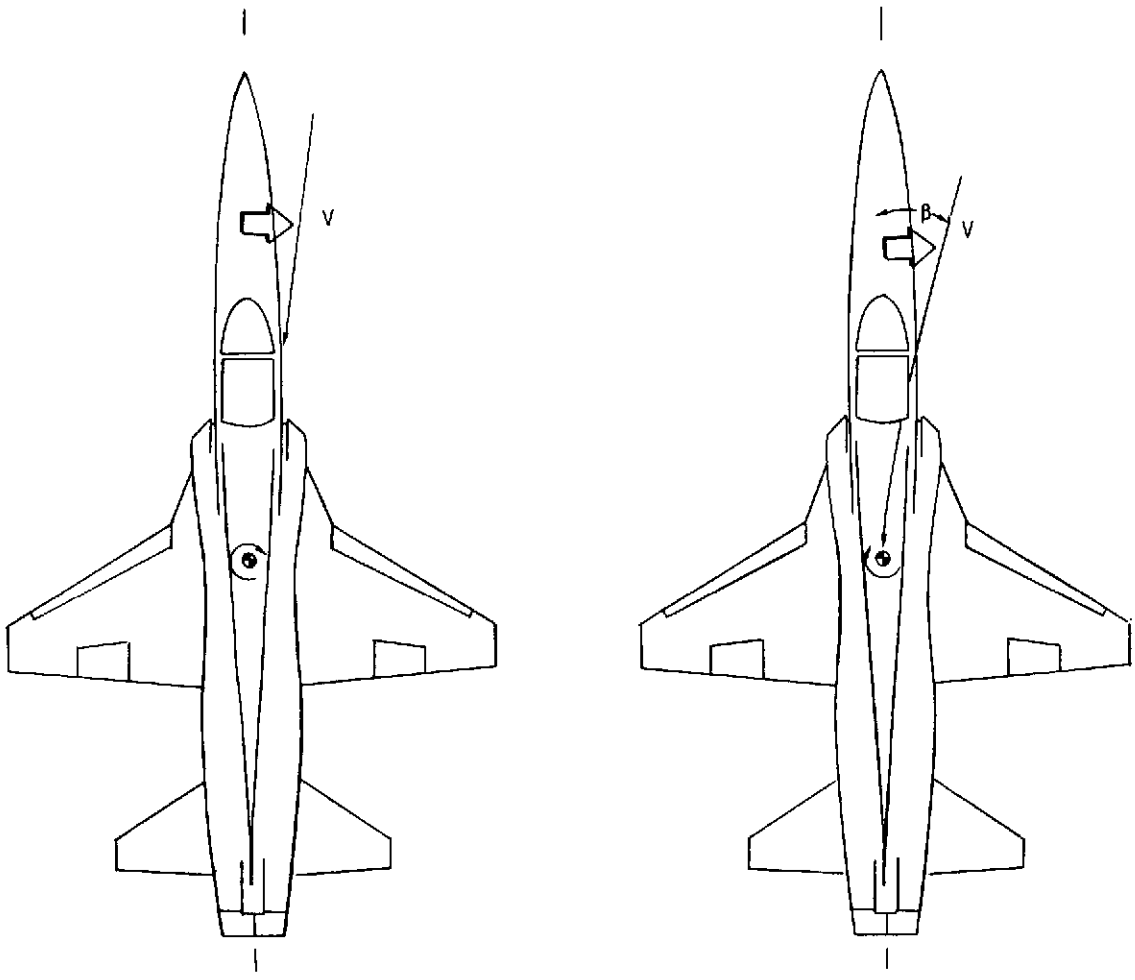

(a) Static, $\beta \neq 0^{\circ}$.

(b) Yawing, $\beta = 0^{\circ}$.

Figure 34.- Illustration of cause of unstable values of damping in yaw.

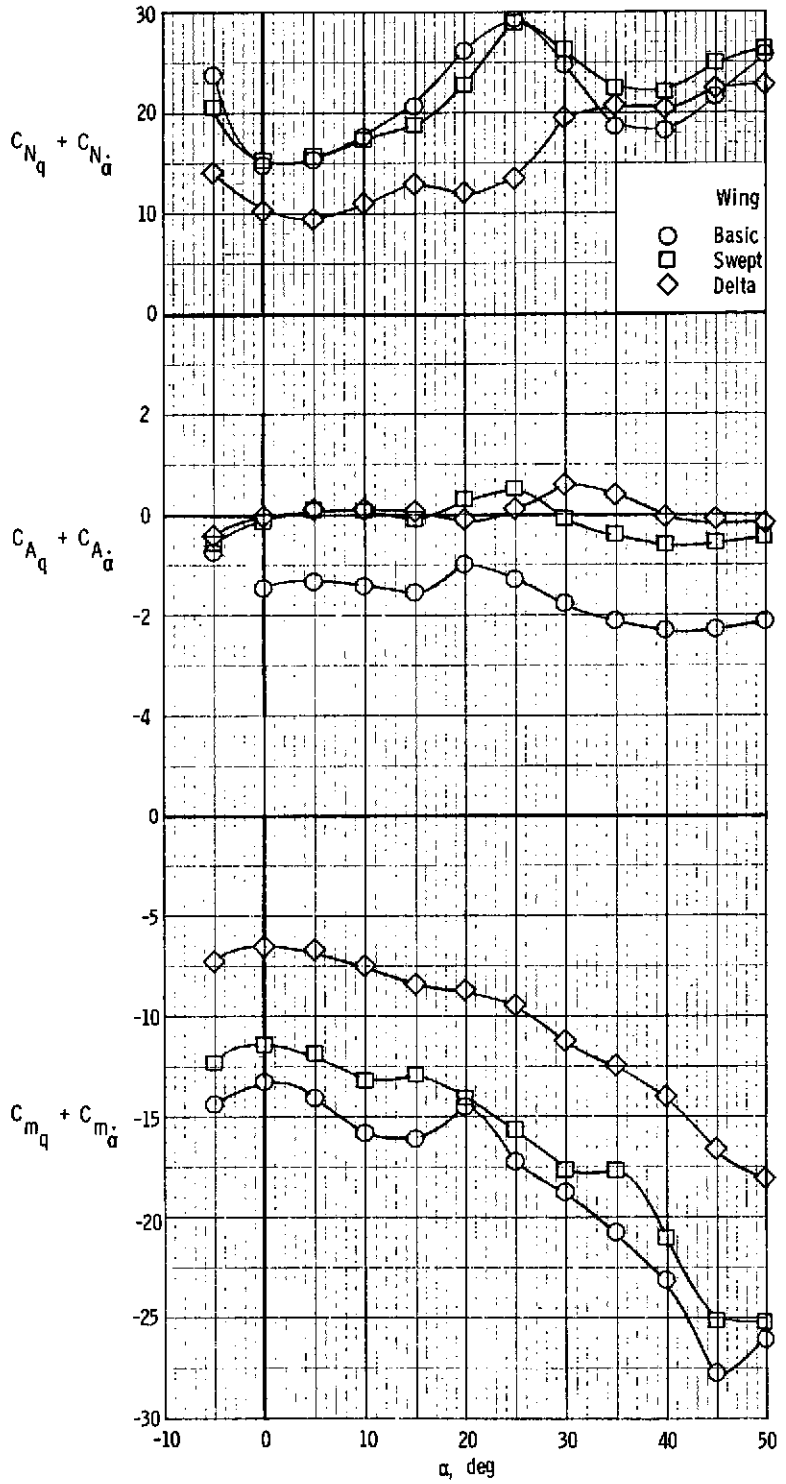

Figure 35.- Dynamic longitudinal stability derivatives obtained during pitching-oscillation tests for three wing configurations.

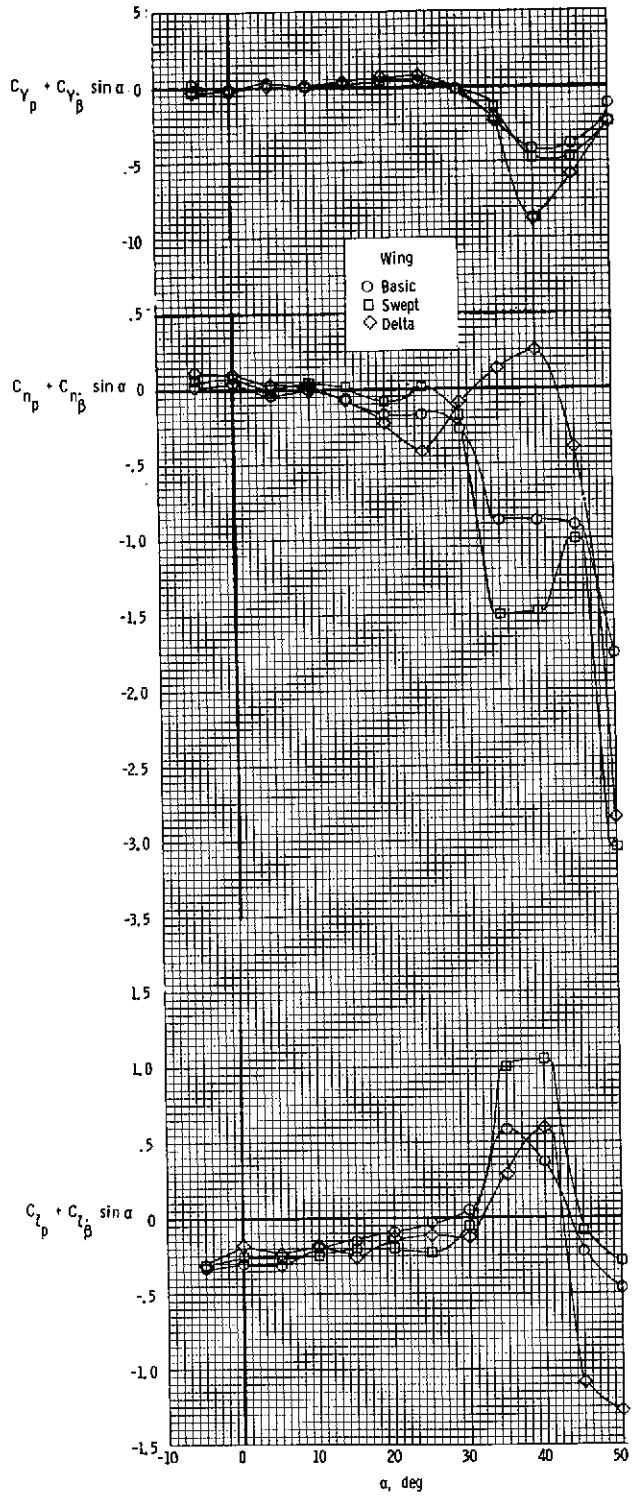

Figure 36.- Dynamic lateral-directional stability derivatives obtained during rolling-oscillation tests for three wing configurations.

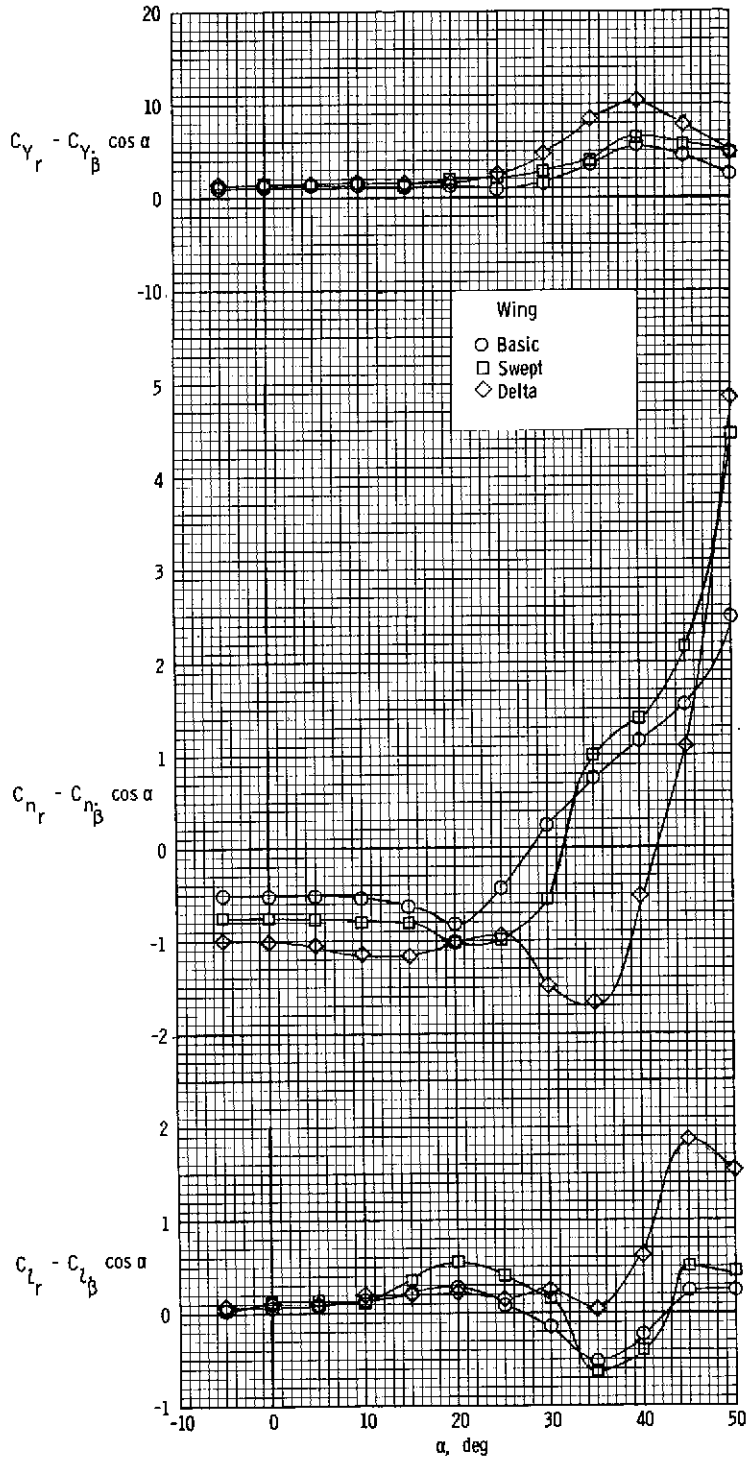

Figure 37.- Dynamic lateral-directional stability derivatives obtained during yawing-oscillation tests for three wing configurations.

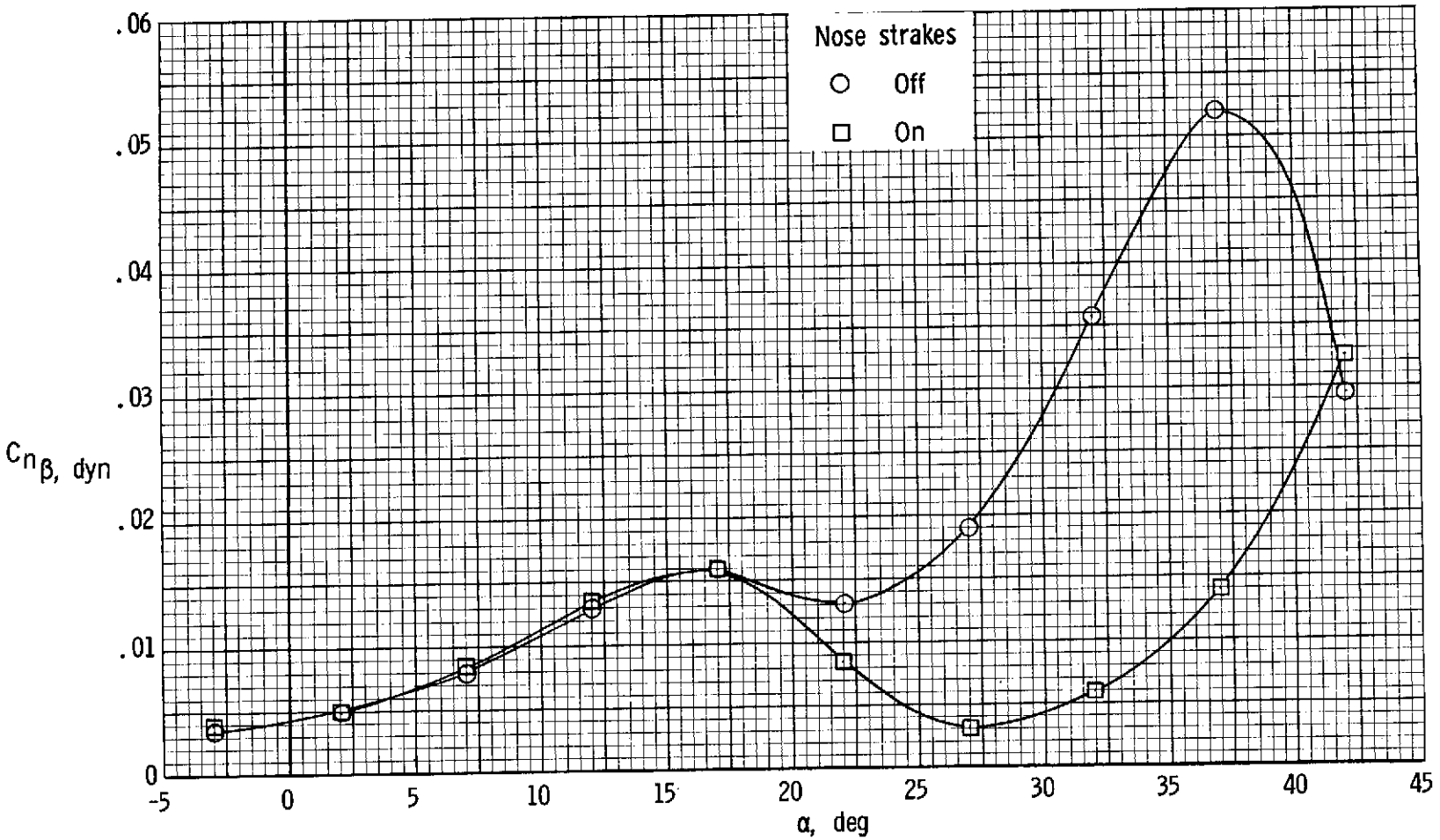

Figure 38.- Variation of $C_{n_{\beta,dyn}}$ with angle of attack. Basic configuration; $\delta_h = 0^\circ$; $\delta_{f,le} = 0^\circ$.

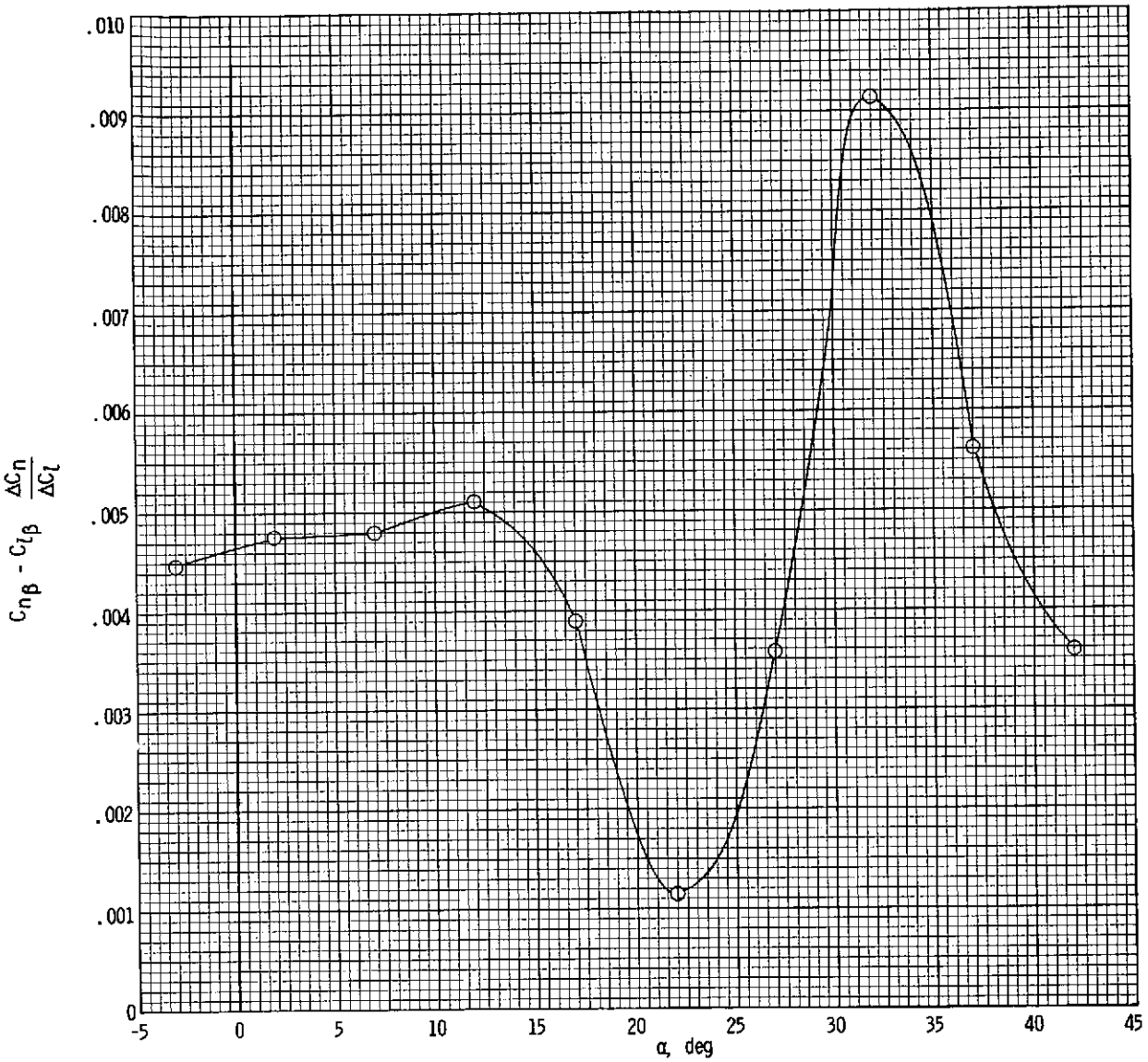

Figure 39.- Variation of aileron-effectiveness parameter with angle of attack. Basic configuration; $\delta_h = 0^\circ$.

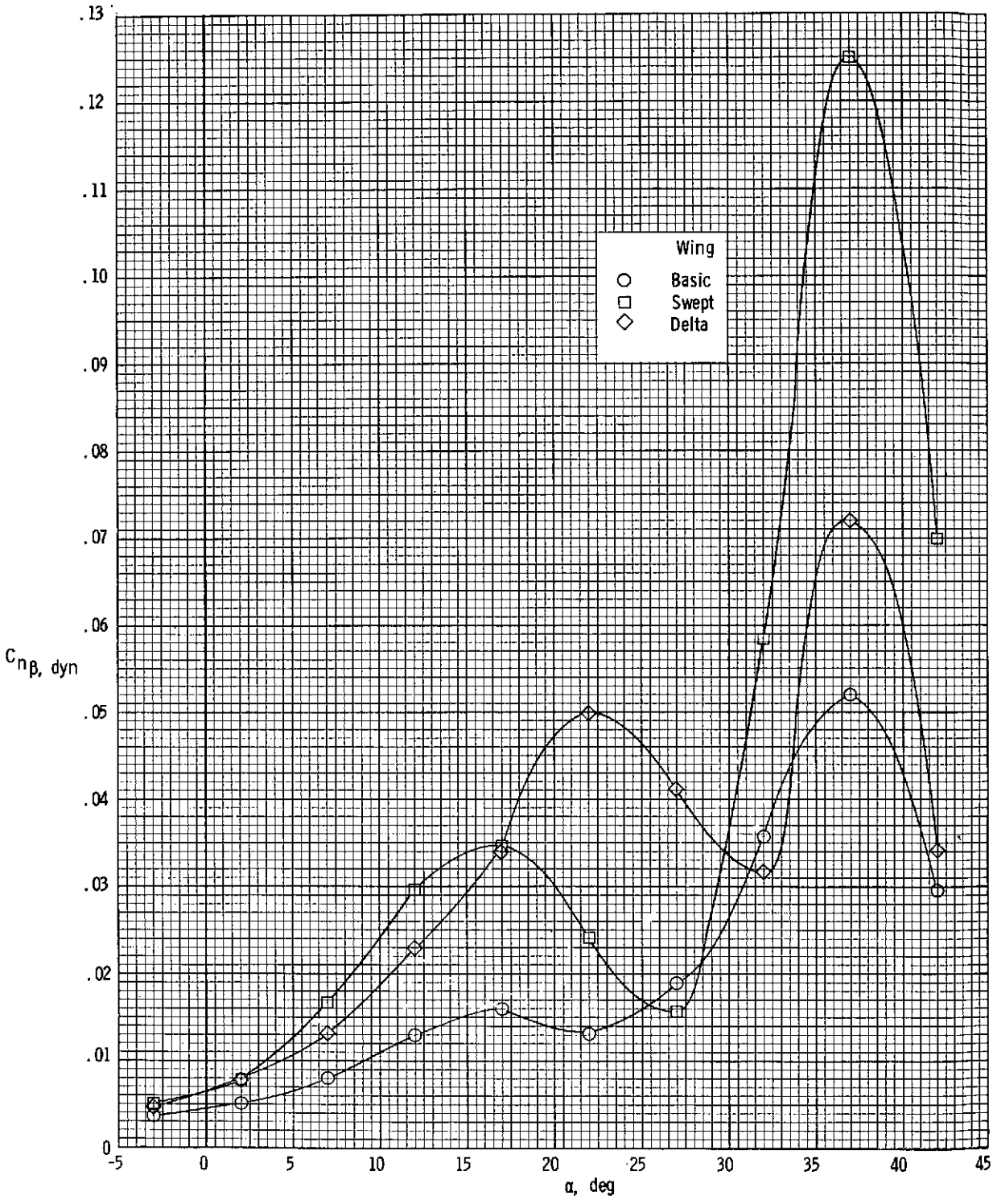

Figure 40.- Effect of wings on variation of $C_{n_{\beta,dyn}}$ with angle of attack.

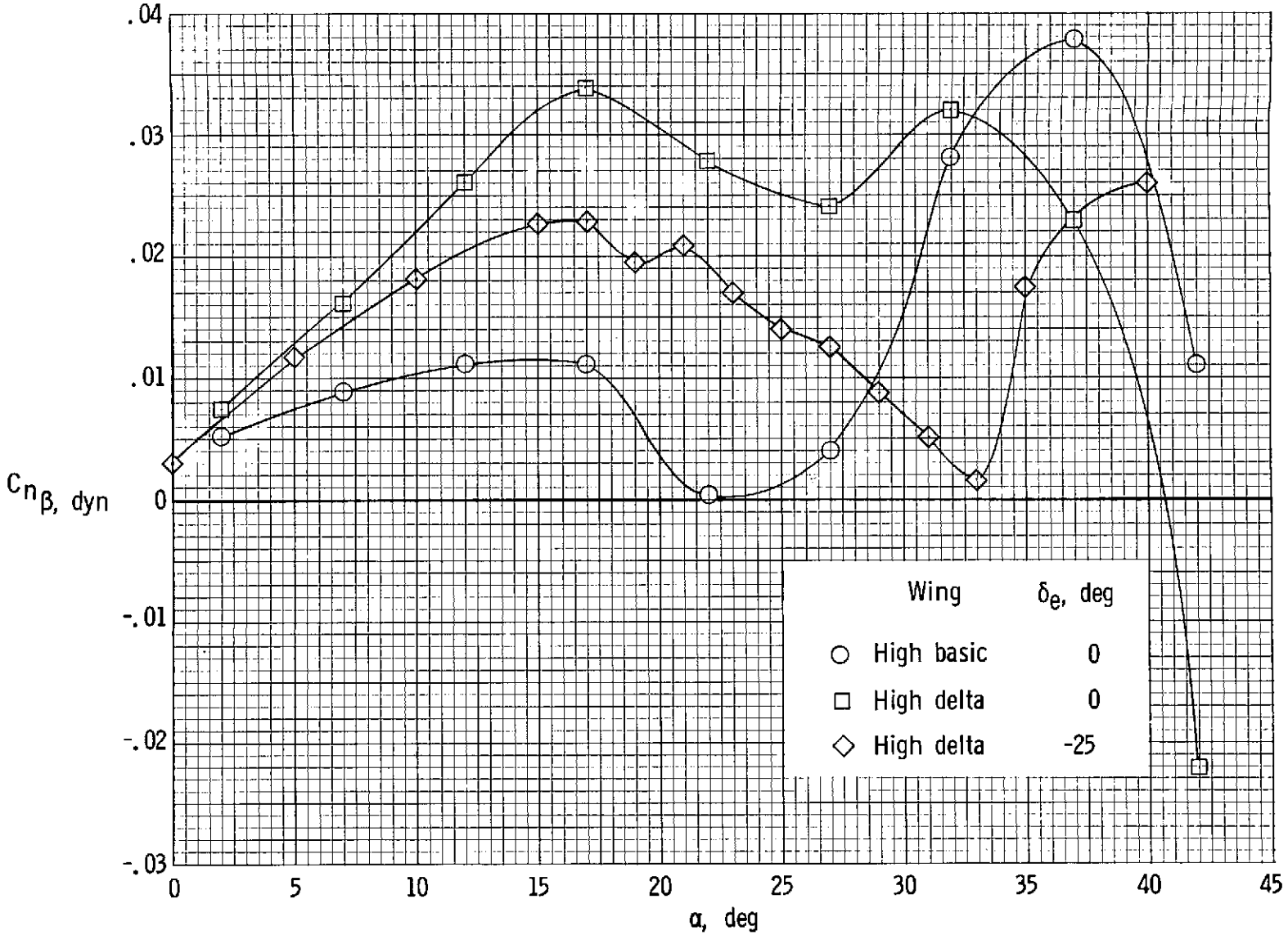

Figure 41.- Variation of $C_{n_{\beta,dyn}}$ with angle of attack for high-wing configurations.

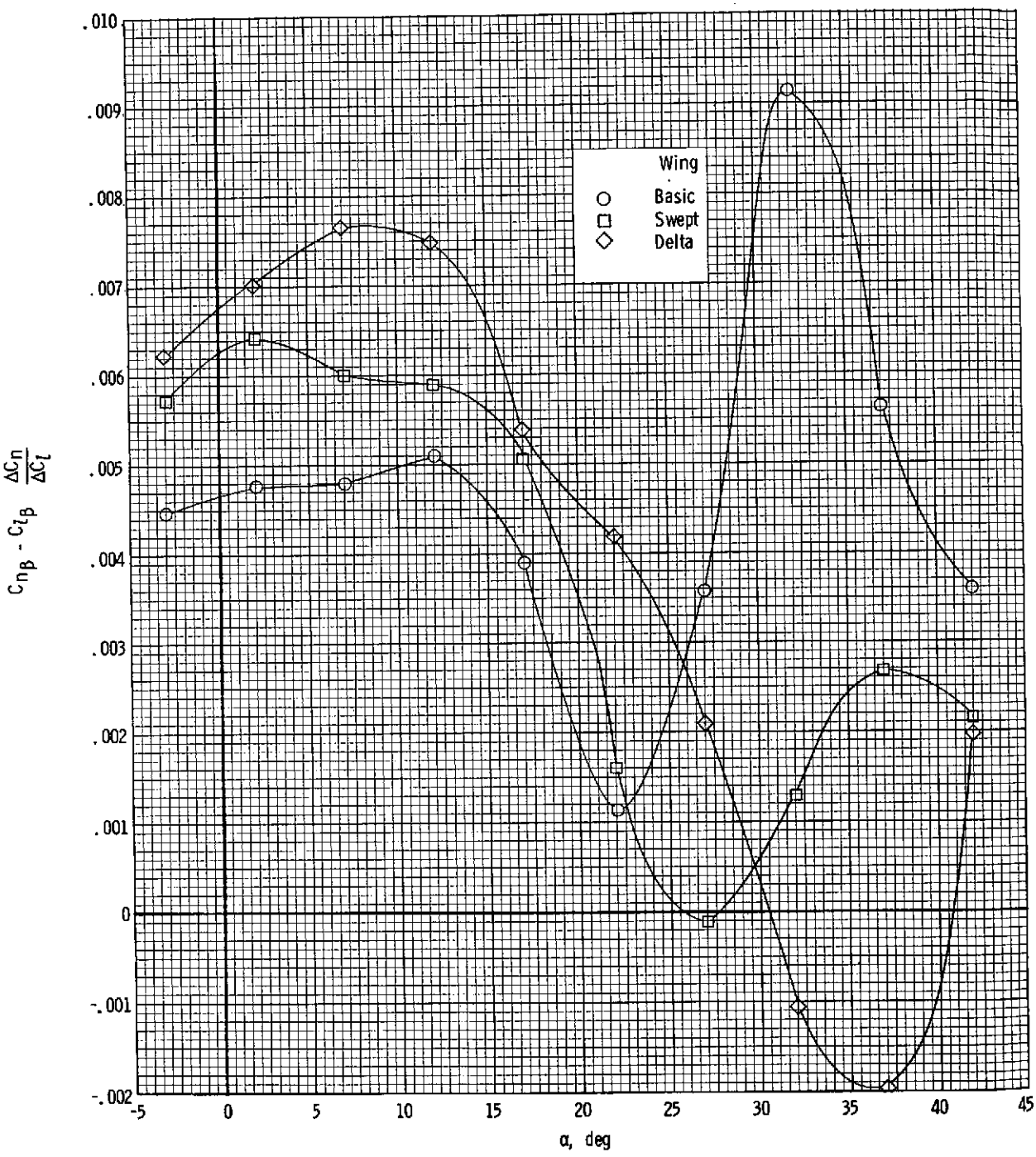

Figure 42.- Variation of aileron-effectiveness parameter with angle of attack for three wing configurations. $\delta_h = 0^\circ$.

NASA-Langley, 1974 L-9681